CHAPTER 1

INTRODUCTION

1.1 Background

Magnesium alloys are gaining attention in the field of automotive, aerospace, electronics and communications industries as they have comprehensive properties such as the improved damping property, excellent machinability, and good castability [1]. Basically there two types of magnesium alloys: aluminum free and aluminum containing. AZ91 magnesium alloy is the most promising alloy. However, the difficulty is that the alloy has a large freezing range, forming the constitutionally undercooled region and thus the formation of dendrites in normal castings which are susceptible to porosity. Hence, for up gradation of the properties of an alloy, quashing the formation of coarse dendrites and reduction of porosity are prime tasks [2].

Rapid cooling, chemical methods (addition of grain refiners) and physical methods (imposition of vibrations) are some of the methods counted as refinement methods in the casting process. Though very fine microstructure is obtained by rapid cooling method, this method is restricted to the size or shape of the casting because of the requisition for attaining an immensely high cooling rate. Addition of grain refiners minimizes the grain size of a microstructure even in bulk castings but most of the refiners are sparse and overpriced. The imposition of vibrations refines the microstructure in bulk castings [3]. In the foundry, vibration cause remarkable and significant effect in metals and alloys [4] such as grain refinement causes an increase in density, degassing and change in shape, size, and distribution of the second phase particles. For microstructural refinement, the vibration of solidifying melt has acknowledged a plenty of consideration from investigators [3]. The mechanical vibrations, ultrasonic vibrations, and electromagnetic vibrations have been reported as vibration processes. In ultrasonic vibrations, on increasing the distance from the transmitter, the intensity of vibration pacifies swiftly. This results confined grain refinement surrounding the vibration source. Therefore, a simple method is required where all such problems can be taken care. Mechanical vibrations are free from above problems and are also economical and simple process [5].

Another technique of grain refinement is the addition of grain refiner. For AZ91 Mg-based alloys, the addition of carbon containing grain refiners such as hexachloroethane (C_2Cl_6), calcium carbide (CaC_6), aluminum carbide (Al_4C_3), silicon carbide (SiC) and magnesium carbonate ($MgCO_3$) are used. There are also some carbon free grain refiners such as strontium (Sr), boron (B), Al-TiB, AlN, calcium, manganese and rare earth elements like cerium (Ce) and Yttrium (Y). Though these refiners were reported as successful refiners, still there is no widespread grain refiner exists for Mg- Al- based alloys that are ecofriendly, authentic and accessible [6]. In contrast, Fu et al. [7] observed ZnO as suitable grain refiner for pure magnesium (Mg) and Mg-3wt%Al alloy. Lee [8] also found ZnO as an effective grain refiner for AZ91E alloy. Saha et al. [6] also reported that ZnO supports in the refinement of grains along with the enhancement of mechanical properties.

The present research work comprised synthesis of AZ91 magnesium alloy. In the present study, the effect of different process parameters: frequency of mechanical vibration, the amplitude of mechanical vibration and addition of grain refiner without and with vibration were carried out.

1.2 Thesis Organization

The present work is organized into five chapters. The first chapter consists of the necessary background information. The motivation and overview of the project have also been presented in **Chapter 1**.

Chapter 2 contains the critical review of fundamental aspects of magnesium and its alloys, formation of the cast microstructure including solidification, homogeneous nucleation, heterogeneous nucleation, growth of the solid, effect of constitutional undercooling and solidification of magnesium alloys. Techniques of grain refinement including grain refinement of Mg- Al alloys through physical methods (vibrations) and grain refinement of Mg- Al alloys through chemical methods have also thoroughly been reviewed. The effect of different process parameters on microstructure and mechanical properties has also been critically reviewed.

Chapter 3 deals with the materials and methods used in the thesis. Synthesis of the AZ91 Mg alloy, compositional analysis of cast AZ91 Mg alloy and grain refining procedure of as- cast Mg- Al alloy are discussed in this chapter. In addition to this, this chapter also provides information about various characterization techniques used in the thesis. The characterization techniques such as optical micrographs, XRD and SEM were employed to analyze the morphology, phases, mode of fracture and worn surfaces. To study the mechanical properties (hardness and tensile properties) Brinell hardness and tensile tests were performed. Experiments for wear analysis of AZ91 alloy were conducted with a pin on disc test machine.

Chapter 4 presents the results and discussions including estimation of optical microstructures, SEM, hardness, tensile strength and XRD characterization of the treated and non-treated AZ91 samples; processed at different frequencies of vibration, amplitudes of vibration and addition of grain refiner without and with the imposition of vibration.

Firstly, the effect of the varied frequency of vibration at constant amplitude on the morphology of α-Mg phase was seen, and it showed that the average grain size decreased for frequency up to 15 Hz. Further increase in frequency increases the grain size. Secondly, the effect of varied amplitude of vibration at constant frequency of 15 Hz was seen and the optimum results were obtained at 15Hz – 2 mm. Thirdly, 2 wt.% of ZnO was added to the AZ91 alloy without and with the imposition of vibration. The mechanical properties and wear analysis of AZ91 alloy in different processing conditions were also studied. A comparative study between as cast, vibration imposed and ZnO added without and with imposed vibration AZ91 alloy for different processing conditions also conceded. Characterization study about the fractured surfaces, worn surfaces and examination of debris was also carried out. The alloy given combined effect showed minimum grain size of 70.2 μm, 64.3 μ and 56.9 μm at the top, middle and bottom portions respectively. On, giving the combined action i.e. addition of the grain refiner along with the imposition of vibration to the AZ91 alloy, the value of density increased to its maximum that further resulted into the improvement of mechanical properties.

This thesis concludes with **Chapter 5** enlisting the significant findings of the study and identification of the areas worthy of further investigation.

1.3 Aims and Objectives

The present work therefore contemplates the following study in respect of AZ91 magnesium alloy having composition Al-8.3-9.7%, Mn-0.15% min, Zn-0.35-1.0%, Si-0.10% max, Cu-0.03% max, Fe-0.005% max, Ni-0.002% max and Mg-90.963% - 89.013%.

(i) Effect of varying frequency (5, 10, 15, 20 and 25 Hz) of mechanical vibration at constant amplitude of 2 mm on the microstructure of the AZ91 alloy during solidification.

(ii) Effect of varying frequency (5, 10, 15, 20 and 25 Hz) of mechanical vibration at constant amplitude of 2 mm on the mechanical properties of the AZ91 alloy during solidification.

(iii) Effect of varying frequency (5, 10, 15, 20 and 25 Hz) of mechanical vibration at constant amplitude of 2 mm on the wear study of the AZ91 alloy during solidification.

(iv) Effect of varying amplitude (1 and 3 mm) of mechanical vibration at constant frequency of 15 Hz on the microstructure of the AZ91 alloy during solidification.

(v) Effect of varying amplitude (1 and 3 mm) of mechanical vibration at constant frequency of 15 Hz on the mechanical properties of the AZ91 alloy during solidification.

(vi) Effect of varying amplitude (1 and 3 mm) of mechanical vibration at constant frequency of 15 Hz on the wear study of the AZ91 alloy during solidification.

(vii) Effect of combined action of mechanical vibration and grain refiner during solidification of AZ91 alloy.

(viii) Effect of grain refiner without and with vibration on the microstructure of the AZ91 alloy during solidification.

(ix) Effect of grain refiner without and with vibration on the mechanical properties of the AZ91 alloy during solidification.

(x) Effect of grain refiner without and with vibration on the wear study of the AZ91 alloy during solidification.

CHAPTER 2

LITERATURE REVIEW

The extensive literature survey that has been done is focused on solidification, microstructural analysis, mechanical properties and wear study of magnesium alloys.

2.1 Classification of Cast Magnesium Alloys

Pure magnesium is light in nature and therefore its alloy is used in automobiles and aerospace industries. Thus, alloying is done to improve the manufacturability and the product properties.

2.1.1 Effect of addition of alloying elements on magnesium

The addition of alloying elements can effectively improve the strength and ductility of magnesium. Direct or indirect increment of the content of the solute element in solid solution affects the development in the mechanical properties [9]. The major alloying elements and their effects in magnesium alloys are [10]:

(i) Aluminum: Aluminum is the most commonly used alloying element. The maximum solubility of Al in Mg is 12.7 wt. % and alloys in excess of 6 wt.% can be heat treated. Aluminum improves strength of the alloy. The optimum combination of strength and ductility observed at about 6 wt.%. The creep resistance is limited due to the poor thermal stability of the $Mg_{17}Al_{12}$ phase. It provides hardness and strength at room temperature, widens the freezing range and makes the alloy easier to cast.

(ii) Zinc: Zinc is one of the commonest alloying additions. It is used in conjunction with Al (e.g., AZ91 or with zirconium, thorium or rare earths). It provides strength but increases microporosity, reduces corrosion resistance.

(iii) Manganese: Manganese is usually not employed alone but with other elements, e.g., Al. In this case compounds MnAl, $MnAl_6$ or $MnAl_4$ intermetallics are formed. It reduces the solubility of iron and produces relatively innocuous compounds. It increases the yield strength and improves salt water corrosion resistance of MgAl and MgAlZn alloys. The maximum amount of manganese

addition is 1.5–2 wt.%. It helps in offsetting effect of trace element on corrosion and provides toughness. To certain extent reduces micro-galvanic corrosion but at high concentration affect corrosion resistance.

(iv) Yitrium: Yitrium is used in conjunction with rare earths to improve high temperature strength and creep resistance up to 300 °C. It provides strength, increases corrosion resistance, but it is expensive.

(v) Silver: Silver increases age hardening and high temperature properties of thorium or rare earth containing alloys e.g. QE22 and QH21. It provides strength but reduces corrosion resistance.

(vi) Cerium: It provides moderate elevated temperature properties and helps in castability.

(vii) Neodymium: It increases elevated temperature properties and assists in castability.

(viii) Heavy rare earths: They improve room and elevated temperature mechanical properties and increases fluidity.

(ix) Zirconium: It works as a grain refiner.

2.1.2 AZ91 cast magnesium alloy

The AZ groups of magnesium alloys are roughly 90% magnesium with aluminum as its major other component. Small amounts of copper, nickel, and iron contribute to corrosion resistance and silicon for strength. The Mg-Al-Zn alloy system, with the most common alloy AZ91D, is most often used in room temperature applications as seat frames and instrument panels. Table 2.1 shows the composition of AZ91 magnesium alloys.

Table 2.1 Composition of AZ91 magnesium alloys [11]

Alloy	Al	Mg	Zn	Si	Cu	Fe	Ni	Other
AZ91 A	8.3- 9.7 %	0.13 %max	0.35-1%	0.50 %max	0.10 %max	-	0.03 %max	0.30 %max
AZ91 B	8.3- 9.7 %	0.13 %max	0.35-1%	0.50 %	0.35 %max	-	0.03 %max	0.03 %max
AZ91 C	8.1-9.3 %	0.13 %min	0.4-1%	0.30 %max	0.10 %max	-	0.01 %max	0.30 %max
AZ91 D	8.3-9.7 %	0.15 %min	0.35-1%	0.10 %max	0.03 %max	0.005 % max	0.002 %max	0.03 %max
AZ91 E	8.1-9.3 %	0.17- 0.35%	0.4-1%	0.20 %max	0.015 %max	0.005 % max	0.001 %max	0.30 %max

2.1.3 Advantages of magnesium and its alloys

Following are the advantages of magnesium and its alloys;

(i) Density and specific strength: In the automotive and aerospace industries in the present era, the augmentation of the fuel efficiency of automobiles and aircrafts is of the major interest and this can be increased by decreasing the weight of vehicles. Since, the cast magnesium alloys have low density (1.74 g/cm^3), high specific strength (175.69 MPa/g/cm^3) and high tensile strength; they are essential material in these industries.

(ii) Castability: Magnesium has a good castability as it requires ease of casting, less cost, defects and lead- time and energy due to its high fluidity.

(iii) Damping capacity: Magnesium and its alloys have excellent damping capacity. The homogeneous distribution of elastic energy results in the increase in damping capacity with the reduction in grain size of the material.

(iv) Machinability: Magnesium and its alloys have very good machinability. In contrast to other frequently machined metals, magnesium and its alloys entail less power to eradicate a given amount of magnesium. Also there is a feasibility of higher speeds, feed rates and greater depths of cuts [12].

2.2 Phase Diagram of AZ91 Magnesium Alloy

Aluminum is one of the most important alloying elements in magnesium. Several systems contain up to 10 wt.%, e.g., AZ, AE (AE42), AM (AM60, AM50, AM20) and AS (AS41, AS21). Figure 2.1 (a- b) shows the Mg- Al system. Aluminum is one of the few metals that dissolve easily in magnesium. Above the solubility limit $Mg_{17}Al_{12}$, a brittle intermetallic phase precipitates out. The solubility limit of aluminum at the eutectic temperature is 12 wt.% and falls to about 1 wt.% at room temperature. Consequently, the $Mg_{17}Al_{12}$ plays a dominant role in determining the properties. The commercial alloys based on Mg- Al involve further alloying additions of zinc e.g., AZ91, AZ81, AZ63 [13]. Two eutectic reactions are important to the phase constitution of Mg-Al binary alloys:

(i) at 450 ºC: $L \longrightarrow Al + Mg_2Al_3$ **(2.1)**

(ii) at 436 ºC: $L \longrightarrow Mg + Mg_{17}Al_{12}$ **(2.2)**

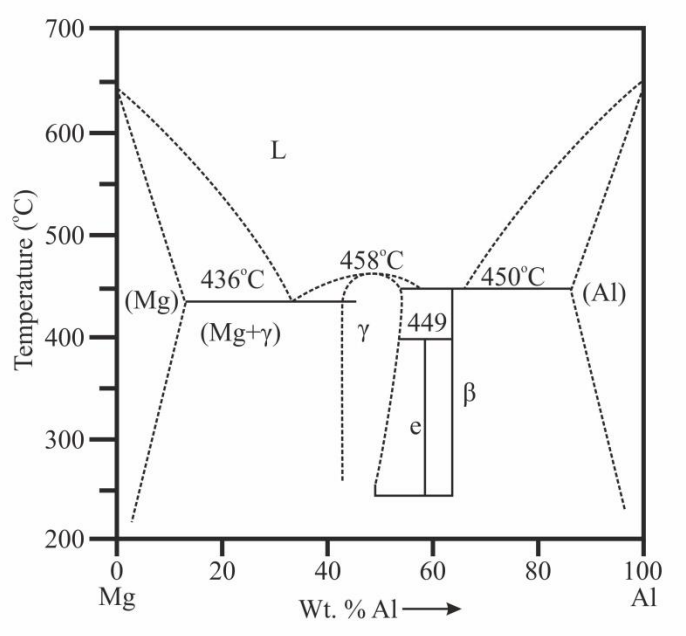

Figure 2.1 (a) Phase diagram of Mg-Al binary alloy [14].

The low eutectic temperature (436 °C) of the $Mg_{17}Al_{12}$ phase limits the application of Mg-Al alloys to temperatures below 125 °C, above which the discontinuous precipitation of the $Mg_{17}Al_{12}$ phase leads to substantial creep deformation [14]. The commercial alloys

fall in the range of 2-9 wt.% aluminum. At the lower end of this composition range, casting becomes difficult, while beyond 9 wt.% aluminum, the alloys become increasingly brittle due to the high fractions of β-($Mg_{17}Al_{12}$) intermetallic phase.

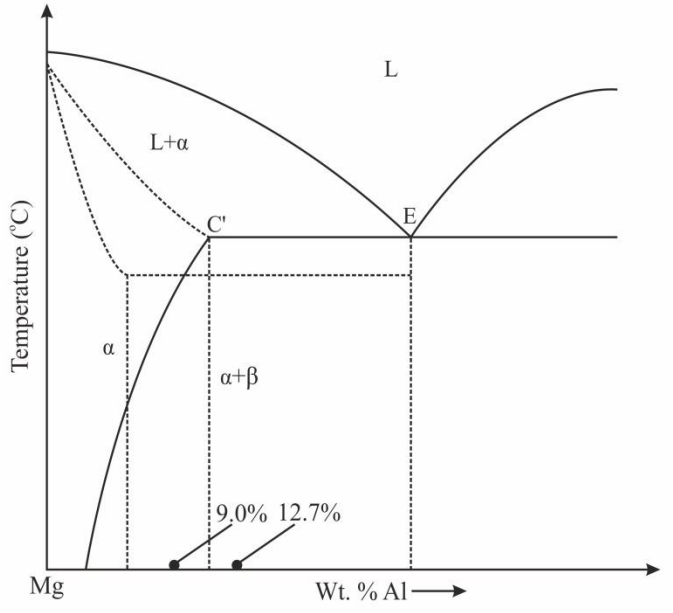

Figure 2.1 (b) Magnesium- rich section of Mg-Al system [15].

2.3 Solidification

At any temperature, thermodynamically stable state is only when it has lowest free energy. The temperature at which the two states have same free energy is known as the equilibrium temperature for transition between the two states. For example, equation (2.3) shows transformation of pure liquid metal to solid crystal of pure metal.

$$L \rightarrow X\ (Solid) \qquad \textbf{(2.3)}$$

The liquid phase will have higher internal energy (equal to heat of fusion) and higher entropy due to its more random structure, while the crystalline solid phase has lower internal energy and lower entropy. Due to this, at equilibrium melting point, T_f, free energy of both the phases is equal. Therefore, the free energy curve of liquid phase will lie below the free energy curve of the solid phase (Fig.2.2). At $\Delta G = 0$, solidification

reaction cannot occur. Above T_f, the liquid phase is more stable as it has a lower free energy. For reaction 2.3, ΔG is positive, so solidification reaction cannot occur. Crystalline solid has a lower free energy than the liquid phase below T_f, so for reaction 3, free energy is negative. Once ΔG becomes negative, very tiny particles of the product phase forms within the parent phase due to thermal fluctuations. These tiny particles separate themselves from the parent matrix by forming an interface, which grows by transfer of atoms across this interface. Grain nucleation and grain growth are two important mechanisms during solidification.

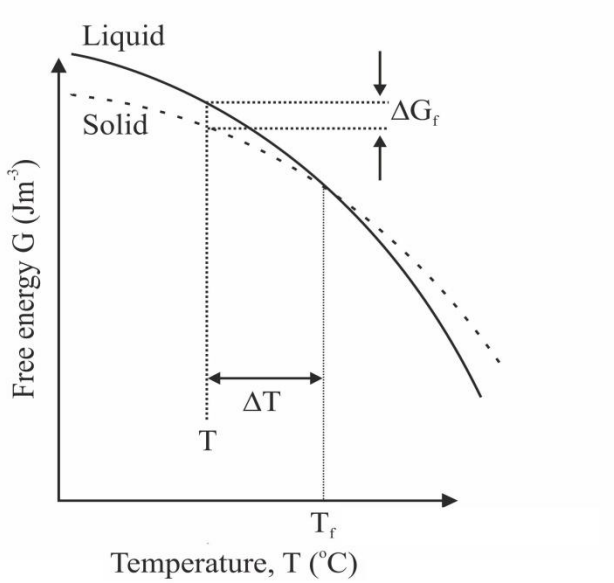

Figure 2.2 Schematic plot of the difference between the free energies of liquid and solid.

2.3.1 Fundamentals of nucleation

Nucleation can be defined as the formation of a new phase in a distinct region, separated from the surroundings by a definite boundary. When a liquid cools, a change of state from liquid to solid may occur corresponding to a discontinuity in free energy. This results in the formation of small particles surrounded by liquid. Nucleation is of two types, namely, homogeneous nucleation and heterogeneous nucleation. Homogeneous nucleation does not involve foreign atoms, particles or surfaces. Heterogeneous nucleation is achieved through the influence of foreign particles and/or surfaces. A good understanding of how

and when nucleation takes place necessitates a look at the problem from both the thermodynamic and the kinetic point of view.

The final microstructure during solidification of alloys depends on the initial nucleation, the growth characteristics of primary phase and the final eutectic solidification. The size and the shape of the primary phase affect the size of the primary pockets that form upon solidification, which change the morphology of the eutectic. However, the cooling rate influences the final microstructure of the alloys by controlling the initial nucleation and grain size [16].

Homogeneous nucleation

When a pure metal cools down in the liquid state, it will transform to the solid state at some temperature. From thermodynamics, there is only one temperature at which a pure solid metal can co-exist with pure liquid metal. At this temperature, corresponding to the equilibrium melting temperature T_f, the free energies of liquid and solid are equal.

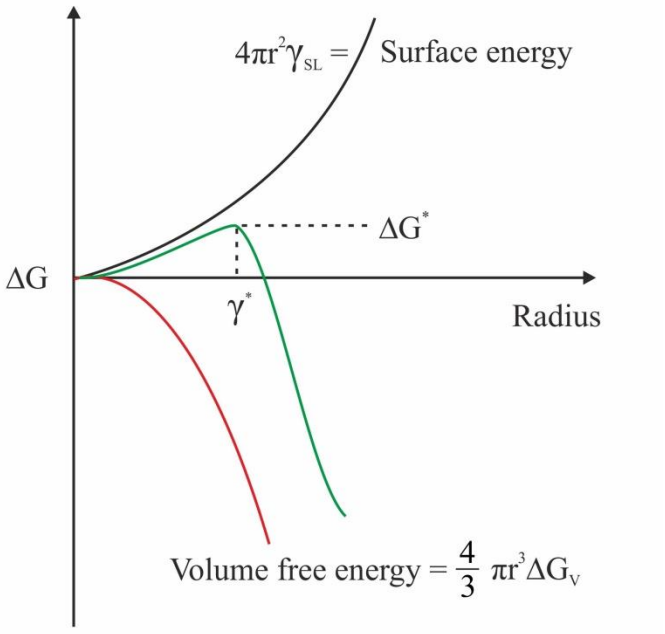

Figure 2.3 Free energy change for cluster formation as a function of cluster size [17].

T_f is also the temperature of melting of the solid on heating. A metal will tend to solidify when its temperature is below the melting point because there is a decrease in free energy

associated with the solid-to-liquid transformation. The larger the degree of undercooling, the larger the driving force to transform from liquid to solid. Figure 2.3 showing Free energy change for cluster formation as a function of cluster size [17].

$$\mathbf{r^* = \frac{-2\gamma}{\Delta G}} \qquad \textbf{(2.4)}$$

Heterogeneous nucleation

In the usual casting processes, nucleation is heterogeneous and occurs on solid surfaces in the liquid. Foreign substances, either the container or insoluble impurities, provide such surfaces. For a metal to solidify on a foreign substance, it is essential that the surface of the substrate should be wetted. The angle of contact θ between the substrate and the solid metal being deposited is important (Fig. 2.4). When θ is small, the interface energy between the solid and the substrate is low.

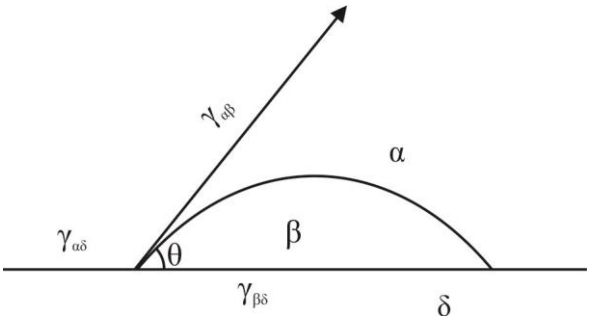

Figure 2.4 The nucleation of a β phase particle on the surface of a nucleating agent δ. The surface tension forces γαβ, γαδ and γβδ act along the indicated directions [17].

Under these conditions, the atoms in the liquid readily form a solid-metal nucleus on the surface of the substrate. If θ = 180° the solid/ substrate surface energy is high and nucleation is in effect homogeneous. The effectiveness of any particle as a nucleation catalyst is a function of the contact angle, which is determined by factors such as the lattice spacing of the two structures (substrate and solid metal) and the chemical nature of the substrate surface [18].

$$\gamma_{\alpha\beta} = \gamma_{\alpha\beta}\mathrm{Cos}\theta + \gamma_{\beta\delta} \qquad \textbf{(2.5)}$$

$$\Delta G^*_{\mathrm{het}} \frac{4\pi\gamma^3\alpha\beta}{3(\Delta G)^2}(2 - 3\mathrm{Cos}\theta + \mathrm{Cos}^3\theta) \qquad \textbf{(2.6)}$$

$$\Delta G^*_{het} = \frac{1}{4}\Delta G^*_{homo} \quad \textbf{(2.7)}$$

2.3.2 Thermal supercooling

Cellular growth, as illustrated in Fig.2.5, occurs when the advancing planar solid-liquid interface becomes unstable, and a small spike appears on the interface that then grows into a cellular type structure. The planar surface becomes unstable because any part of the interface that grows ahead of the remainder enters a region in the liquid that is at a lower temperature. The initial spikes that form remain isolated at first, because as they grow by solidification, they release their latent heat of fusion into the adjacent liquid, causing a localized increase in the temperature. Consequently, parallel spikes of almost equal spacing advance into the liquid [19].

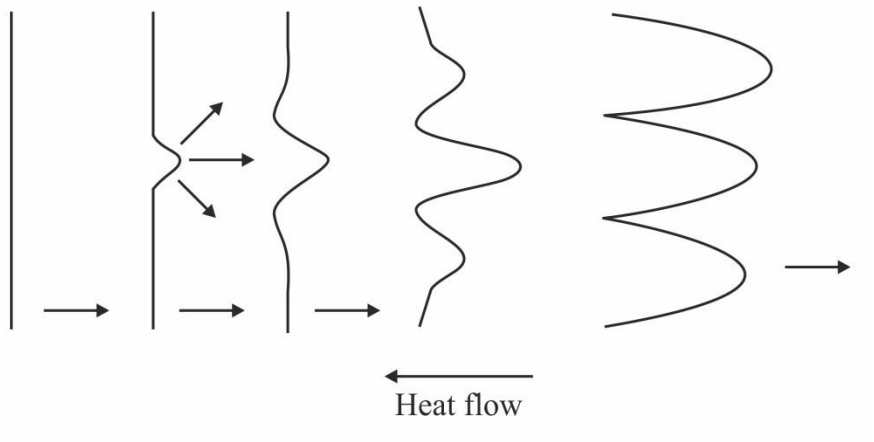

Figure 2.5 Transition from planar to cellular growth [19].

Dendritic growth is a further manifestation of cellular growth in which the spikes develop side protrusions. At still higher undercooling and higher growth velocities, the cells grow into rapidly advancing projections, sometimes of complex geometry. Their tree like forms (Fig. 2.6) have given them the name dendrites, after the Greek word dendrites for tree. The secondary arms of dendrites develop perpendicular to the primary arms because, as the primary arm solidifies and gives off its latent heat of reaction, the temperature

immediately adjacent to the primary arm increases. This creates another temperature inversion in the liquid between the primary arms, so secondary arms shoot out in that direction. A similar explanation can be given for the formation of the tertiary arms.

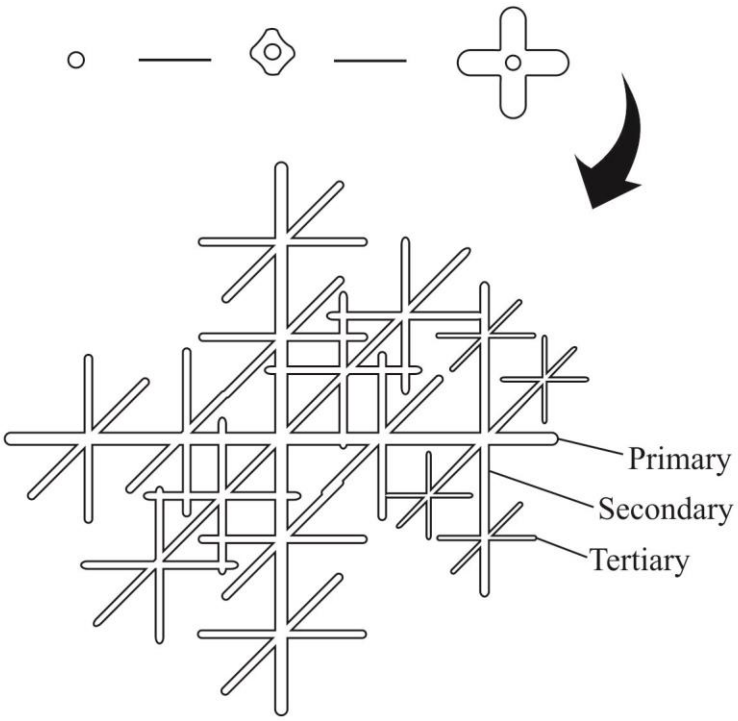

Figure 2.6 Dendrite formation [19].

The spacing of the secondary arms is proportional to the rate at which heat is removed from the casting during solidification, with faster cooling rates producing smaller dendrite arm spacing. Dendrites start as long thin crystals that grow into the liquid and thicken. The change in interface morphology of a succinonitrile- 4% acetone solution with increasing solidification velocity (Fig.2.7) demonstrates the evolution of a dendritic structure [19].

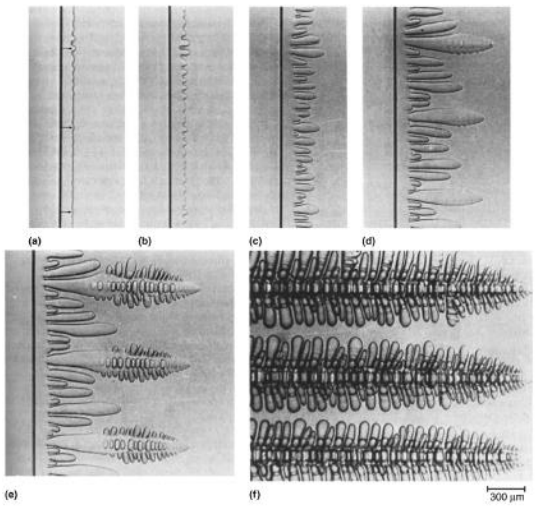

Figure 2.7 Dendrite formation in succiononitrile-4% acetone solution [19].

2.3.3 Effect of constitutional undercooling

Constitutional supercooling occurs as solute is rejected at the solid-liquid interface during solidification as shown in Fig. 2.8. During growth, solute rejection builds up a constitutionally supercooled zone ahead of the interface. This supercooled zone facilitates further nucleation and initiates a new grain if nucleant particles are available**.** In hypoeutectic Al and Mg based alloys, constitutional undercooling is a result of solute enrichment. In the case of peritectic systems and hypereutectic alloys, the constitutional undercooling is caused by the solvent (aluminum or magnesium respectively) [20]**.** For example addition of Zirconium (Zr) results in retarded grain growth. Zr addition to Mg alloys provides good nucleant substrates and enhances constitutional undercooling, which restricts dendrite growth and facilitates further nucleation [21]**.**

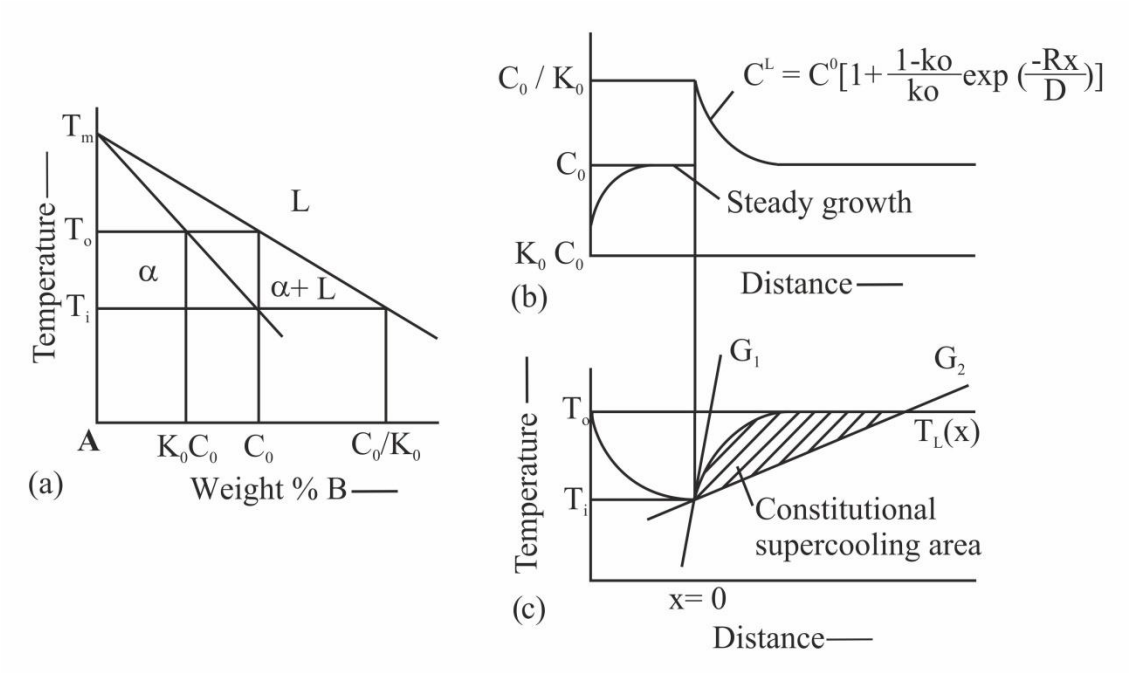

Figure 2.8 Temperature vs. distance from solid/ liquid interface [21].

2.3.4 Growth of the solid

Mostly, solute diffusion in the liquid restricts the homogenization. In aforesaid cases, there is a solute concentration gradient before solidifying front. The liquidus temperature (T_{mp}) increases with the distance, as on increasing the distance before the solid- liquid interface, attain less concentration of solute. Nevertheless, due to casting conditions, the rate of heat transfer from the system is fixed. Casting condition controls the overall temperature distribution. Therefore, there exists a temperature difference between T_{mp} and T which is called constitutionally undercooled region. During solidification the morphology of the solid- liquid interface is deeply affected by the constitutional undercooling of the melt. Planar to cellular morphology transition endorse higher rate of solute rejection whereas highest rate of solute rejection is endorsed by transformation to a dendritic morphology. That is why constitutional undercooling plays a vital role in the determination of the eventual solidified microstructure. Figure 2.9 shows the transformation in the morphology of solid- liquid interface [22].

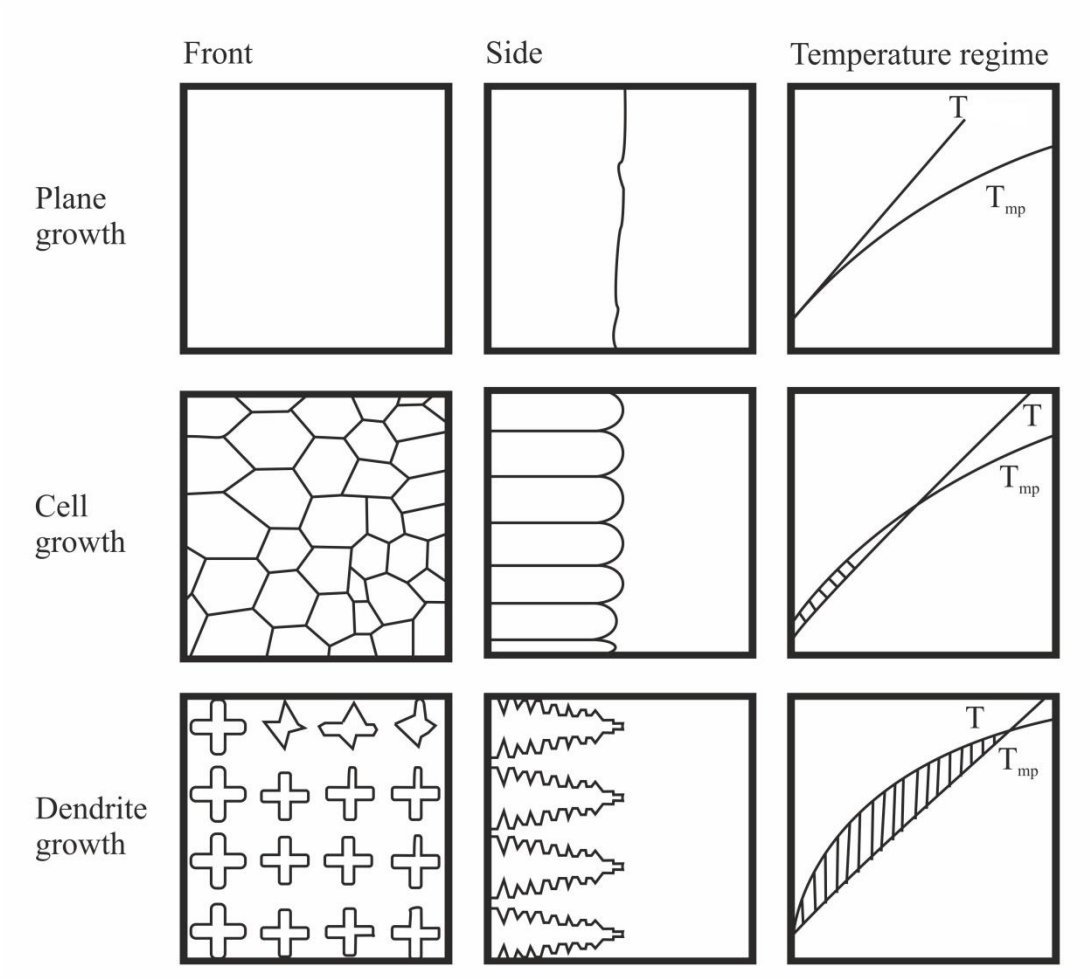

Figure 2.9 The transition of growth morphology from planar, to cellular, to dendritic [22].

Magnesium castings having HCP structure are produced in non- equilibrium conditions and has a dendritic microstructure with six- fold symmetry. The morphology of the growing solid does not only get affected by the constitutional undercooling of the melt but it also affects the nucleation event sites. New crystals nucleate and begin to grow in the undercooled region as constitutional undercooling reaches ΔT_n. These crystals further grow leading further constitutional undercooling around them. This process continues and the rapid closely packed crystals restrict the further crystal growth resulting in fine grained crystal. Easton et al. [23] schematically illustrated this phenomenon in a diagram which is reproduced below in Fig.2.10.

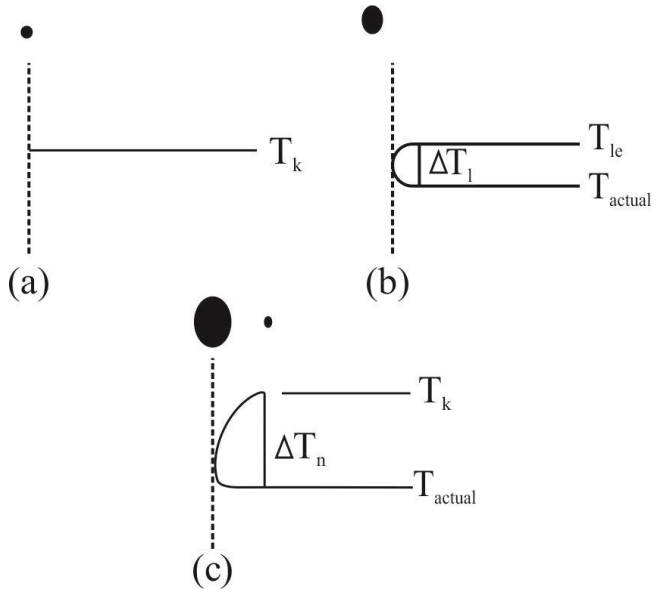

Figure 2.10 (a) through (c) shows the development of the constitutionally undercooled area in front of the growing interface so that further nucleation events can occur. In (b) a constitutionally undercooled area exists but is not sufficient to activate further nucleation. In (c) undercooling reaches T_n the sufficient level for nucleation to occur. T_{le} is the equilibrium liquidus temperature of the alloy. The dark circle represent growing solid crystals [23].

2.4 Solidification of Magnesium Alloys

During solidification, alloying elements, grain refiners, cooling rates and vibrations affect the solidification behavior of magnesium alloys. Both the aluminum content and cooling rate are responsible for the growth morphologies of primary dendrites and the eutectic. α-Mg starts to form during primeval stage of solidification in all the magnesium alloys. Occasionally addition of grain refiners control the primary phase of nucleation. The production of commercial magnesium products by High Pressure Die Casting (HPDC) has a very high cooling rate, resulting in high driving force for nucleation. Thus, increasing the nucleation and production of numerous primary grains, that reduces the need for effective grain refiners. The eutectic constituents in most commercial Mg- Al alloys can be observed even at the low Al content i.e. as low as 2 wt.%. The eutectic solidification plays a vital role in alloy development which controls the size, shape and distribution of more brittle γ- $Mg_{17}Al_{12}$ phase in the final microstructure that sequentially influences both the ductility and creep strength of the alloy. Moreover, when feeding is

interdendritic and large pressure differentials are required to draw liquidus through the dendritic network, eutectic growth, being the final state of solidification process affects the feedability at a critical stage [10].

As it has been found that depending upon the composition and cooling rates in hypoeutectic magnesium alloys, eutectic shows a wide range of morphologies. The regular lamellar or fibrous eutectic morphologies form in alloys with Al content tending towards the eutectic composition (33 wt.% Al). But in aluminum content less than 10 wt.%, a fully or partially divorced eutectic appears [24]. Figure 2.11 shows the different morphologies of the [α-Mg + γ- $Mg_{17}Al_{12}$] eutectic.

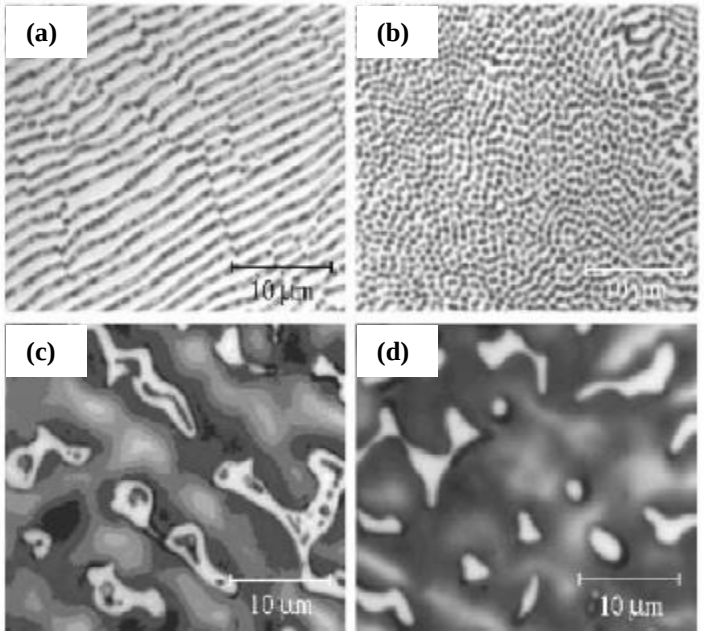

Figure 2.11 (a) lamellar (b) fibrous (c) partially divorced (d) fully divorced morphologies in Mg- Al alloys of various compositions [25].

Cooling rate decides the morphologies of an alloy i.e. when the cooling rate is extremely high (600 ˚C/min), fully divorced morphologies usually appear whereas lower cooling rates exhibit partially divorced morphology [10]. In the fully divorced there is a complete separation between two eutectic phases. Eutectic α-Mg (high Al content) that has grown from the primary dendrites surrounds every dendritic region having single β- $Mg_{17}Al_{12}$ particle (Fig. 2.11 d). The partially divorced eutectic has islands of α-Mg within β- $Mg_{17}Al_{12}$ phase, but the greater part of α-Mg is still on the outer side of $Mg_{17}Al_{12}$ particle

[24]. It has been found that after solidification via discontinuous precipitation from α-Mg supersaturated solid solution, the lamellar γ- $Mg_{17}Al_{12}$ structure is formed. At higher solidification rates in magnesium casting, aforesaid lamellar structure do not emerge, which is sustained by the aforementioned substantiality that at higher cooling rate tendency to form divorced eutectic structure gets embellished whereas on the other hand, lower cooling rates exhibit partially divorced morphology. There is also a less pronounced interrelationship between grain size and the cooling rate i.e., on increasing the cooling rate, grain size decreases. It has already been discussed the grain size may be affected by the addition of grain refiners. Thermodynamic modelling noticed that in the interdendritic regions alloys solidified as primary α-Mg dendrites with eutectic as well as intermetallic phases. It has also been seen that the eutectic containing α-Mg and γ- $Mg_{17}Al_{12}$ is present as divorced eutectic microstructure.

2.5 Techniques of Grain Refinement

Current processes for grain refinement during solidification of Mg- Al alloys to enhance the microstructure and mechanical properties include physical methods (vibrations), chemical methods (melt addition) and thermal methods (heating and chilling).

2.5.1 Grain refinement of Mg- Al alloys through physical methods (vibrations)

Vibration involves the oscillatory kinetics of physical systems, that may be harmonic, periodic or a general kinetics where the amplitude varies with time. For instance, vibration of turbine blades, chatter vibration of machine tools, electrical oscillations, sound waves, vibrations of engines, torsional vibration of crankshafts and vibration of automobiles. Vibrations are experienced in many mechanical and structural applications, such as, machines, building, bridges, vehicles, and aircrafts. Also too much vibration creates high stress levels resulting into mechanical failure [26].

(i) Ultrasonic vibrations

Ultrasonic vibration generators are of two types. One is the magnestostrictive vibrator and the other is a piezo- electric vibration generator. The magnestostrictive vibrator employs a ferromagnetic material that undergoes elastic expansion and contraction under the

influence of an alternating magnetic field. Generally this basic principle permits generation of vibration frequencies upto 100 kHz. The effective heat dissipation problem imposes a limit on still higher attainable frequencies. Amplitude of vibration is considerably small in these vibration generators.

The piezo- electric vibration generators contain crystals of quartz or Rochelle salt. These crystals undergo changes in physical dimensions when subjected to electric field along with certain crystallographic directions. Vibrational frequencies up to 200 kHz or more are possible in piezo- electric vibrations.

Likewise other alloys, AZ91 alloy has tendency of microporosity, a solidification defect which could be overcome by refining the microstructures according to various researchers. Socolov [27] was the first to report on UST in 1936 on molten zinc, tin and aluminum. Campbell [28]**,** Eskin [27] and Abramov [29] gave the detailed critique on ultrasonic vibration. At particular sonification intensities acoustic cavitation and streaming in UST refined the cast microstructure, withdrawal of gasses and oxides from the melt. During UST, formation of cavity occurs if the local pressure in the melt during half period of expansion during random compression- expansion (tension) cycles becomes less than its vapour pressure.

In AZ91 magnesium alloy, the effect of ultrasonic power results into the formation of fine non- dendritic grains. UST could lead to refinement only in the presence of enough solute elements. According to Ramirez et al. [30] and Qian et al. [31], the enhancement of the nucleation and activating potential nucleation sites developed the initial crystallites was the primary role of UST in magnesium alloys. Mostly all the researchers who have worked on UST on magnesium alloys have only mentioned the influence of UST on the morphology of α- Mg and very trivial reports have been mentioned on the influence of UST on intermetallic phases like Mg_2 Si, MnFeAl(Si) and Mg_{17} Al_{12}. Effects of ultrasonic treatment on microstructures of AZ91 alloy was examined by Yang et al. [32]. Wang et al. [33] applied UST in AZ91D magnesium alloy to acquire metal matrix nano-composites. Khosro et al. [34] studied the UST on microstructure and tensile strength of AZ91 magnesium alloy at different power levels for 5 min with frequency of about 20kHz and maximum power of 600W**.** Gao et al. [35] applied ultrasonic power in AZ91

alloy from 0 to 700W during solidification process of AZ91 alloy and found that at high intensity ultrasonic vibration gradually decrease grain size and improve mechanical properties with increasing ultrasonic power. Figure 2.12 Microstructure of AZ91 alloy treated by different ultrasonic powers. Nie et al. [36] examined the effect of ultrasonic vibration and solution heat treatment on microstructure and tensile properties of AZ91 alloy with frequency 20kHz and power 350W. Ultrasonic vibration significantly improved the ultimate tensile strength and elongation to fracture of the alloy.

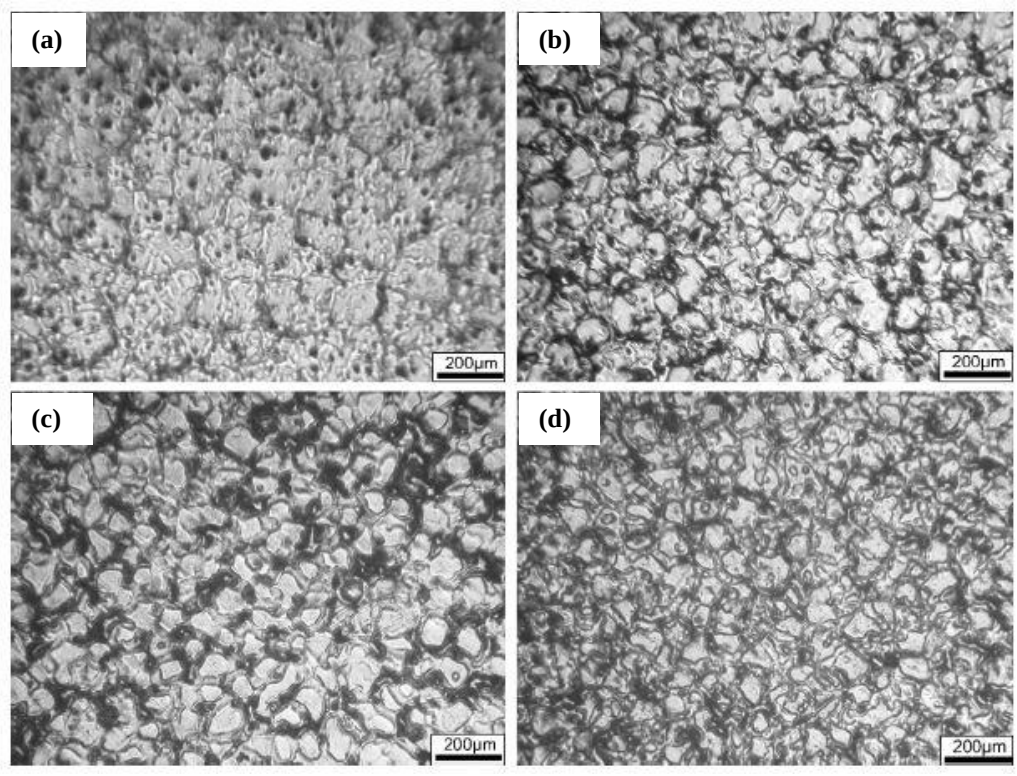

Figure 2.12 Microstructure of AZ91 alloy treated by different ultrasonic powers (a) 0W, (b) 300W, (c) 500W, and (d) 700W [35].

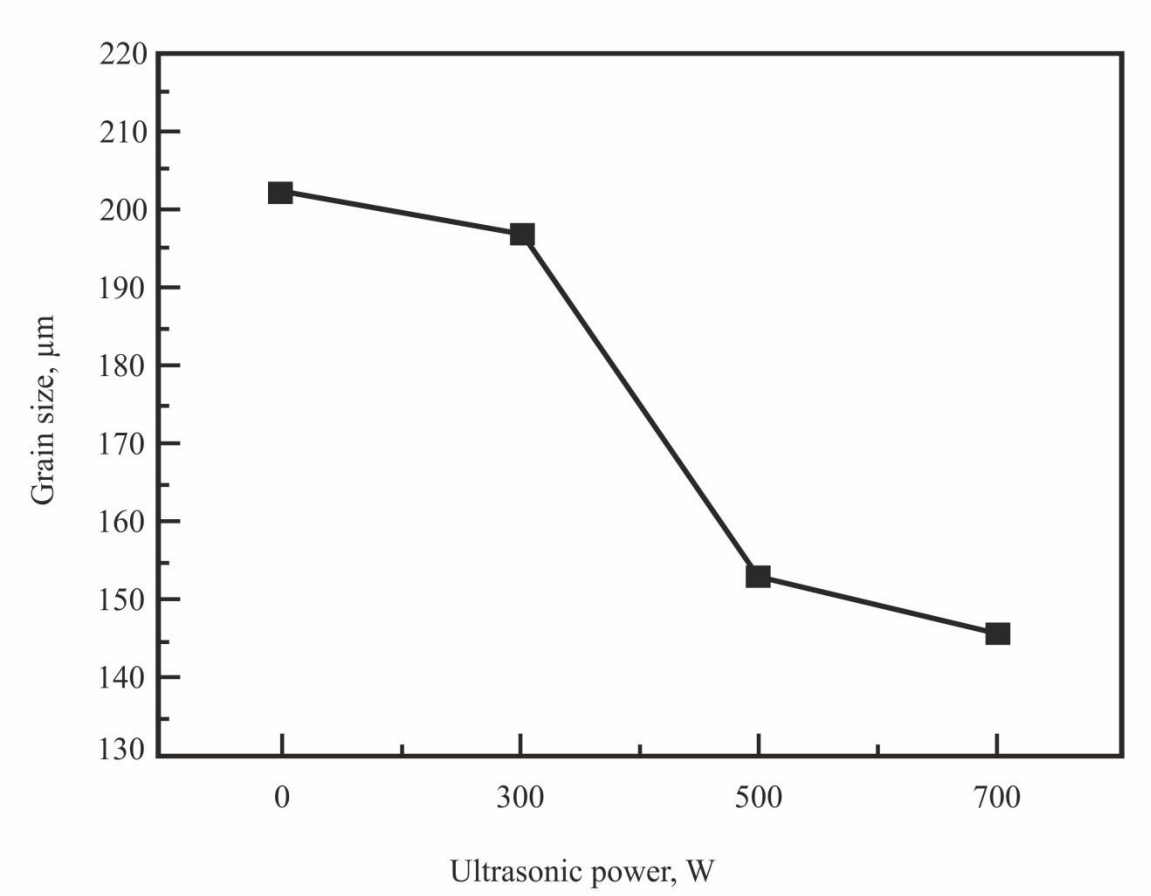

Figure 2.13 Grain size of AZ91 alloy as a function of ultrasonic power [35].

The mechanism of UST involves cavitation phenomenon which in melt develops localized high pressure points on the temporary basis. In many alloys melting point of the alloys increase with the local pressure according to Clausius- Clapeyron, whenever applied consciously in the melt might depict large undercooling resulting into intensified nucleation. By increasing the heterogeneous nucleation, cavitation clear the surface of the particles poorly wetted by the melt. During the half period of compression, the breakdown of bubbles is accompanied by propagation of large pressure pulses (100- 1000 MPa). These pulses result in the breakdown of large dendritic grains. From the surface of the bubbles, the vaporization of the melt occurs when there is deterioration of local pressure in the developed bubbles during half period of expansion. As vaporization is an endothermic process, reducing the surface temperature of the bubbles thereby assisting the nucleation of the solid particles on the surfaces. Soon these particles scattered in the melt as the bubbles in the melt broke

down. At high ultrasonic intensity in the melt, the process of streaming results in the evolution of mechanical pressure fragmenting the dendrite arms. During half period of compression, due to raise in local temperature of the melt roots of the dendrite arms separate from the mother dendrite. Further these assorted particles grow contouring new grains [35].

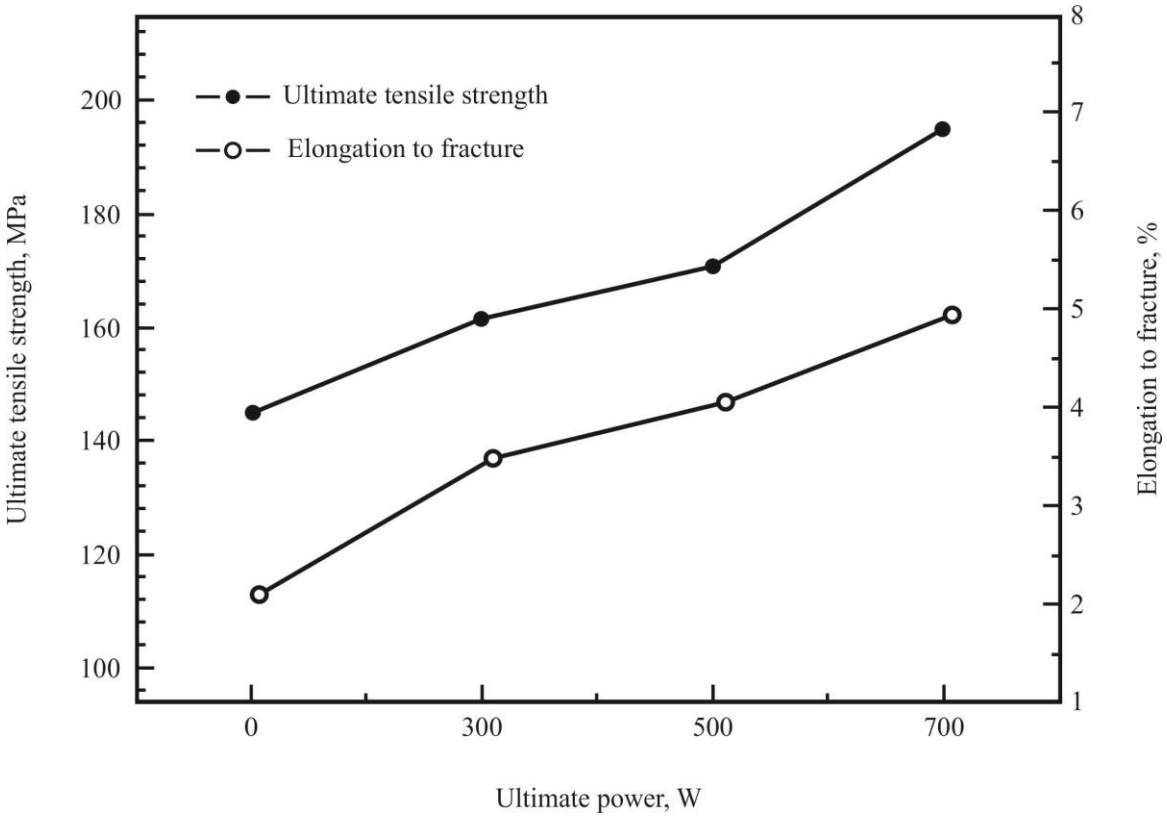

Figure 2.14 Mechanical properties of AZ91 alloy as function of ultrasonic power [35].

(ii) Electromagnetic vibrations

For medium frequency applications the electromagnetic vibrator is preferred. In this vibrator, the magnetic field of a solenoid is directed to the center of a beam fixed at both ends, which exerts a bending load on the beam. This load is proportional to the ampere- turns and demagnetization factor to the magnetic circuit. If the magnetic field is caused to fluctuate as when an alternating current is applied to the solenoid, the beam can be set into flexural vibrations. By adjusting the frequency of electromagnetic field, the amplitude of flexural vibration can be maximized. This

relatively simple arrangement can produce vibration frequencies up to 1200 Hz when used in conjunction with a frequency oscillator. This type of vibrator cannot develop large thrust. Therefore, it is used to vibrate objects of relatively low mass only.

The latest design that has gained popularity is the electrodynamic vibrator. It employs a steady magnetic field induced into an iron body having an air gap. The moving platform consists of a drive coil through which an alternating current is passed. The platform coil assembly is suspended in the air gap. It oscillates due to the alternating force produced by the coil. This type of vibration generator has the greatest accuracy and flexibility of control together with a wide frequency range and lower distortion than any other type.

During EMV processing the mechanism interpreted in the last two decades was cavitation [2]**.** In cavitation the shock pressure is yielded resulting into the fragmentation of growing dendrites that provide an artificial source of effective nuclei for grain multiplication. A new technical term proposed by Miwa and co- workers [3, 38- 40] "micro- explosion" was considered to be the cause for grain refinement of various metals and alloys. The above process is based on the proposal that during vibration the gaseous bubble may be produced around the primary solid. Substantial shock wave can be yielded by the breakup of the bubble resulting into the segmentation of the solid into fine pieces, thus refining the microstructure. This mechanism may be viable for grain refinement. The occurrence of cavitation only at a very narrow frequency interval has not been well interpreted theoretically. For example, for the AZ91D alloy it is around 900 Hz [2]. Cavitation becomes less effective on considering the frequencies at too low or too high region. Taken this problem of cavitation model into account, a new mechanism was projected on referring the considerable difference of electrical resistivity between the solid and the liquid in mushy zone, plausibly explaining the effect vibration frequency on the microstructure formation.

Segmentation of some of the growing crystals occurs into fine pieces. This results into the limited number of grain nuclei and bare suspension of these in the melt. In front of the growing interface, the solute diffusion boundary can be established to form a

constitutionally undercooled region, on the growth of the grain nucleus. Until all liquid get crystallized to form a dendrite, interface can be readily destabilized. On increasing driving force the fluid flow may become comparatively severe to break down more dendrites to form more grains. This condition brings the formation of basic dendritic skeleton. Nevertheless, as grain nuclei increases, direct contact of neighboring crystals make further development of each immature dendritic structure more difficult. This results into the formation of more rosette dendrites and less coarse dendrites.

(iii) Mechanical vibrations

This method is carried out by setting the vibrations into entire mold by means of a vibration source. It is the most encouraging process of applying vibrations to solidifying melts owing to its simplicity and ruggedness of the equipment needed. It allows limited degree of freedom to the operator. The amount of fragmentation increases with the amplitude of vibration. Kocatepe [37] also reported that vibrations increases diffusivity of silicon in the liquid resulting in coarsening of the eutectic silicon. The observed grain refinement was mainly due to the fragmentation of dendrites and the growing crystallites. Abu Dheir et al. [38] used electromagnetic shaker in the permanent mold to induce mechanical vibrations. The vibrations were imposed in the mold at frequencies ranging from 100 Hz to 2 kHz and amplitudes ranging from 18 μm to 199 μm. They observed that vibration homogenizes the temperature distribution in the mold and encourages faster cooling. Abu Dheir et al. [39] observed fragmentation of the dendritic structure in Al-12.5Si alloy. They noticed that amount of fragmentation increased with the increase in amplitude of vibration. Olufemi and Ademola [40] investigated the effect of mechanical mould vibration during melt solidification on the mechanical properties of an AZ91 magnesium alloy. This was tested in the frequency range from 0 to 24 Hz and at two vibration intensities; 5V-peak to peak and 10V-peak to peak. Mechanical tests such as tensile test, hardness test and impact test were carried out on the samples. Improvements were observed in the mechanical tests within the frequency threshold

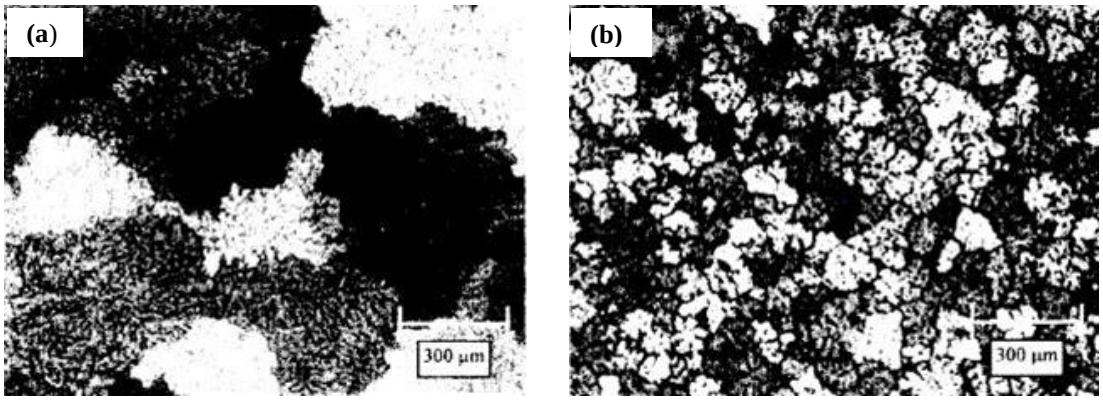

Figure 2.15 Typical microstructures of as cast (a) unvibrated and (b) vibrated AZ91D [41].

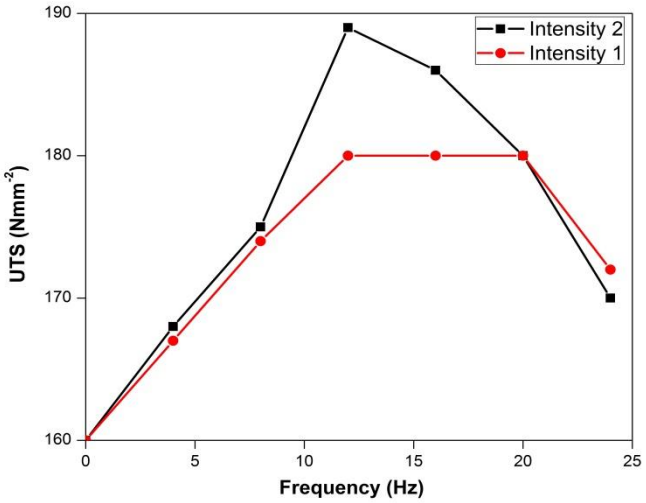

Figure 2.16 Relation between the frequency of vibration and ultimate tensile strength of the samples [40].

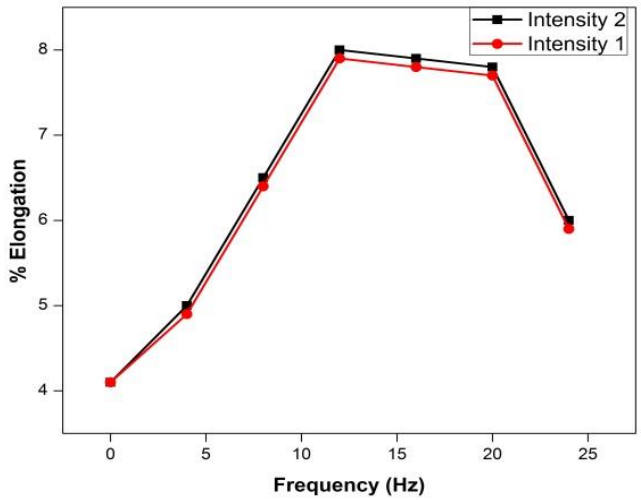

Figure 2.17 Effects of frequency of vibration on the percentage elongation of the samples [40].

of 12 and 16 Hz. It was concluded that increased frequency of mould vibration during solidification causes refinement of the grain in the alloy. This refinement of the grains results in an increased ductility, percentage elongation, UTS, impact strength and hardness of the said alloy samples. Increase in vibration intensities results in higher maximum values of these mechanical properties. The mechanical mold vibrations increasingly improve the mechanical properties of the alloy, with the optimum mechanical properties occurring at a frequency of 12Hz. A moderate application of this optimum frequency of mold vibration during alloy solidification in foundry will improve workability of the alloy for all applications involving plastic deformation of the cast alloy without necessarily subjecting it to annealing.

It had been investigated during the solidification of metals and alloys by mechanical vibrations of both sonic and ultrasonic character that the macrostructures and microstructures obtained get conventionally modified. The suppression of undesirable dendritic and columnar zones and the development of the fine grained equiaxed structure is the most observed effect [41]. The three effects propagated by ultrasonic waves are grain refinement, dispersive effects and degassing resulting in reduced porosity. It has also been found that vibrations of mechanical origin are effective in increasing the ability of mold filling. There are two more concepts related to mechanism which will clear the doubts: cavitation and fluid flow.

It is well known that when the molten metal is poured into the mold, the solidification process occurs firstly in the low temperature region near the mold wall. Then the solidified region make wider towards the center. But if mechanical vibration (MV) is applied in solidification process, the situation will be changed. Heat flow is disturbed and the disturbance affects heat and mass transport during crystal growth from the molten steel. It alters the status of the structural and energy fluctuations in the melt and makes crystal nucleating easier. Meanwhile the disturbance of MV breaks off dendrites, which decreases the size of constitutional supercooling zone and suppresses growth of dendrite. The broken dendrites grow into equiaxed grains, and the amount of equiaxed grains increases.

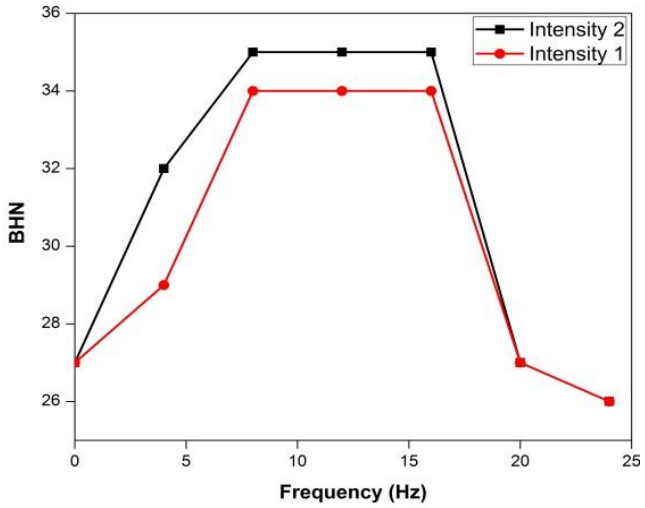

Figure 2.18 Effects of frequency of vibration on the hardness of the samples [45].

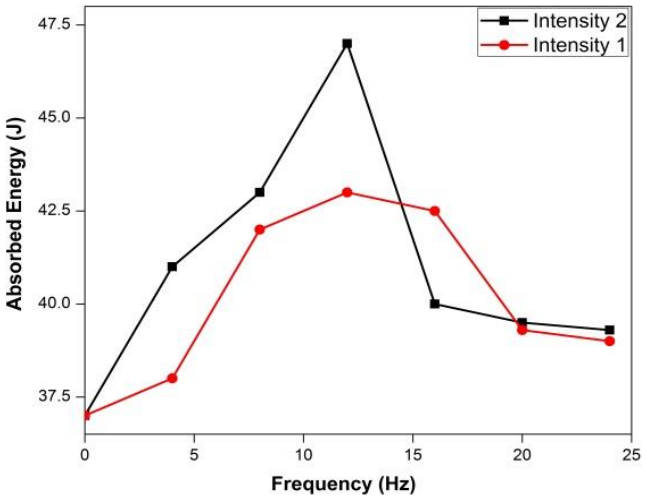

Figure 2.19 Effects of frequency of vibration on the impact strength of the samples [45].

Based on the analysis, it can be concluded that if the MV is applied at the beginning of the solidification process, the nucleation would occur in the whole molten metal or in a larger region. It will make the growth of grains proceed in the mold wall and in the internal region simultaneously. During the solidification, dendrites can be broken up before they grow into the large dendrites. Those effects can break off the dendrites growing from mold wall towards to center. Therefore, the growth of the dendrites is restrained and the microstructure of alloy treated by MV is refined [42].

Effect of vibration on metallographic structure

The influence of vibration on solidifying melts can be affected by several parameters. These include the amplitude of vibration, the amount of superheat of the metal when poured, the temperature of the mold, the rate of cooling in the mold and the presence of grain refiners or inoculants in the melt. It has been reported [43] that vibration influences the cast structure only when it is applied during the solidification process.

Increased frequency of mold vibration during solidification causes refinement of grains in the alloy [40]. Maltais et al. [44] concluded that grain refinement enhanced in cast plates by vibrations is comparable to that produced by carbonaceous compounds. Grain refinement can be explained by surface waves during filling as well as enhanced dendrites detachment from the mold wall due to vibrations. Guo et al. [45] accomplished that mechanical vibration causes vigorous melt convection and rapid cooling due to the melting of the vibrating horn. When the vibrations were imposed in molten AZ31 billets from 646.85 °C to 629.85 °C the coarse dendritic microstructure transformed into fine, uniform and non- dendritic microstructure on increasing vibration acceleration from 2.5 to 19 m/s^2. Fine and globular primary α-Mg could form in the initial stage of solidification. It was found that free space area for vibrating the melt affects the microstructure refinement. The effect of mechanical vibrations on the microstructure weakens when the melt cannot vibrate freely. The primary crystal particles become rosette- like and fine when the mechanical vibrations are applied to the melt from about 649.85 °C and 614.85 °C. Thus, it was found that the mechanical vibrations promote heterogeneous nucleation just under the liquidus temperature [46]**.** It was found that the velocity of vibrations is important factor for primary crystal refinement. The mechanical vibrations with high velocity regardless of frequency can refine the primary crystals [47]**.** The vibrations with high velocity increase the cooling rate and decrease the supercooling by strong vibration stirring [48]**.** On the other hand, the microstructure refinement by mechanical vibrations with high acceleration or amplitude is affected by the mechanical frequency. The square of the velocity corresponds to the energy of mechanical vibrations. Thus, the energy of mechanical vibrations promotes microstructure refinement during solidification [47].

Naoki et al. [49] found that the grain size in the inner area of columnar rod tends to decrease by the imposition of the mechanical vibration in AC4C aluminum alloys. Furthermore, the inner casting defects reduce and become smaller. The cooling rate of melt increases by imposition of the mechanical vibration and increases with the increase of the vibration frequency. The dendritic arm spacing of the outer region of specimens decreased by the mechanical vibrations and decreases with the increase of the vibration frequency [50]**.**

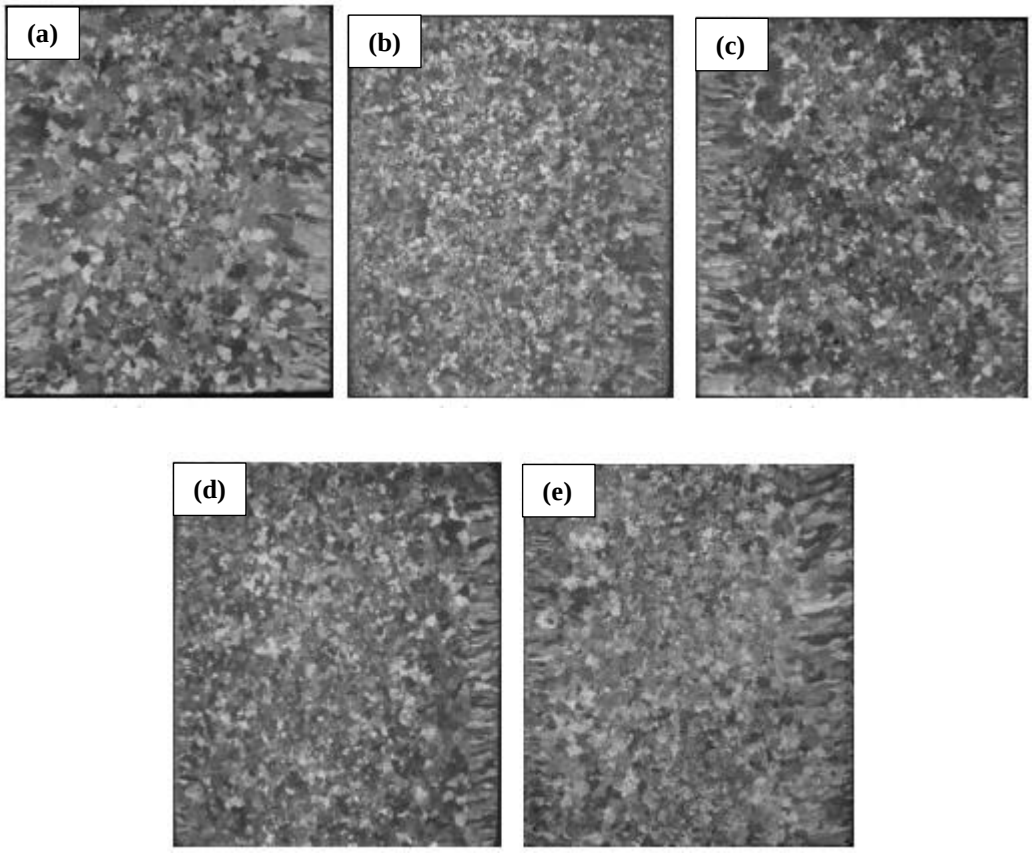

Figure 2.20 Macrostructures of specimens cast under different vibration frequencies of (a) 0 Hz, (b) 112 Hz, (c) 132 Hz, (d) 148Hz and (e) 157 Hz [51].

Zhao et al. [52] concluded that in hypoeutectic Al- Si alloy, the intense convection can be caused in melt by vibration, which is generated from the free surface of the bulk melt and spreads downwards, consequently leading to the convection in the bulk. Non- dendritic primary α-Al crystals become finer and rounder with the increase of vibration. In A356 alloy it was seen that size of primary solid phase decreased and their morphology increased with increasing vibration frequency and also with

increasing vibration time. Shape factor of primary solid phase increased with increasing vibration times at all frequencies [53].

Ultrasonic vibrations when applied during solidification of alloy cause considerable grain refinement of the as cast structure [43]. Yang et al. [32] observed the effect of ultrasonic treatment on microstructures of AZ91 alloy. It was seen that phase composition does not get affected by the ultrasonic treatment but has impact on the microstructures. The percentage area of the lamellar eutectic phase first increased to the maximum on increasing the ultrasonic power and then decreased on further increasing the ultrasonic power. The effect of ultrasonic treatment during solidification of AZ91 alloy at various power was studied by Gao et al. [35]. It was found that the dendrites were coarse and large in the AZ91 alloy without being subjected to vibrations. But on the imposition of the vibration to the alloy the grains obtained were globular. Nie et al. [36] in his study found that the morphology of $Mg_{17}Al_{12}$ in AZ91 alloy changed from coarse to lamellar. Osawa et al. [54] reported that with ultrasonic vibration the microstructure of the AZ91 alloy obtained was fine and uniform. Khosro et al. [34] in his study found that ultrasonic treatment had a substantial effect on the size and shape of α- Mg dendrites as well as on the size, shape and distribution of β- $Mg_{17}Al_{12}$ phases in the AZ91 alloy.

Mizutani et al. [55] studied the effect of electromagnetic vibration frequency in the range of 150- 500 Hz. It was observed that on increasing the vibration frequency, the grains became small. But on increasing the frequency more than 1 kHz, the effect of refinement became weak and similar to the non-vibrated alloy. Refined area surprisingly extends as the longitudinal temperature gradient become gradual in the specimen. It could be believed that refinement through electromagnetic vibration is substantially influenced by the temperature gradient. Mingjun et al. [2] found finer and equiaxed grains on imposing the electromagnetic vibration during solidification of AZ91D alloy. Guo et al. [56] observed the effects of electromagnetic vibrations on macrosegregation in AZ80 Mg alloy billets. It was found that intensity of electromagnetic vibrations results in uniform distribution of metallic elements in the billet. Mizutani et al. [57] studied the effect of electromagnetic vibration intensity on

microstructural refinement of Al-7wt% Si alloy. During solidification the imposition of electromagnetic vibration refines the primary α- dendrite particles. Coarse dendrite particles decreased and primary α- dendrite attain globular shape as the vibration intensity increased. Collapse of dendrite arms due to micro- explosion and stirring of the melt is probably responsible for the refinement of primary α- dendrites. No single theory is exclusively capable of explaining the various aspects of modification in grain structure.

Tian et al. [58] studied the effect of vibration on microstructure of AZ91 Mg alloy via lost foam casting (LFC). They also analyzed the mechanism for the microstructure refinement of the cast alloy. It was also found that in AZ91 Mg alloy finer dendrites can be produced by mechanical vibration. It was revealed that the microstructure of AZ91 Mg alloy via LFC mainly consists of α- Mg and β- $Mg_{17}Al_{12}$ along with a new phase $Al_{13}Mn_{12}$ which is quite different from the $Al_{32}Mn_{25}$ in the untreated alloy via LFC. Tamura et al. [59] investigated the factors responsible for refinement of mechanical vibrations on microstructure of Al- 7mass% Si alloys. Frequency, amplitude, velocity and accelerations are the factors considered in mechanical vibrations. 20 experiments were performed by varying the amplitude, velocity, acceleration and frequency. The value of acceleration and velocity were illustrated by 0 to peak value and amplitude by peak to peak value. The effect of velocity of vibrations on cooling rate and effect of imposition temperature region on microstructure were seen. It was concluded that for refinement of primary crystals velocity of mechanical vibrations relating to the vibration energy is important factor. High velocity vibrations increase the cooling rate and decrease the supercooling. Furthermore, refinement of primary crystals by mechanical vibrations was found at temperature just below the liquidus temperature. Taghavi [60] studied the effect of prolonged mechanical vibration on the grain refinement of α- Al primary solid phase and density of A356 aluminum alloy. Melting of 1.5 kg of an alloy was done in an electrical resistance furnace, in silicon carbide crucible. As soon as the temperature of the melt reached 700 ˚C, vibration was imposed to the molten metal and poured into the preheated mold. To examine and control the temperature of the molten metal, thermocouple was inserted. To avoid the cooling or solidification of the melt surface,

covering was done with asbestos. A combined effect of vibration during solidification and isothermal vibration of semisolid alloy was also studied. Firstly vibration was imposed at a cooling rate of 0.33˚C/s. As soon as the temperature of the melt reaches 600˚C, at the same frequency vibration continued isothermally at second stage. It was seen that grain refinement and density of A356 Al alloy can be increased by imposing mechanical vibration but there was a reduction in the size of α- Al phase on increasing the vibration time up to 15 min for all frequencies and on increasing the vibration frequency up to 50 Hz for all the vibration time. Maximum achieved density and grain refinement was at 50 Hz and 15 min. At this condition grain refinement was 53% and density improved from 2.40 g/cm^3 to 2.66 g/cm^3.

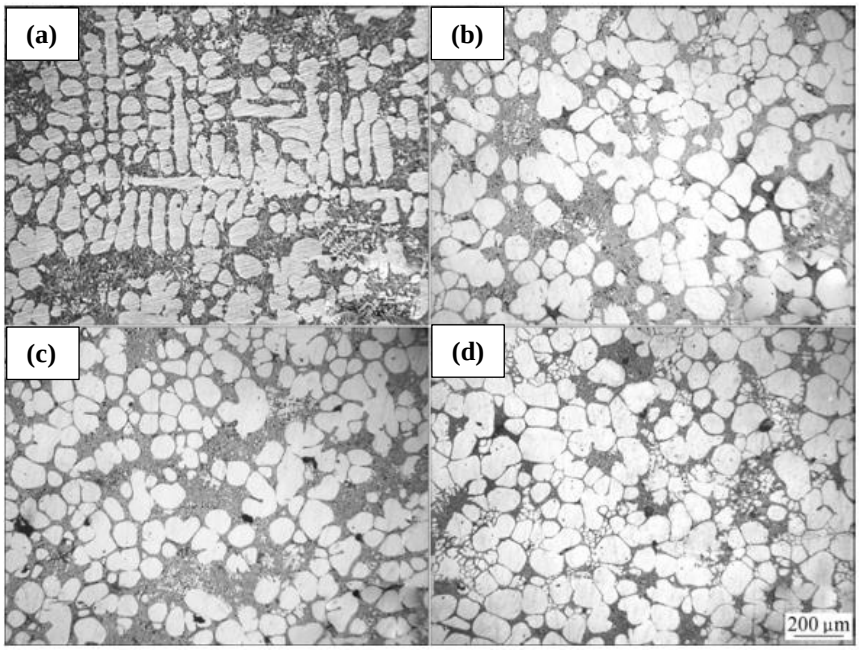

Figure 2.21 Microstructures of semisolid 356 slurry processed by different frequency vibration: (a) 0 Hz; (b) 12 Hz; (c) 20 Hz; (d) 35 Hz [52].

Zhao et al. [61] observed the influence of mechanical vibration on the size and morphology of α- Al dendrites. Mechanical vibration with different peak acceleration is perfectly applied to the solidification of LFC 356 alloy. Without mechanical vibration, the coarse primary α-Al dendrites are presented in the alloy, demonstrating a normal dendrite growth mode. However, if solidification is carried out with

vibration, the grains will be refined gradually as the peak acceleration increases. When the peak acceleration is between 1 and 4 g, the primary α-Al grains are refined significantly, secondary dendrite arms are broken, the average grain size is reduced.

2.5.2 Grain refinement of Mg- Al alloys through chemical methods

Various grain refiners are added in Mg alloys such as carbon addition, elfinal process, manganese addition, titanium addition, vanadium addition and zinc oxide.

(i) Carbon addition

To reduce the grain size of Mg- Al alloys one of the most common and efficacious process is carbon addition. According to Moetgi [62] carbon is added in the form of chlorides powder such as hexachloroethane (C_2Cl_6) and carbon tetrachloride (CCl_4). Karlsen et al. [63] added carbon in the form of wax CaF_2, wax CaF_2-C, C_2Cl_6 and C into AZ91. Some of the authors like Xue et al. [64] and Lue et al. [65] added 0.5 wt.% Al_4C_3 directly to pure magnesium and Mg- 3Al respectively. The usual mechanism showed the formation of Al_4C_3 particles on the interaction of carbon with aluminum in the melt. Jin et al. [66] proposed that there was no manifestation for Al_4C_3 particles as nucleating sites. Rather, grain refinement occurs due to rejection of carbon at solid- liquid interface causing constitutional undercooling. If grain refinement occurred because of segregation of carbon, then it would have occurred in Al- free magnesium alloys too. Most of the researchers affirm the estimation of heterogeneous nucleation across Al_4C_3 particles as the approach for grain refinement. Han et al. [70, 71] formulated an Al- C master alloy for the refinement of AZ31 and intended duplex nucleation with Al_4C_3 coated Al- Mn particles. Pan et al. [67] used Al- 1.5C master alloy to refine AZ63 B and detected Al_4C_3 nucleating particles.

(ii) Elfinal process

The Elfinal process postulates the accession of ferric chloride ($FeCl_3$) into the melt of magnesium alloy, resulting in the formation of intermetallics of Al- Fe or Al-Mn-Fe in the melt exemplifying the nucleation sites for primary Mg. It was also discovered by John

et al. [68] that Al and Fe- rich intermetallics assist the nucleation of grains merely got the presence of Zr and Be that would impede the procedure since these factors can remove iron. Nevertheless, toxicity and the traumatic ejection of chlorine and hydrochloric acid are the major pertaining factors for the accession of $FeCl_3$. Moreover, corrosion resistance of an already corrosion- prone metal could be dropped- off by adding Fe into Mg.

(iii) Manganese addition

By using several Al levels Cao et al. [69] examined the efficiency of Mn grain refinement and determined that on increasing the Al content, grain refinement efficiency with Mn enhances. Elsayed et al. [70] studied the effect of addition of Mn on Mn- 25Al master alloy and noticed the reduction of average grin size of AZ91D from 215 μm to 174μm and related the mechanism with Elfinal process. Du et al. [71] suggested another mechanism concerning the nucleation of grains by adding Mn, pointing the formation of film of Al_4C_3 acting as nuclei for Mg grains all around Al- Mn intermetallic compounds. It was concluded that on adding Mn, this coating mechanism explicated the efficiency of grain refinement.

(iv) Titanium addition

In Al alloys, the application of Al- 5Ti- 1B is very popular but it is not so noticeable in case of Mg alloys. The formation of TiB_2 particles is the cause of grain refinement in Ti- B based refiners. Currently, within Mg melts, researchers have explored on the viability of the addition of master alloys forming TiB_2 particles, which are mainly Al- Ti- B based. According to Wang et al. [72] use of 0.3wt% Al- 4Ti- 5B in AZ31 alloy prospered the refinement of grains. Moreover, heterogeneous nucleation had been shown by TiB_2 particles in energy dispersive X- ray (EDX). Wang et al. [73] also used Al- TiB_2 master alloy. The addition of 7.5 wt.% TiB_2 particles formed metal- matrix composites AZ91/TiB_2. On subsequent solidification, TiB_2 particles solidified at the last with eutectic $Mg_{17}Al_{12}$. Moreover, at the center of Mg grains, very less TiB_2 particles were observed. Therefore, it was concluded that AZ91 is refined by TiB_2 mainly via growth restriction. That is why; the grain refinement mechanism of TiB_2 is a combination of heterogeneous

nucleation and growth restriction not exclusively heterogeneous nucleation or growth restriction.

(v) Vanadium addition

Buha [74] noticed that vanadium addition in Mg- Zn alloys reduces its grain size. The interesting prospect regarding vanadium addition is that it has a BCC crystal structure although Mg has a HCP structure. It was found that instead of dissimilar crystal structures, heterogeneous nucleation occurred during solidification as vanadium (V) particles were the best nucleating sites. On adding 0.3wt% V for Mg- Zn alloys, the study of V has not been done. Therefore its research is justified, but its commercial usage is admonished as V is quite expensive element.

(vi) Zinc oxide addition

According to Fu et al. [7], zinc oxide (ZnO) is a latent grain refiner from th edge- to- edge crystallographic model. The crystal structure and lattice parameters of ZnO and Mg are alike as shown in Table 2.2. According to the given reaction,

$$Mg + ZnO \longrightarrow Zn + MgO \qquad \textbf{(2.8)}$$

ZnO is reduced to Zn on adding it to molten Mg. The researchers considered that Zn impart grain growth restriction whereas remaining ZnO offer/ render desirable sites for heterogeneous nucleation. The only weakness of ZnO addition is the formation of MgO, which can reduce the castability and mechanical properties if not withdrew. On the ground of its grain refinement efficiency in pure Mg and Mg- 3Zn, ZnO can be used for refining the grain size in AZ91 Mg- Al alloys [6].

Table 2.2 Lattice parameters of Mg and ZnO [6]

	Lattice parameters	
	a (˚A)	c (˚A)
Mg	3.209	5.211
ZnO	3.265	5.219

2.6 Effect of Vibration on Mechanical Properties

It has been seen that application of vibration produced invariably a fine grained structure, suppresses columnar growth and eliminates dendritic grain geometries. On the basis of these observations one would expect a corresponding increase in mechanical properties also. Macrostructural control is related to the overall thermal and constitutional environment and is thus closely allied to microsegregation leading especially to porosity and second phase distributions [43]. Olufemi et al. [40] studied the effect of mechanical vibration during solidification of AZ91 Mg alloy and found mechanical vibration improves the mechanical properties of the alloy and also improves the workability of the alloy for all applications including plastic deformation of the cast alloy without subjecting it to annealing. Mishra et al. [75] studied the effect of mechanical vibration on the mechanical properties of Al- Cu alloy. Graphite mold was used to prepare the castings. The results showed substantial and remarkable enhancement in the mechanical properties. Pillai [5] concluded that density and elongation of cast component could be improved through mechanical vibrations. Omura et al. [51] conducted mechanical vibration on AC4C Al alloy and found increment in the average density and reduction in the casting defect of the specimen due to which dispersion in mechanical properties reduced. Vibration performance of the vibrator for mechanical vibration casting is given in Table 2.3. The temperatures of the melt and mold at which vibrations were given were 759.85 °C and 299.85 °C. The vibrations were started before pouring and given for a period of 80s after pouring.

Table 2.3 Vibration parameters for mechanical vibration casting [81]

Air pressure (MPa)	0	0.2	0.3	0.4	0.47
Centrifugal force (kN)	0	0.7	0.97	1.23	1.37
Frequency (Hz)	0	112	132	148	157

The tests that were carried out after mechanical vibration were density measurement and macrostructure observation, X- ray computer tomography (CT) analysis and tensile test. It

was concluded that on imposing the mechanical vibration the grain size in the inner area of columnar rod decreases. Also there is a reduction of inner casting defects resulting in the scattering of the mechanical properties of the cast alloys after vibration decrease unusually and slight increase in elongation.

Zhao et al. [42] studied that imposition of mechanical vibration on the cast hot working die steel during solidification process could reduce the casting defects like shrinkage, inclusion, porosity. Tian et al. [58] studied the effect of vibration on mechanical properties of AZ91 Mg alloy via lost foam casting (LFC). These researchers also stated that the mechanical properties of AZ91 Mg alloy can be strongly improved by mechanical vibration. It was found that the tensile strength of the vibrated AZ91 Mg alloy was increased by 27% when compared to unvibrated alloy. It was predicted that on increasing the vibration force strength of AZ91 alloy decreased by virtue of the presence of the microporosity. In mechanical vibrations finer dendrites get produced on amplifying the cooling degree, by shear stress dendrites broke down into pieces and melting of secondary dendrite arm took place.

Kocatepe [76] in effect of low frequency vibration on porosity of LM25 and LM26 alloys investigated the effect on porosity of unmodified and metallic sodium modified LM25 (Al- 7.15%Si) and LM6 (Al- 12.3%Si) alloys. During solidification vibrations were given at different frequencies and amplitudes to both unmodified and metallic sodium modified alloys. The parameters are given in the Table 2.4. The conclusions that were made from the investigation are that in LM25 and LM26 pore volume can be reduced with nucleant 2 when grain refined. In unmodified LM25 and LM26 alloys on increasing the vibration intensity, the amount and size of pores decreased in comparison to modified LM25 and LM26 alloys with metallic sodium. In unmodified and modified LM25 and LM26 alloys large holes on the top of the ingot were seen on applying the vibrations at frequencies and amplitudes in the ranges from 31.7- 41.7Hz and 0.375- 0.5mm respectively. Long freezing range eutectic Al7Si0.3Mg (LM25/356) and narrow freezing range eutectic Al-Si alloys Al12Si (LM6/ 413) were studied. It was found that mechanical properties of the long freezing range Al7Si0.3Mg alloy solidified in a permanent mold without and with tilting has got meliorated by using simple, inexpensive technique. By hand tapping with

mold tilting of undegassed melt subjected to vibration exhibited properties analogous to degassed Al7Si0.3Mg alloy melt. The latter also assist in minimizing the turbulence experienced by an Al melt during pouring and mold filling and hence in the enhancement of the mechanical properties. Nevertheless, on comparing the undegassed melt, degassed melt has the potency of both mold tilting and hand tapping. In addition very marginal improvement was seen in the properties of narrow freezing $Al_{12}Si$ eutectic**.**

Table 2.4 Application of vibration at different frequencies and amplitudes to the unmodified and modified LM25 and LM6 alloys [82]

Frequency (Hz)	Amplitude (mm)	Angular frequency (Rad/s)	T, Period (s)
41.7	0.125 0.250 0.375 0.500	261.7	0.024
31.7	0.125 0.250 0.375 0.500	198.9	0.031
21.7	0.125 0.250 0.375 0.500	136.1	0.046
15.0	0.125 0.250 0.375 0.500	62.8	0.1

Chirita et al. [77] studied the influence of vibration on the solidification behavior and tensile properties of Al- 18 wt.%Si alloy. The chemical composition (wt.%) of the alloy is $18 \leq Si \leq 22$; Fe ≈ 0.75; $1.5 \leq Cu \leq 3.0$; Zn ≈ 0.2; Mg ≈ 0.1; Mn ≈0.3; Ni ≈ 0.5; Pb ≈ 0.1; Sn ≈ 0.05; Ti ≈ 0.2. The melting and pouring of the alloy was carried out at 800 ˚C and 130 ˚C respectively. The vibrations were imposed at constant amplitude of 0.5mm and varied frequencies 0, 8 and 24 Hz. After that the castings were given heat treatment with a temper for 8 h at 200 ˚C. It was determined that during solidification vibration affects the mechanical properties due to heat transfer related aspects. It also increases the rate of heat transfer in the liquid metal. Owing to

loss of contact vibration can considerably decrease the heat transfer in the metal- wall interface.

2.7 Wear study on magnesium alloy

Wrought magnesium alloys have extensively been used in the substitution of aluminum and steel parts. Cast magnesium alloys are not passing to congregate a large amount of the requirements [78]. In certain applications like automotive brakes, engines components etc. light weight alloys and composites are imposed to sliding motion. Therefore, sliding wear is an important consideration in material processing. Hiratsuka et al. [79] used pin-on- disc apparatus to study dry sliding wear of pure magnesium against an alumina counterface at a normal load of 9.8N, sliding velocity of 1.6 m/s and a total sliding distance of 2.5 x 103 m. Role of fiber friction volume was studied by Alahelisten [80] on the wear behavior of alumina fiber reinforced AZ91 magnesium alloy. On increasing the fiber content, wear resistance in two body abrasion increases but solid particle erosion resistance decreases. Veeresh et al. [81] made an attempt to consolidate some of the aspects of mechanical and wear behavior of Al-MMCs and the prediction of the Mechanical and Tribological properties of Aluminum MMCs. They concluded that mechanical, physical factors and material factors also with the effect of lubrication, work hardening, mechanical mixed layer, heat treatment etc. have considerable effect on the tribological performance of Al-MMC and counterface metal couples. Chen and Alpas [82] gave the sliding "wear map" for the AZ91 magnesium alloy. They performed the tests on block- on- ring apparatus against AISI 52100 steel within a load range of 1- 350 N and sliding velocity range of 0.1- 2.0 m/s. The wear behavior was classified into two main regimes- mild and severe wear. Mild wear accelerate under steady state conditions due to thermal equilibrium of contact surfaces whereas severe rate progressed continuously with sliding distance. There are two sub regimes of mild wear- oxidational and delamination wear. For severe wear also there are two sub regimes- severe plastic deformation induced wear and melt wear. For AZ91 alloy severe wear occurred on exceeding the surface contact temperature by 73.85 °C. It was also found that mild wear and severe wear are associated with oxidational wear mechanism and metallic wear mechanism respectively. An et al. [83] in dry sliding wear behavior of $Mg_{97}Z_1Y_2$ and

AZ91 magnesium alloys studied the coefficient of friction and wear rates by using pin-on- disc configuration. They also studied the worn morphologies of $Mg_{97}Z_1Y_2$ and AZ91 using scanning electron microscopy. Five wear mechanisms were observed- abrasion, oxidation, delamination, thermal softening and melting. It was found that $Mg_{97}Z_1Y_2$ showed better wear resistance in comparison to AZ91 in terms of thermal stability of intermetallic phase and by using surface temperature analysis elevated temperature mechanical properties of the two materials tested. In sliding friction and wear of magnesium alloy AZ91D produced by two different methods Blau and Walukas [84] mentioned in 2000 that friction and wear data in AZ91 seem to be absent from the tribology literature. Researchers studied the friction and wear behaviour on die cast (DC) and thixomolded (ThM) AZ91D magnesium alloy in both unidirectional and reciprocating sliding motion against 440C stainless steel. The tests conditions are given in Table 2.5. It was found that without additional surface treatments, coatings or lubricants magnesium alloys would not be suitable to produce bearing surfaces against stainless steel. Morsy [78] in dry sliding wear behaviour of hot deformed magnesium AZ61 alloy as influenced by the sliding conditions used pin-on- ring type wear apparatus against a stainless steel counterface. The tests were performed in the load range of 50- 350N and sliding velocity in the range of 0.2- 1.8 m/s. Aung et al. [85] in wear behaviour of AZ91D magnesium alloy at low sliding speeds studied wear behaviour of AZ91D surface layers against stainless steel under dry and slow sliding condition. The tests were carried out on pin-on- disc tribometer.

Table 2.5 Tests conditions for AZ91D magnesium alloy against 440 C stainless steel [90]

Motion	Applied conditions	No. of Tests
Reciprocating	Load=25 N, Stroke=10mm, Frequency=5cycle/s, Sliding distance=50 m	5
Reciprocating	Load=5 N, Stroke=10mm, Frequency=1cycle/s, Sliding distance=6 m	6
Unidirectional	Load=5 N, Speed=0.1±0.03m/s, Sliding distance=6 m	4 (DC), 5 (ThM)

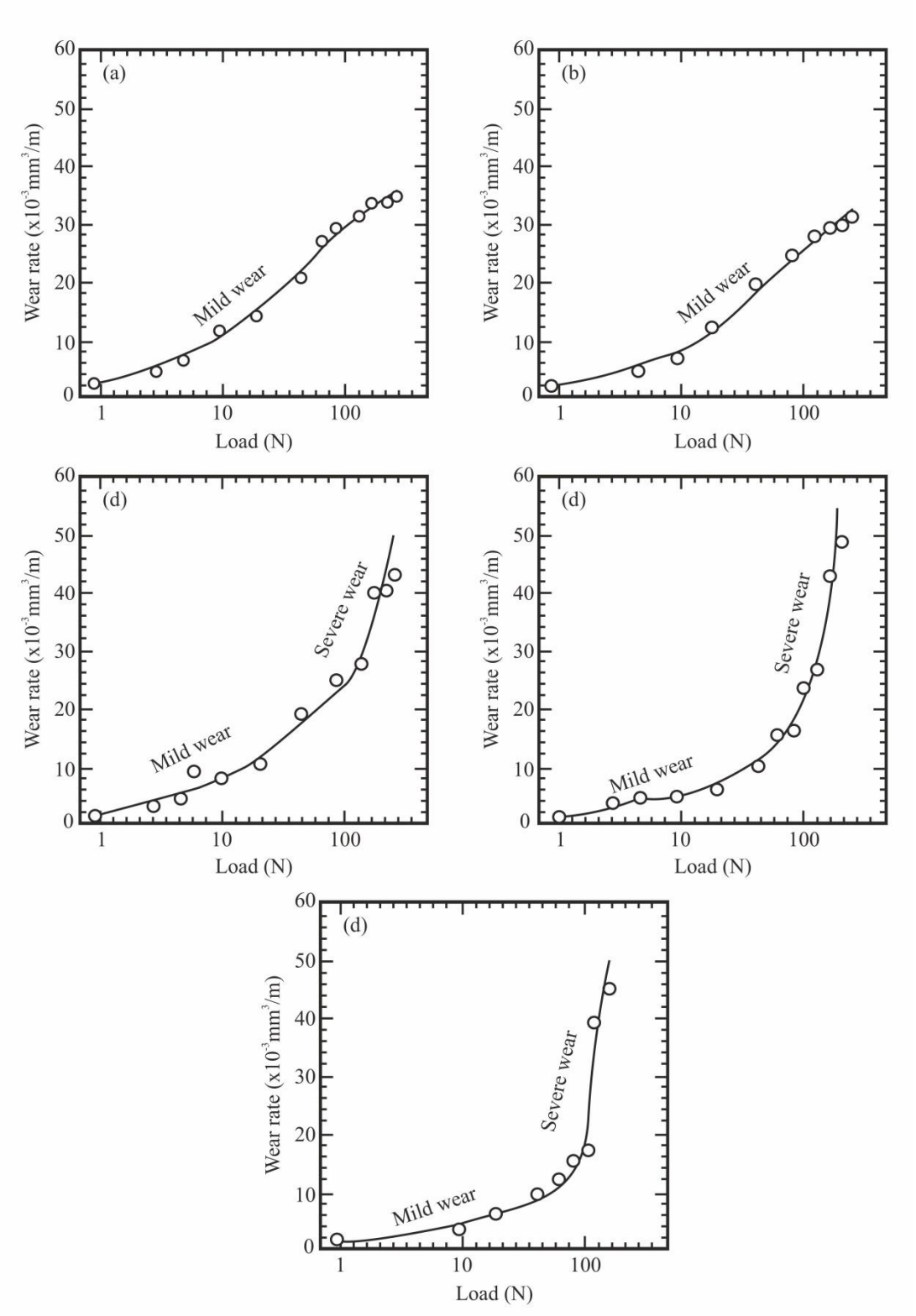

Figure 2.22 Wear rates of AZ91 as a function of applied load for tests conducted at the following speeds: (a) 0.1 m/s; (b) 0.3 m/s; (c) 0.5 m/s; (d) 1.0 m/s; (e) 1.5 m/s. Loads are rounded to the nearest integer [82].

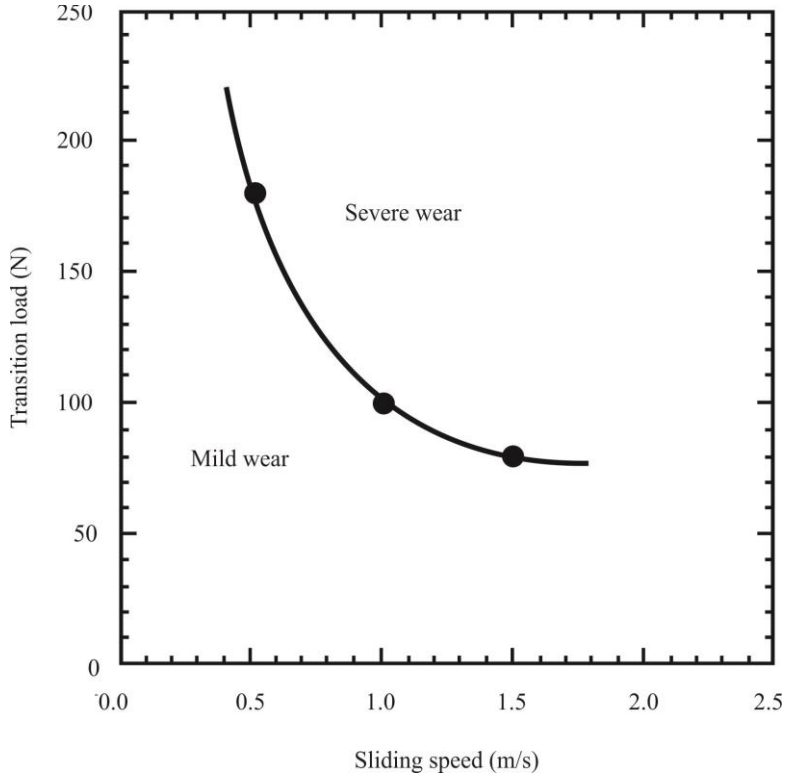

Figure 2.23 Transition load (mild to severe wear) vs. sliding speed [82].

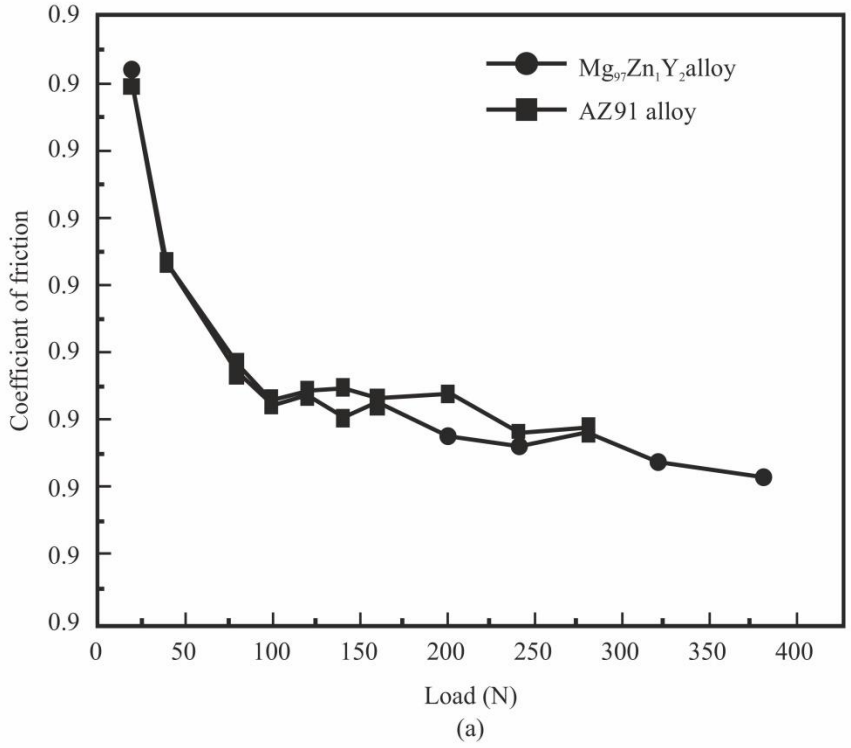

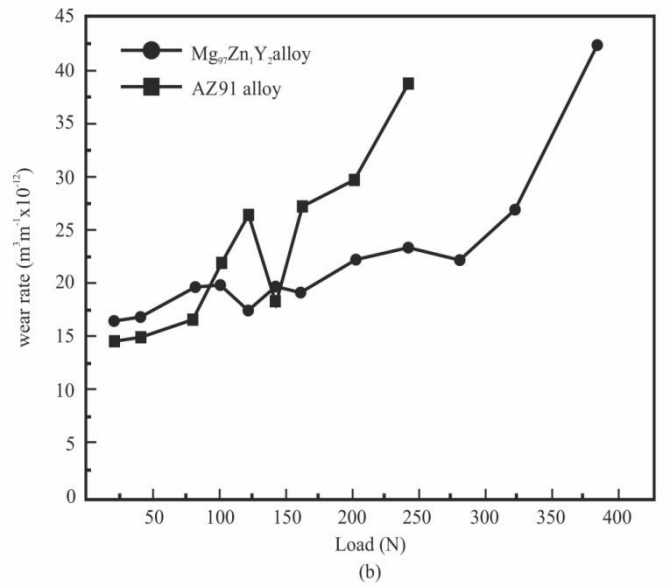

Figure 2.24 The variation in coefficient of friction (a) and wear rate (b) with load for Mg97Zn1Y2 alloy and AZ91 alloy [83].

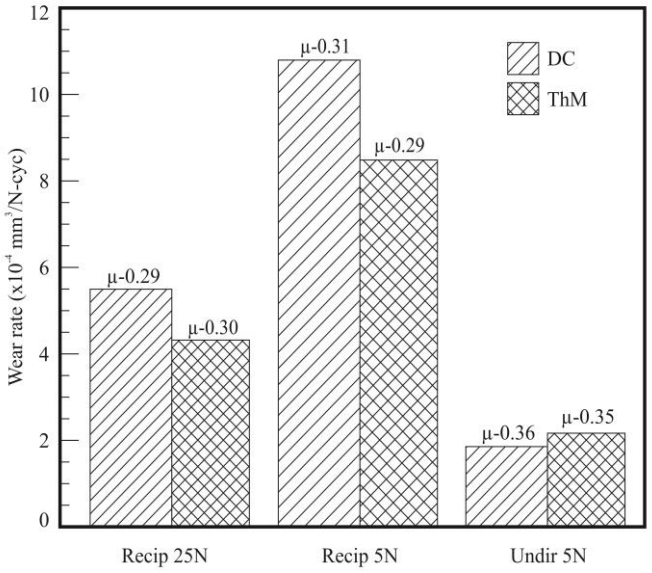

Figure 2.25 Summary of average, steady-state friction coefficients and wear rates for magnesium alloys in two processed conditions [84].

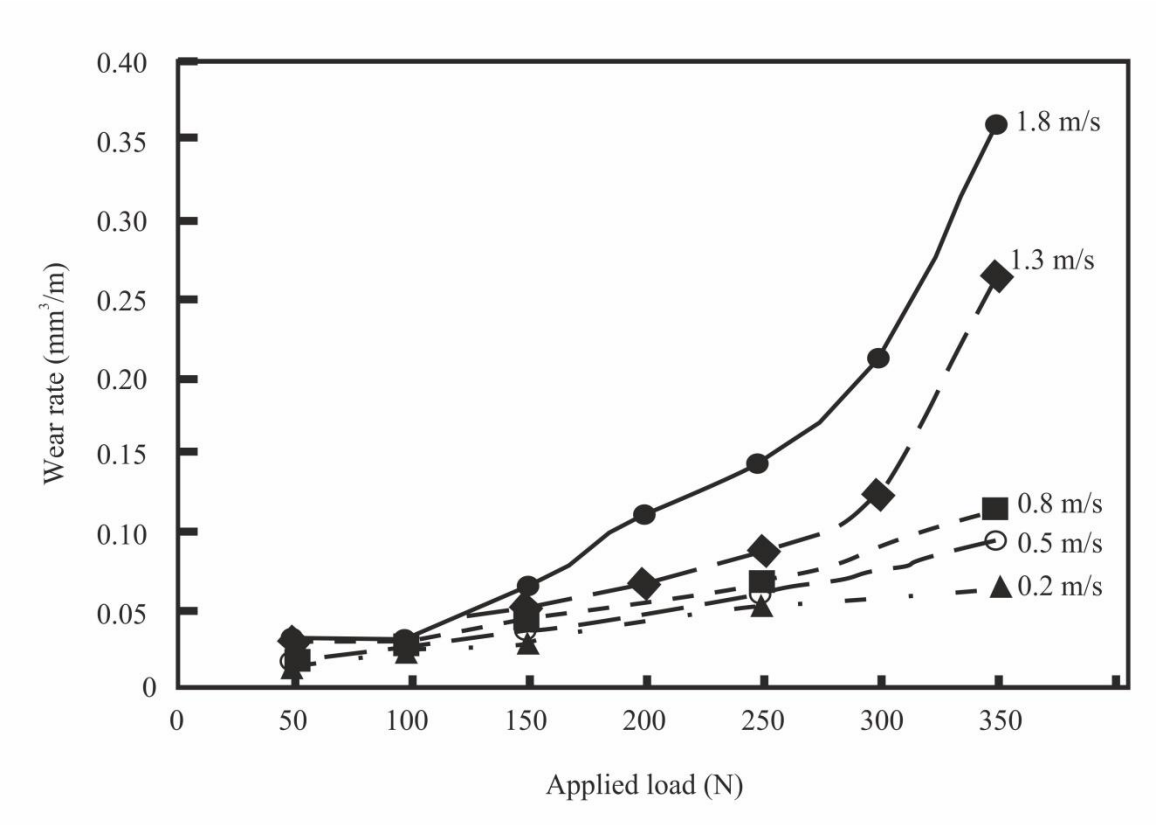

Figure 2.26 Effect of applied load on the wear rate of AZ61 at sliding velocity [78].

The parameters for conducting the tests are given in Table 2.6. It was concluded that abrasive wear was prevalent at sliding speed less than 0.1m/s resulting in the highest wear rate. Higher sliding speed more than 0.1m/s causes oxidational wear by assisting frictional heat. At higher speeds or at 0.5m/s delamination wear took place.

Table 2.6 Test parameters for conducting wear tests [84]

load	50- 350 N
sliding velocity	0.2- 1.8 m/s
sliding distance	1500m

In friction and wear characteristic of AZ91D magnesium alloy under dry friction reciprocating sliding motion Jun et al. [86] studied the friction and wear characteristics of conventional casted (CC) and Thixoformed (ThF) AZ91 magnesium alloy against GCr15 steel counterface. The test parameters are given in Table 2.7.

Table 2.7 Parameters for dry friction reciprocating sliding motion [92]

Steel ball GCr 15(SAE52100)	3.0 mm dia
frequency	5 Hz
time	10 min
load (in gms)	10, 50, 100, 200

It was concluded that under the experimental conditions the friction and wear behavior was from slight to serious wear. At low load the wear mechanism of AZ91D magnesium alloy under friction reciprocating sliding motion execute peel and grit wear. At higher load complete peel wear, adhesive wear and melting wear mechanisms were executed.

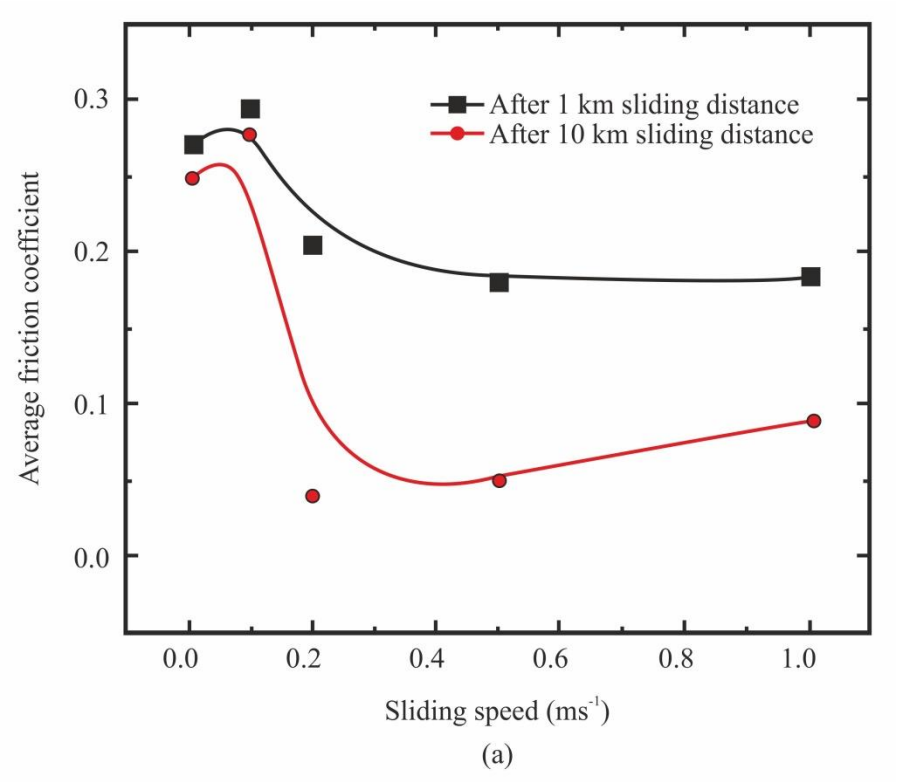

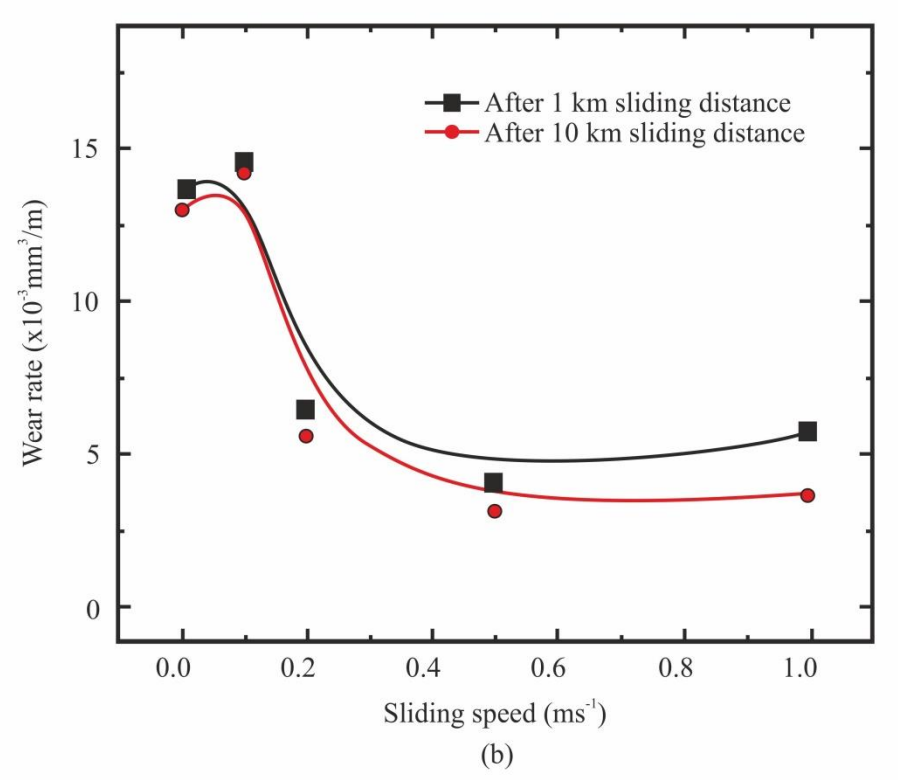

Figure 2.27 Variation of (a) average friction coefficient and (b) wear rate with sliding speed for fixed applied load and different sliding distances [85].

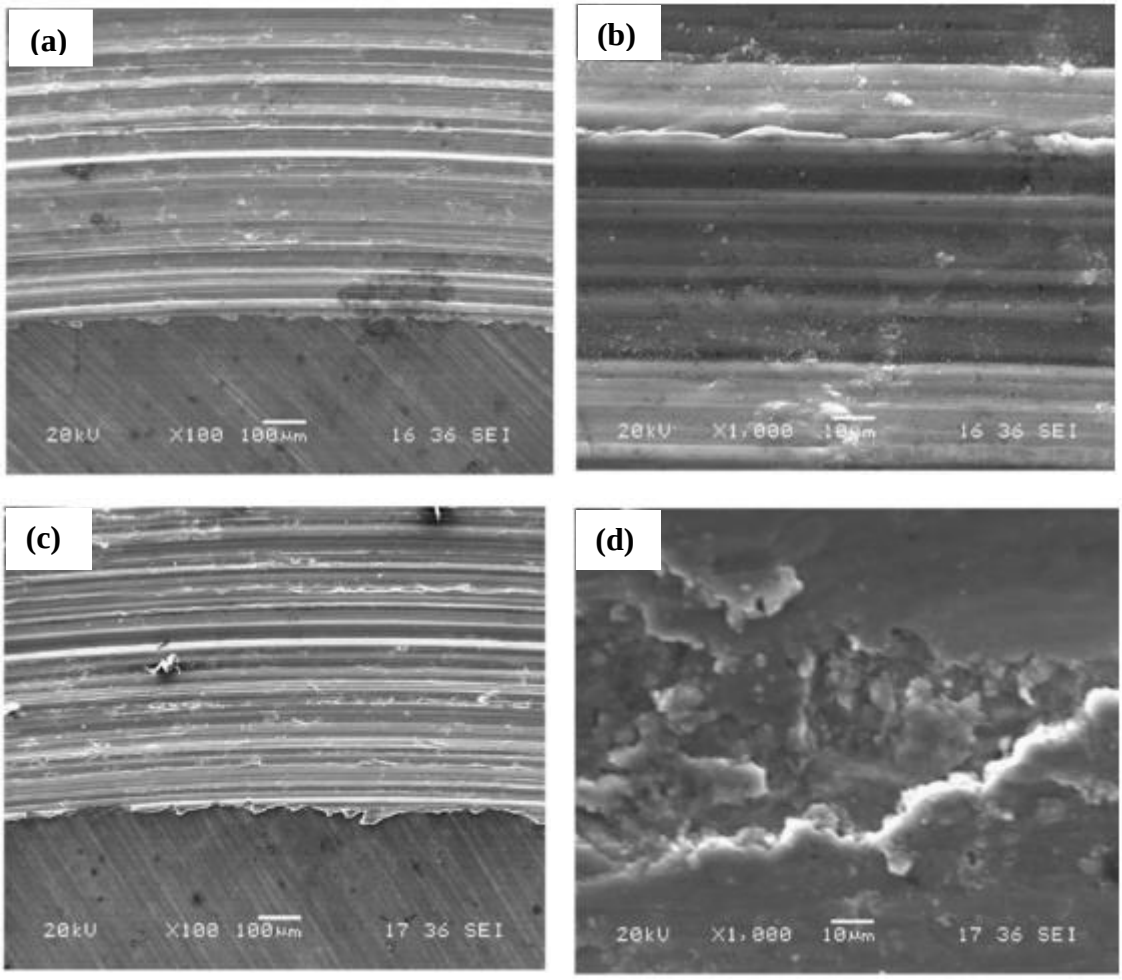

Figure 2.28 Scanning electron micrographs showing the wear track and worn surface morphologies of AZ91D alloy for 10 km sliding distance under different sliding speeds: (a) 0.01ms−1; (b) close-up of (a); (c) 0.1ms−1; (d) close-up of (c) [91].

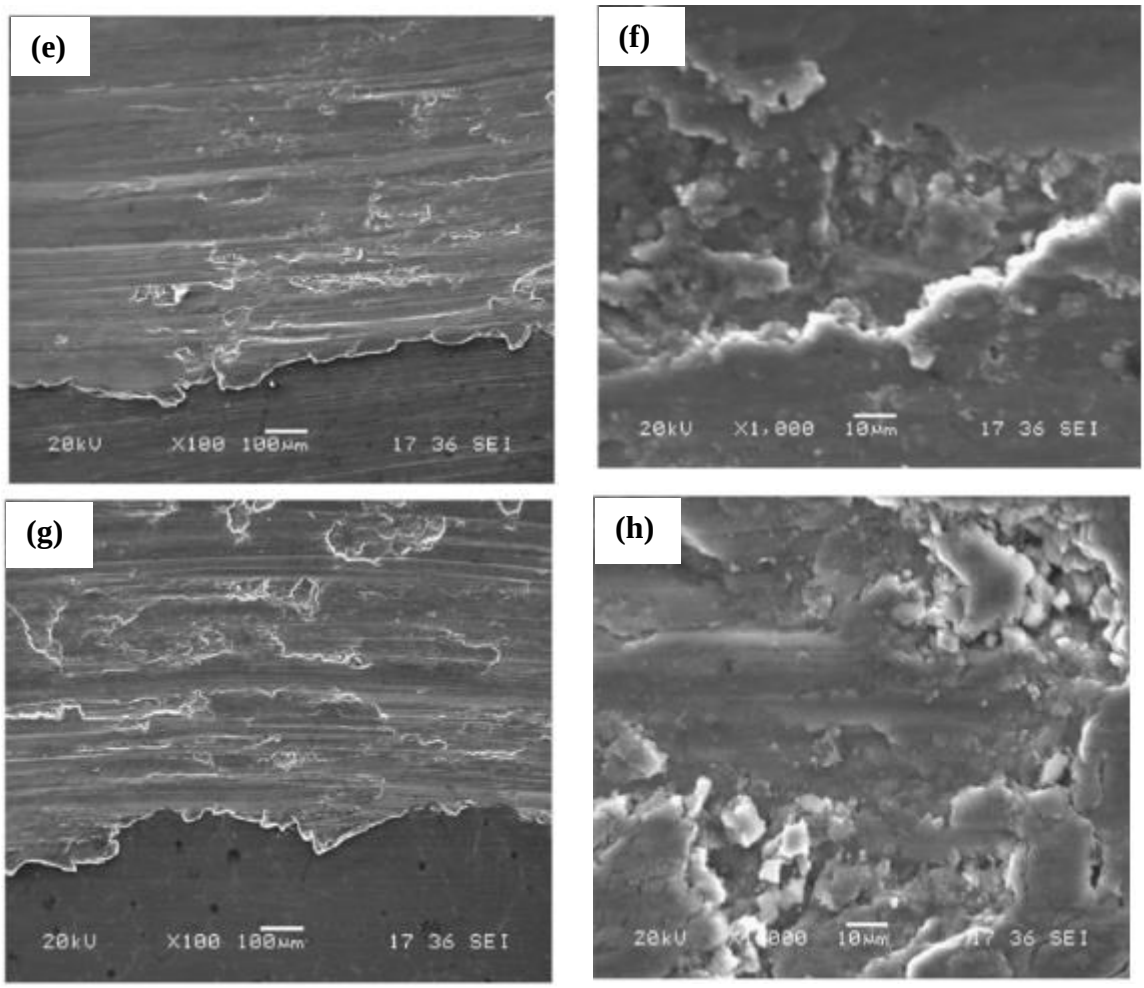

Figure 2.28 Scanning electron micrographs showing the wear track and worn surface morphologies of AZ91D alloy for 1 km sliding distance under different sliding (e) 0.5 ms^{-1} f) close-up of (e); (g) 1.0 ms^{-1} and (h) close-up of (g) [91].

2.7.1 Wear mechanisms

Abrasion

The grooves that occur parallel to the direction of worn surface, indicates that wear is taken place by abrasion wear mechanism. The grooves occur generally due to the existence of hard particles that plough into the pin. When these particles move over the surface of the pin removes the material along its direction on the surface of the Mg alloy [87]**.** Ploughing and cutting of hard particles between the pin and disc are the prime cause of emergence of grooves. Aung et al. [85] observed that surface deformation and damage in the form of deep grooves occurred through abrasive wear in the sliding direction.

Delamination

The entrapped debris particles produce further damage on both surfaces as a third-body abrasive and the debris itself undergoes delamination during the sliding. Short cracks occur in delamination wear [88]. Suh [89] proposed the delamination theory for non-lubricated sliding situations. Craters produced by delamination wear are eminent characteristic of mild wear regime. Delamination occurs due to the formation and propagation of cracks at the surface. Dry sliding results into different shapes and sizes of wear debris, which include flakes, chips and oxide powder. These debris particles basically comprised of laminates created by fractured compacted material. According to Das et al**.** [90], stresses generated during the wear causes delamination, subsurface cracks, that might either exist initially or became nucleated. When subsurface cracks and wear surface comes in contact with each other, delamination wear mechanism plays a leading role.

Oxidation

A very thin layer of fine particles significantly covered the dark surface, this mechanism is known as oxidational wear [82]**.** Oxidation of the surface with the removal of oxide fragments is due to the frictional heating during sliding. Oxides wear debris seal the valleys on the pin surface due to continual sliding and become embedded forming a protective layer, avoiding metallic contact and resulting in minimum wear rates [91]. According to An et al. [83], thick oxide layer is effective in protecting the sliding surface.

Plastic deformation

Adjacent to contact surface, extensive surface damage results from the plastic deformation [92]**.** According to Kumar et al. [93], plastic deformation also results in higher structural disruption [88]. The higher plastic deformation does not support any oxides on the wear surface leading to higher wear rate [94]. According to Tatavull et al. [95] massive surface deformation and local melting of material are the two important features of the plastic deformation mechanism [88].

From the literature survey it is observed that most of the studies of vibrations during solidification have taken place for aluminum alloys. Studies on magnesium alloys have also been carried out by ultrasonic vibration and electromagnetic vibration. However, the study of mechanical vibration during solidification of AZ91 Mg alloy has not been paid due attention. In addition to this, the combined effect of mechanical vibration with grain refiner addition has not taken place so far. Therefore, the research gap on the study of mechanical vibration during solidification of AZ91 alloy without and with the addition of grain refiner creates the scope for research work.

CHAPTER 3

EXPERIMENTAL PROCEDURE

This chapter elucidates the procedures used to perform the experiments. Optimization of process parameters includes; varying frequency of vibration, amplitude of vibration, addition of grain refiner without and with vibration during the solidification of AZ91 Mg alloy. In addition, the casting process, XRD, microscopy, porosity, tensile testing, hardness and wear testing are also covered.

3.1 Synthesis of Cast AZ91 Mg Alloy

In present work, weighed pieces of Mg, Al and Zn were kept in stainless steel crucible to get the 650 g of melt. Argon gas was passed through the melt at a rate of 0.28m^3/min to avoid oxidation. 1wt.% of flux (39% $MgCl_2$, 30% $CaCl_2$, 30% NaCl and 1% MgO) was used to remove dross. An argon gas cylinder is used for maintaining inert atmosphere, the furnace was specially designed for above purpose and furnace was fully protected from outer atmosphere. The schematic diagram of the experimental set up used for melting AZ91 alloy is shown in Fig. 3.1. The top of the experimental set up consisted of bottom pouring furnace with a maximum temperature of 1000˚C, a stainless steel crucible (76.2mm x 203.2mm), stainless steel stirrer rod (381mm long and 6mm diameter) to stir the melt during melting. Stainless steel stopper rod having 10mm diameter is used to prevent the flow of the melt during melting through the hole at the bottom of the crucible. There is also supply of argon gas through inlet to create the inert atmosphere in the crucible during melting so that no oxidation could take place. The bottom part of the experimental set up consists of mechanical vibration system. The cast iron mold (76.2mm x 228.6mm) is placed on the vibrating plate underneath the furnace attached with a spring that helps the plate to vibrate. The permanent mold used in this investigation is depicted in Fig. 3.1. The mold was made of cast iron and coated with lime for ease of casting ejection and thermal insulation. The effectiveness of the vibrations in AZ91 alloy during permanent mold casting was investigated. The castings were produced by inducing the mechanical vibrations. All the vibrations were imposed to the melt at 750 °C. The pouring temperature used for the permanent mold castings was 720 °C.

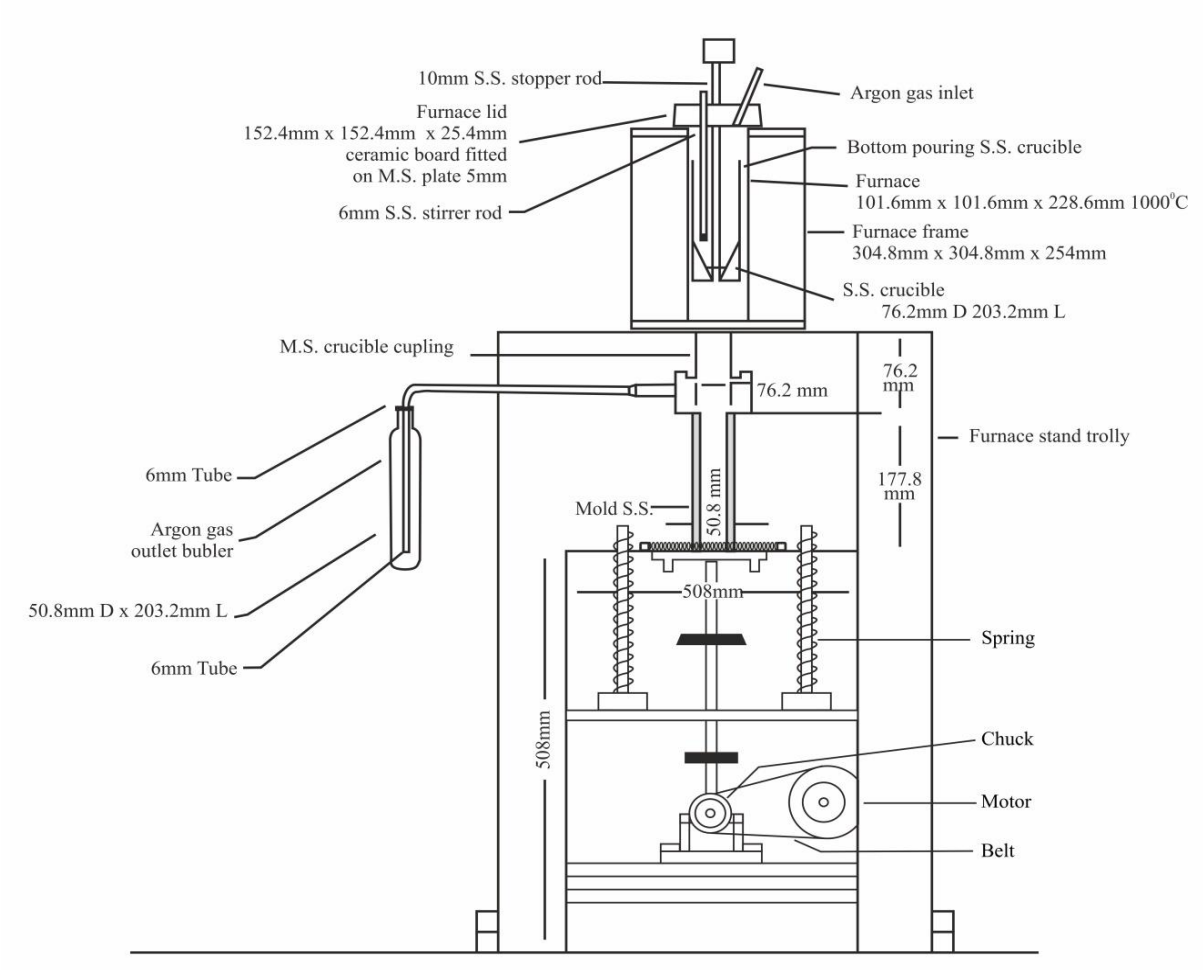

Figure 3.1 Schematic representation of experimental set up.

3.2 Compositional Analysis of Cast AZ91 Mg Alloy

The spectroscopic analysis of the cast samples was carried out at Spectro Analytical Lab limited and the compositional percentage of each element in the AZ91 Mg alloy found to be as given in the Table 3.1.

Table 3.1 Compositional analysis of AZ91 Alloy

Element	Cu	Si	Fe	Ni	Mn	Zn	Al	Mg
Nominal composition	0.003	0.060	0.102	0.026	0.011	1.53	8.27	Remainder

3.3 Grain Refining Procedure of As- Cast AZ91 Mg Alloy

Castings produced with metal mold were used to establish the effectiveness of the mechanical vibrations and grain refiner used in this study. Three set of experiments has been performed in this study. A vibrator device which converts electrical signals to mechanical vibrations was coupled to the target molds. This vibrator produced vertical vibrations. The 650g of AZ91 alloy was melted in a steel crucible to 750 ˚C for approxiately 45 minutes in bottom pouring furnace under argon (Ar) atmosphere at a flow rate of 0.28 m^3/ min. The argon cover gas was used to prevent the oxidation and formation of porosity in the molten AZ91 alloy. The salt based flux ($MgCl_2$.$CaCl_2$. NaCl and MgO) was added to it to coagulate slag and de-slag the melt. The first melt was poured into non-vibrating permanent molds (76.2mm x 228.6mm). While the subsequent some of the melt was poured into permanent molds (76.2mm x 228.6mm) being vibrated. The first set of experiment was performed by vibrating the permanent mold at varied frequencies (0- 25 Hz) and at constant amplitude of 2mm and the optimum results were found at 15 Hz frequency. So after getting the optimum result at 15 Hz, second set of experiment was performed by setting the frequency constant and varying the amplitude (0- 3 mm) and the optimum results were obtained at 15 Hz frequency and 2 mm of amplitude. After that third set of experiments was performed with addition of 2 wt.% ZnO powder (with particle size < 1μm) as a grain refiner (without and with vibration) to the melt. 1 wt.%, 2 wt.% and 3 wt.% ZnO was added to the AZ91 alloy. It was observed that the best results were obtained at 2 wt.% ZnO. This was in accordance with the earlier finding [8]. Therefore, 2 wt.% ZnO was chosen for the conducting the third set of experiments. The experimental parameters are summarized in Table 3.2.

Table 3.2 Experimental parameters

SET OF EXPERIMENTS	AMPLITUDE (mm)	FREQUENCY (Hz)
A	2	5 10 15 20 25
B	1 3	15
C	1 (2 wt.% ZnO addition) 2 (combination of 15 Hz- 2mm + 2 wt.% ZnO)	

3.4 Characterization of As Cast and Grain Refined Samples

The Mg- Al alloy prepared without and with grain refinement has been subjected to microscopy, grain size analysis, mechanical properties (tensile strength, yield strength, % elongation and hardness) and wear studies. Selected fractured samples of tensile test, worn out pin surfaces and debris collected during wear test were subjected to FESEM studies.

3.4.1 X-ray diffraction (XRD) analysis

The XRD of as cast and grain refined AZ91 alloy samples was done at D8 advanced automated XRD unit from PANalytical X' per powder China. The diffraction angle of 20 to 90 degree with Cu target was used. Consequently, intensity peak at different angles showing the element presents with its specific orientation.

3.4.2 Optical micrographs and field emission scanning electron microscopy (FESEM)

Samples of as-cast and grain refined AZ91 alloy for optical microscopy as well as for field scanning scanning electron microscopy (FESEM) were taken from 25 mm, 50 mm and 75 mm above the bottom part of the castings as shown in Fig.3.2. The samples were first polished using successively finer silicon carbide discs (320, 600, 800 and 1200 grit), and finally with diamond suspension of 9μm and 3μm followed by alumina suspension

compound of 0.5 μm. An etchant (15 vol. % $C_2H_4O_2$, 10 vol. % H_2O and 75 vol. % C_2H_5OH) was used to reveal the grain boundaries. The samples were slightly agitated in the etching solution for two minutes, then quickly rinsed with running water and dried using drier.

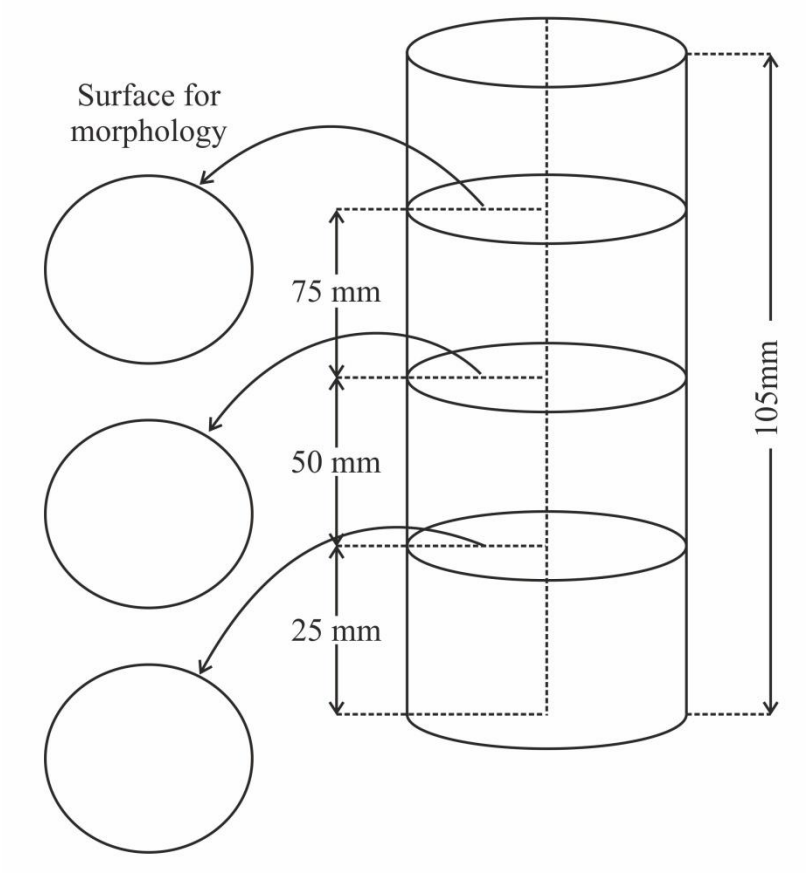

Figure 3.2 Sample position for microstructure.

3.4.3 Porosity measurement

The porosity measurement of AZ91 alloy in present study was measured as per ASTM B962-15 [5] standard using Archimedes principle in the following manner:

$$P(\%)=[1-(D_a/D_m)]x100 \qquad \textbf{(3.1)}$$

Where;

D_a = Experimental density of sample

D_m = Theoretical density of sample

Here D_m = 1.80 g/cm^3 for AZ91 alloy.

The experimental density of the samples was measured using the Mettler Toledo, ME-DNY-4 density measurement kit.

3.5 Mechanical Properties

3.5.1 Tensile properties

The tensile test gives the information about yield strength, ultimate tensile strength, % elongation and as a mean for specification of material. The tensile test was done with the help of tensile testing machine. Tensile specimen as shown in Fig 3.3 with dimension was set into the tensile testing machine followed by a load of 2000N with uniform strain rate of 1.5 mm/min by feeding data on computer system which sense the tensile testing machine. After substantial period of time, yielding began which showed specimen deformed plastically. When specimen started to neck it means UTS has reached and then specimen will got failed within seconds. Five specimens were used for each test.

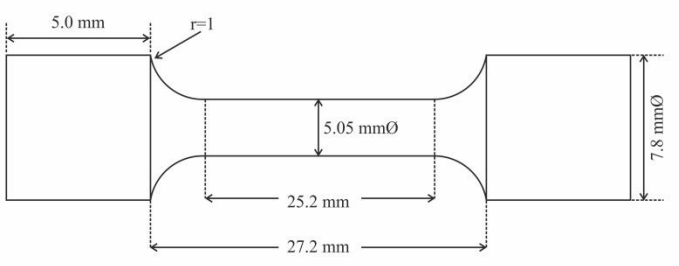

Figure 3.3 Schematic diagram showing a tensile specimen.

3.5.2 Fractography

Characterization studies were carried out on the tensile fractured samples in order to provide insight into the various fracture mechanisms operative during tensile loading of

samples. Fracture surface characterization studies were primarily accomplished using a scanning electron microscope.

3.5.3 Hardness test

The hardness testing of the as-cast and vibrated AZ91 magnesium alloy samples was done through Brinell hardness testing machine. The sample size that was used in the hardness testing was circular having diameter of 10 mm. the polished samples were placed under the microscope for selecting the proper area to get proper indentation. The sample was fitted on the sample holder one by one and a load of 500 kgf was applied for a dwell time of 15s using the ball indenter of 10 mm to get the indentation mark. Five readings were taken for each test and the hardness value was calculated by using the formula given below:

$$\text{BHN} = \frac{P}{\frac{\pi D}{2}(D-\sqrt{D^2-d^2}} \qquad \textbf{(3.2)}$$

Where;

P= load

D= diameter of ball indenter

d= diameter of indentation

3.5.4 Wear and friction analysis

Figure 3.4 shows the pin-on-disc type wear and friction monitor (DUCOM, TL-20, Banglore) machine which was used to study wear and friction behavior of magnesium alloys. The schematic representation of the pin-on disc apparatus is shown in Fig.3.5. Wear and friction tests were conducted on pin-on- disc apparatus. Wear test samples in the form of cylindrical pin (7mm dia and 20mm length) were machined from the castings. The wear test samples were wet grounded using SiC paper from 320 to 1500 grit step-by-step followed by polishing with 1.0μm and 0.5μm alumina suspension using a slow speed polishing machine. The polished surfaces were ultrasonically clean in acetone and dried prior to test. The narrow circular faces of the specimens were kept in contact with the

slider disc. The counterface disc was made of EN31 steel (0.9-1.20% C, 0.10-0.35% Si, 0.30- 0.75% M, 0.05%S, 0.05%P, 1.0- 1.60%Cr). The diameter of the disc was 50 mm and was cleaned with acetone before each wear test. The tests were carried out at a sliding velocity of 1 m/s and loads of 5N and 10N for a total sliding distance of 1500m. Mass losses from the surfaces of specimens were determined as a function of sliding distance and sliding velocity at each load. The mass losses were calculated from the differences in weight of specimens measured before and after the sliding tests (after removing any loose debris) using an analytical balance having an accuracy of 0.01 mg. Pin- on- disc test conditions used in present investigation are given in Table 3.3. Volumetric wear loss was estimated by dividing the mass loss to density of the alloy. A separate specimen was used to measure the mass loss for each load. Microstructural analysis on the worn surfaces and the loose debris particles were undertaken using a field emission scanning electron microscope (FESEM).

$$\text{Volume loss} = \frac{\boldsymbol{weight\ loss}}{\boldsymbol{density}} \qquad \textbf{(3.3)}$$

Table 3.3 Pin- on- disc test conditions

Disc Material	EN31 steel
Applied Load	5N and 10N
Sliding speed	1m/s
Disc diameter	50mm
Test length (sliding distance)	1500m
Room temperature	22˚C
Humidity	38%

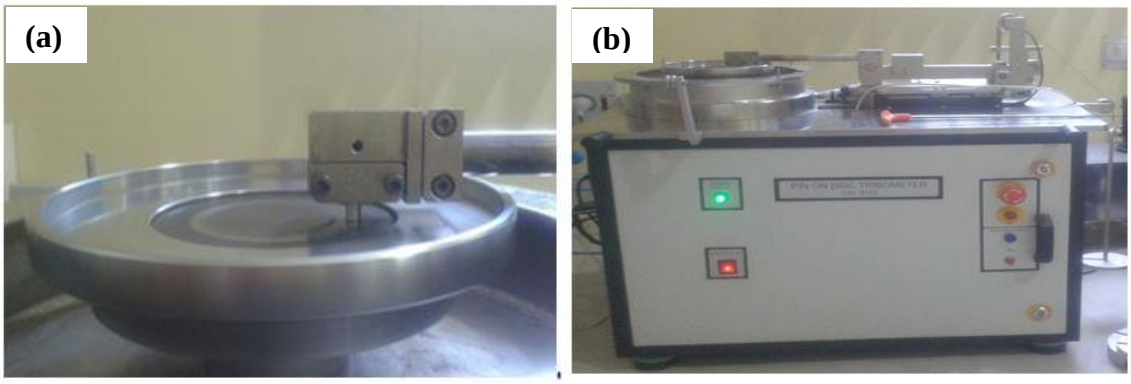

Figure 3.4 Pin- on disc wear unit.

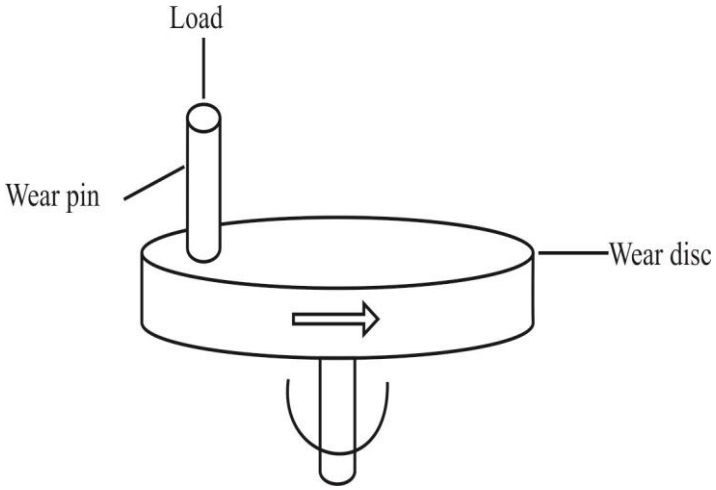

Figure 3.5 Schematic representation of the pin-on-disc wear apparatus.

CHAPTER 4

RESULTS AND DISCUSSIONS

This chapter follows the experimental procedures described in the previous chapter. The following section presents and analyzes the results of the casting performed with the imposition of vibrations at various frequencies and amplitude as well as with the addition of grain refiner.

4.1 Phase Analysis

Figure 4.1 shows the X-ray diffraction patterns of the as cast and grain refined AZ91 magnesium alloy. The diffraction pattern of the cast AZ91 magnesium alloy showed that the alloys mainly consist of α-Mg phase (hcp) and β- $Mg_{17}Al_{12}$ (cubic crystal) phase inter-metallic compound. After alloy was given mechanical vibration at 10 Hz frequency and 2 mm amplitude the magnesium peak becomes sharper and more intense. This indicates that the magnesium phase is stable at frequency of 10 Hz- 2mm amplitude and the intensity of diffraction peak significantly increases. The mechanical vibration treatment at frequency of 10 Hz- 2mm amplitude almost dissolved the intermetallic phase β- $Mg_{17}Al_{12}$. This is evidenced from Fig. 4.1 (b) as characteristic peaks of intermetallic phase β- $Mg_{17}Al_{12}$ are not possible to identify in the X-ray diffraction pattern. Though the magnesium peaks are sharp at frequency of 15 Hz- 2mm amplitude, there are also peaks of β- $Mg_{17}Al_{12}$ with lower intensity (Fig. 4.1c) as compared to as cast AZ91 magnesium alloy. For the alloy with the addition of 2 wt.% ZnO (Fig.4.1d) and the alloy given the combined effect of mechanical vibration treatment (15Hz- 2mm) as well as addition of 2 wt.%ZnO grain refiner (Fig.4.1e), there are peaks of Mg_2AlZn with minimum intensity along with sharp peaks of Mg and lower intensity peaks of β- $Mg_{17}Al_{12}$.

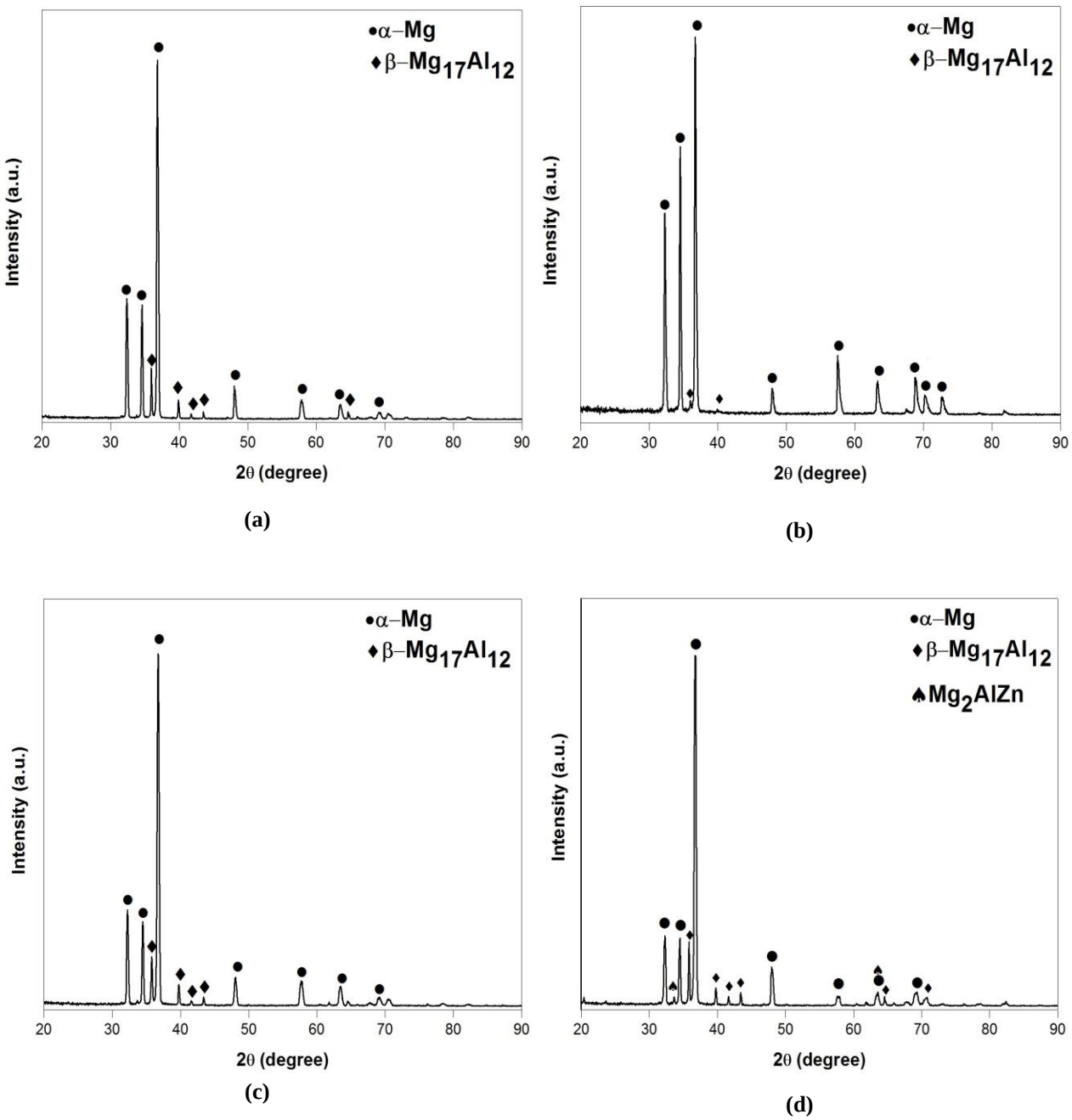

Figure 4.1 X-ray pattern of AZ91 magnesium alloy (a) as cast (b) vibration treated at 10 Hz frequency at 2mm amplitude (c) vibration treated at 15 Hz frequency at 2mm amplitude (d) with addition of 2% ZnO.

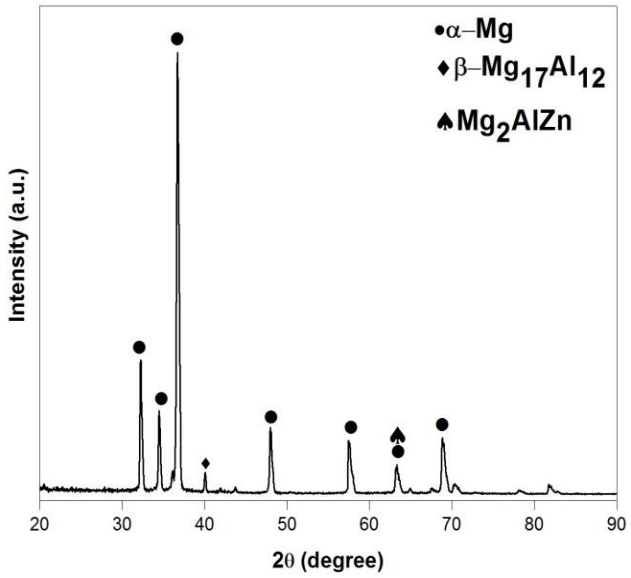

Figure 4.1 X-ray pattern of AZ91 magnesium alloy (e) combination of 15Hz- 2mm + 2% ZnO.

4.2 Microstructures of the Cast AZ91 Mg Alloy

4.2.1. Optical microscopy of the cast AZ91 Mg alloy

Figure 4.2 – Fig.4.10 show the optical microstructures of top, middle and bottom sections of as cast AZ91 magnesium alloy, condition A: mechanical vibration treated AZ91 alloy at constant amplitude and varied frequency, condition B: mechanical vibration treated AZ91 alloy at constant frequency and varied amplitudes and condition C: addition of grain refiner without and with vibration respectively.

As cast AZ91 alloy

Figure 4.2 (a, b and c) show the microstructures of the top, middle and bottom portions of the as cast alloy. The as cast AZ91 alloy consists of coarse dendritic and non- uniform distribution of α-Mg primary phase, eutectic β-$Mg_{17}Al_{12}$ phase and secondary precipitated β-$Mg_{17}Al_{12}$ phases [15]. The eutectic phase precipitates in the form of network at grain boundaries. Difference is observed in the microstructure taken at the top, middle and bottom samples. The microstructure observed at the top showed coarser grain structure and β- precipitates. Microstructure at the middle portion showed little fine α- Mg and β- precipitates. While at the bottom the microstructure showed finer α- Mg and β-

precipitates. This could happen due to different cooling rates at the top, middle and bottom of the mold. At the bottom the melt is in close contact of the mold. Therefore, cooling rate was faster at the bottom as compared to at the middle and top [96].

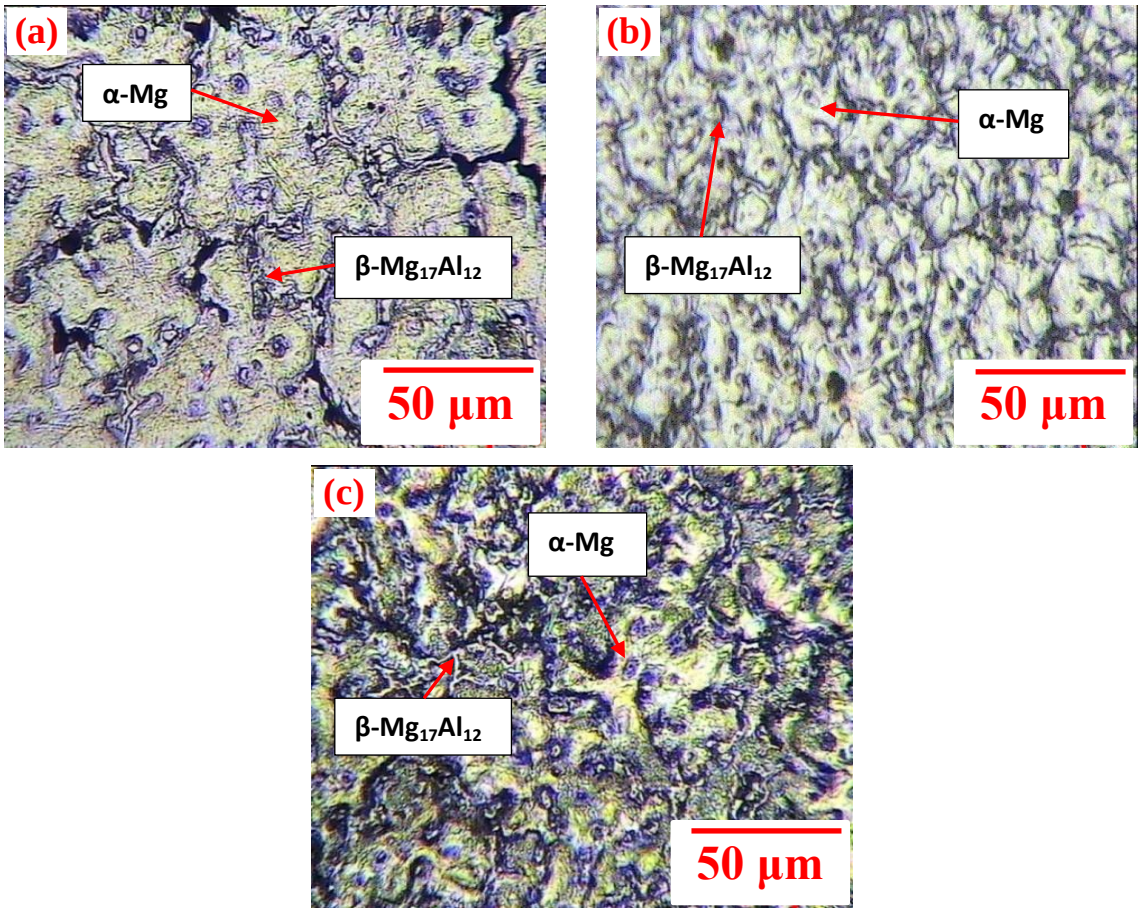

Figure 4.2 Optical microstructures of as cast AZ91 alloy at 200x (a) Top section (b) Middle section (c) Bottom section.

Under condition A: At constant amplitude and varied frequency

On imposing vibrations, coarse eutectic phase is refined and became discontinuous and new granular phases formed. Like as cast alloy, in all the cases, bottom section of the castings has finer structure as compared to middle and top sections. Imposing vibrations during solidification of AZ91 alloy causes morphological changes in different phases under different conditions. When the alloy was treated by mechanical vibration at constant amplitude of 2mm and varied frequency (5- 15 Hz). With the application of mechanical vibration, in the microstructure obtained from the sample with a low-

frequency vibration at 5 Hz and 2mm amplitude, the grain sizes of α-Mg primary phase begin to decrease. However, some dendrites still can be observed, as shown in Fig. 4.3.

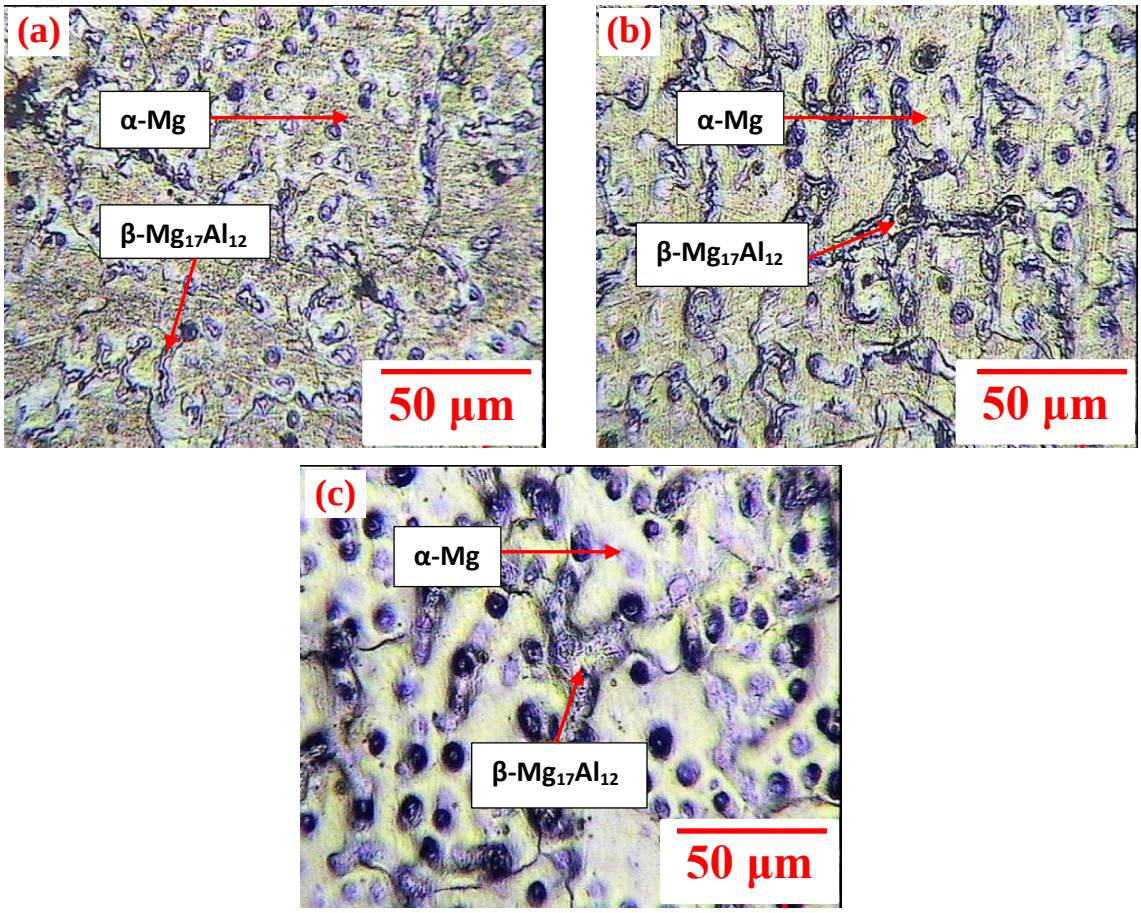

Figure 4.3 Optical microstructures of AZ91 alloy at 5 Hz at 200x (a) Top section (b) Middle section (c) Bottom section.

With increasing vibration frequency, the grain sizes of α-Mg primary phase gradually decrease. When the vibration frequency reaches 10 Hz and 2mm amplitude, it is evident that the grain sizes of α-Mg primary phase are much finer than that of the sample without vibration, and the coarse dendrites have almost disappeared, massive β–$Mg_{17}Al_{12}$ eliminates and the microstructure mainly consists of fine equiaxed grains with a uniform distribution as shown in Fig. 4.4 [15].

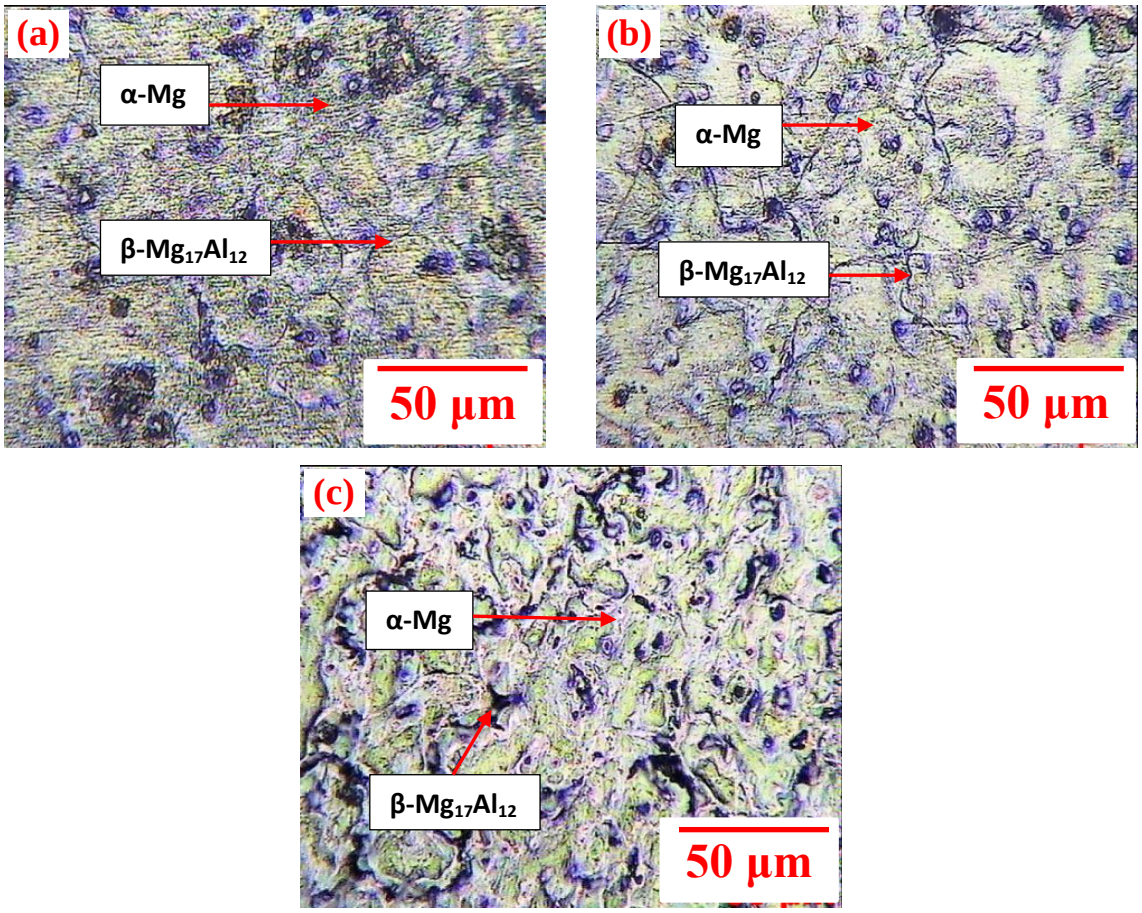

Figure 4.4 Optical microstructures of AZ91 alloy at 10 Hz at 200x (a) Top section (b) Middle section (c) Bottom section.

When the frequency is increased from 10 to 15 Hz- 2 mm amplitude (4.5), the vibrations bestow many nucleation sites in melt forming the fine grain sizes [97]. That is why, at vibration frequency of 15 Hz- 2 mm amplitude, the grain size of α-Mg primary phase decreases and fine precipitates of β-$Mg_{17}Al_{12}$ phase reappears.

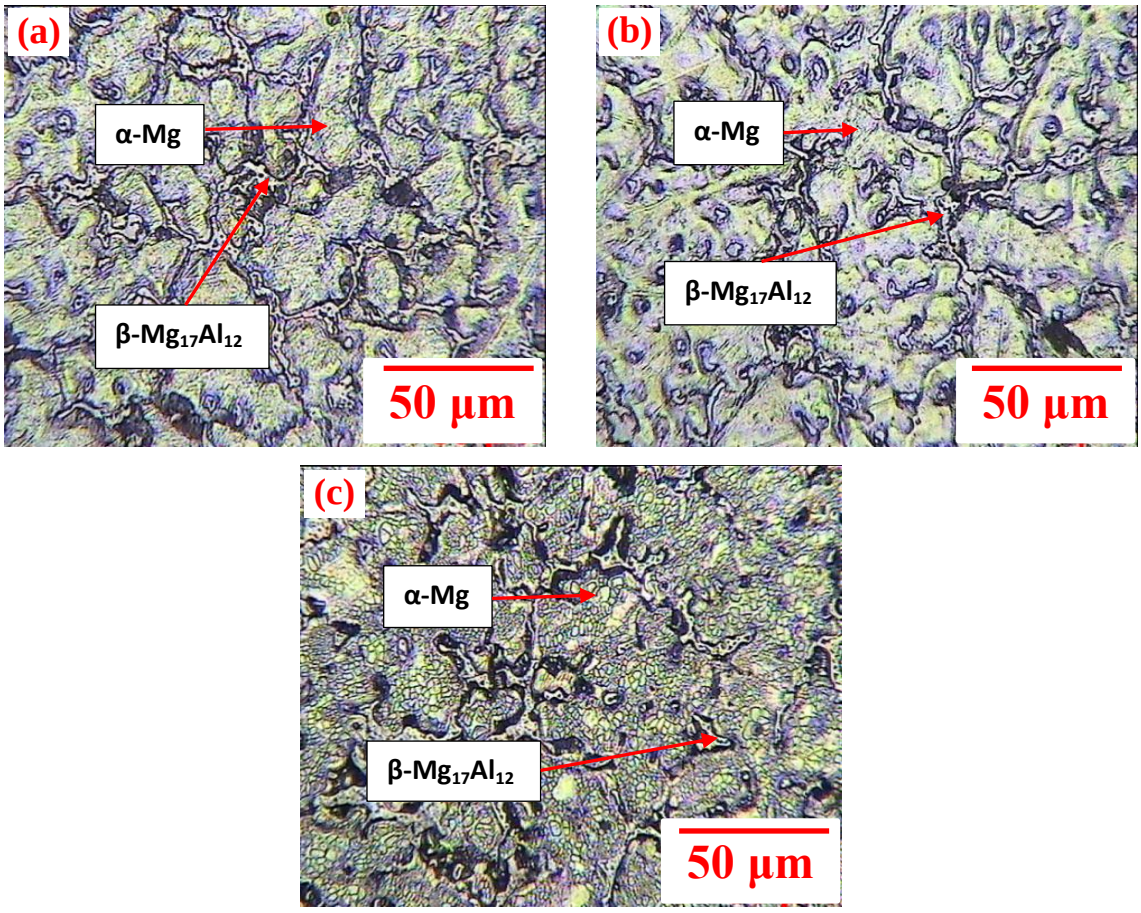

Figure 4.5 Optical microstructures of AZ91 alloy at 15 Hz at 200x (a) Top section (b) Middle section (c) Bottom section.

Thereafter, at 20 Hz frequency- 2 mm amplitude and 25 Hz frequency- 2 mm amplitude (Fig.4.6 & Fig.4.7), the grain size of α-Mg primary phase and β-$Mg_{17}Al_{12}$ phase increases. This may be due to the quicker movement of the liquid due to vibration inside the mold. Though, loss of contact as well as origination of low pressure bubbles in cavitation occurs due to the high frequency between the liquid metal and mold resulting in coarser microstructure [77].

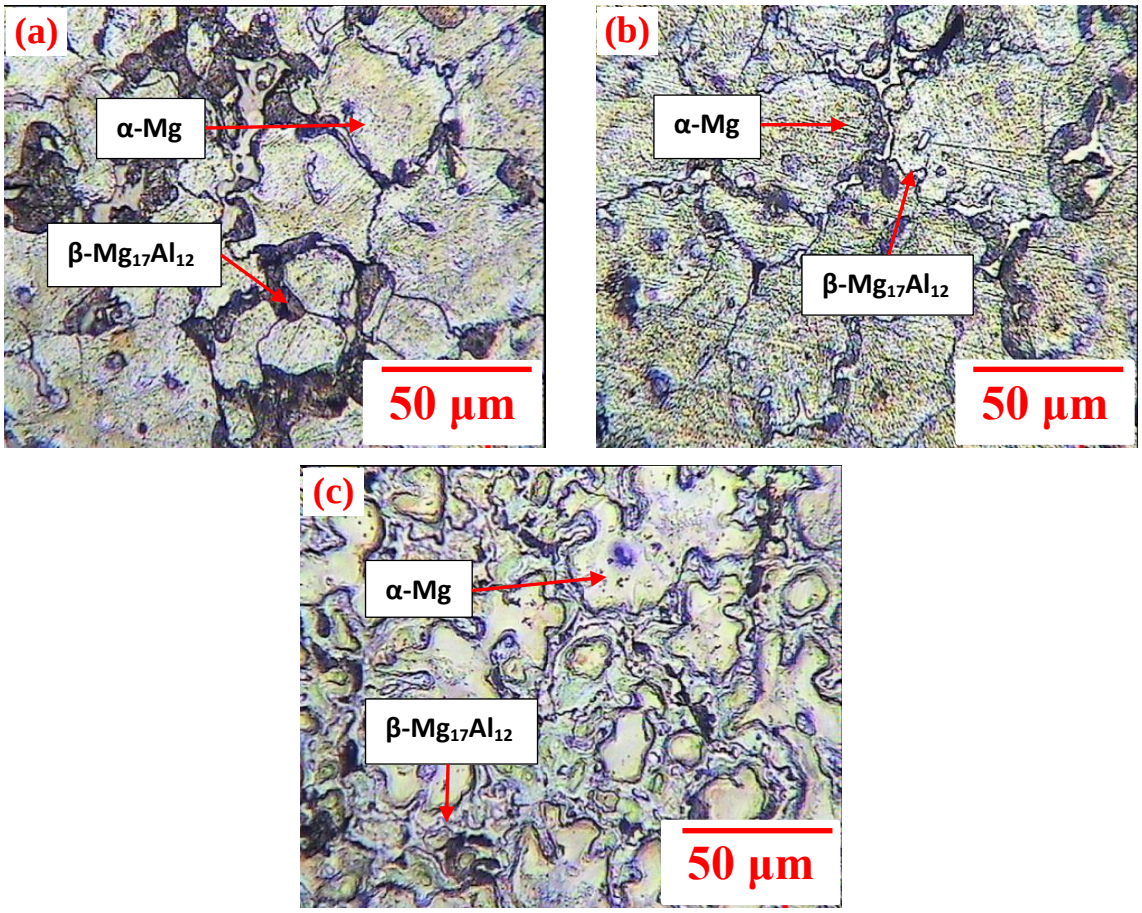

Figure 4.6 Optical microstructures of AZ91 alloy at 20 Hz at 200x (a) Top section (b) Middle section (c) Bottom section.

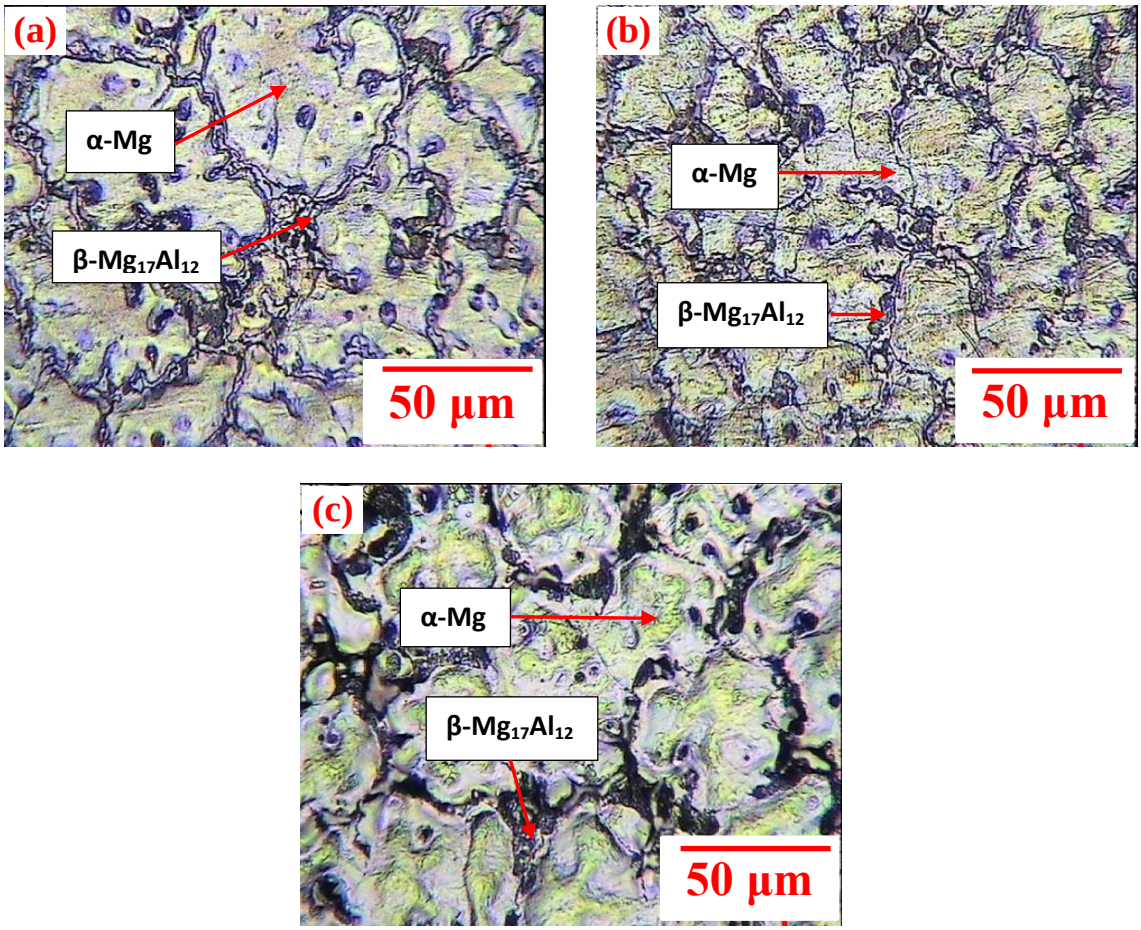

Figure 4.7 Optical microstructures of AZ91 alloy at 25 Hz at 200x (a) Top section (b) Middle section (c) Bottom section.

Figure 4.8 shows the grain size of the as cast and the alloy with the imposition of vibration at constant amplitude and varied frequency. It is well known that the nucleation stage and subsequent growth condition is the base of microstructure and adequate nuclei are vital for the microstructural refinement.

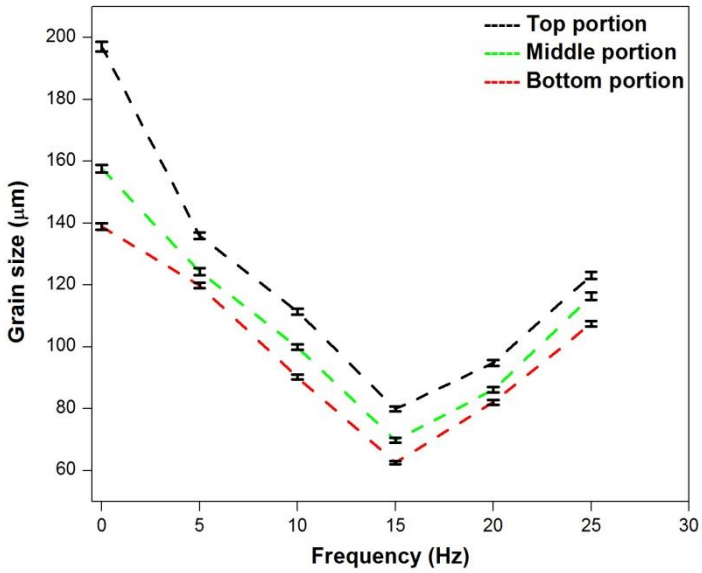

Figure 4.8. Effect of frequency of vibration on grain size of AZ91 alloy.

Under condition B: At constant frequency and varied amplitude

The similar pattern was observed in the third set of experiments when mechanical vibrations were imposed on the alloy at constant frequency of 15 Hz and varied amplitude (1mm- 3mm). The grain sizes of α-Mg and β-$Mg_{17}Al_{12}$ phases begin to decrease on imposing the vibration at amplitude of 1 mm- 15 Hz frequency (Fig.4.9) and 2 mm amplitude- 15 Hz frequency (Fig.4.10), the coarse dendritic structure became finer.

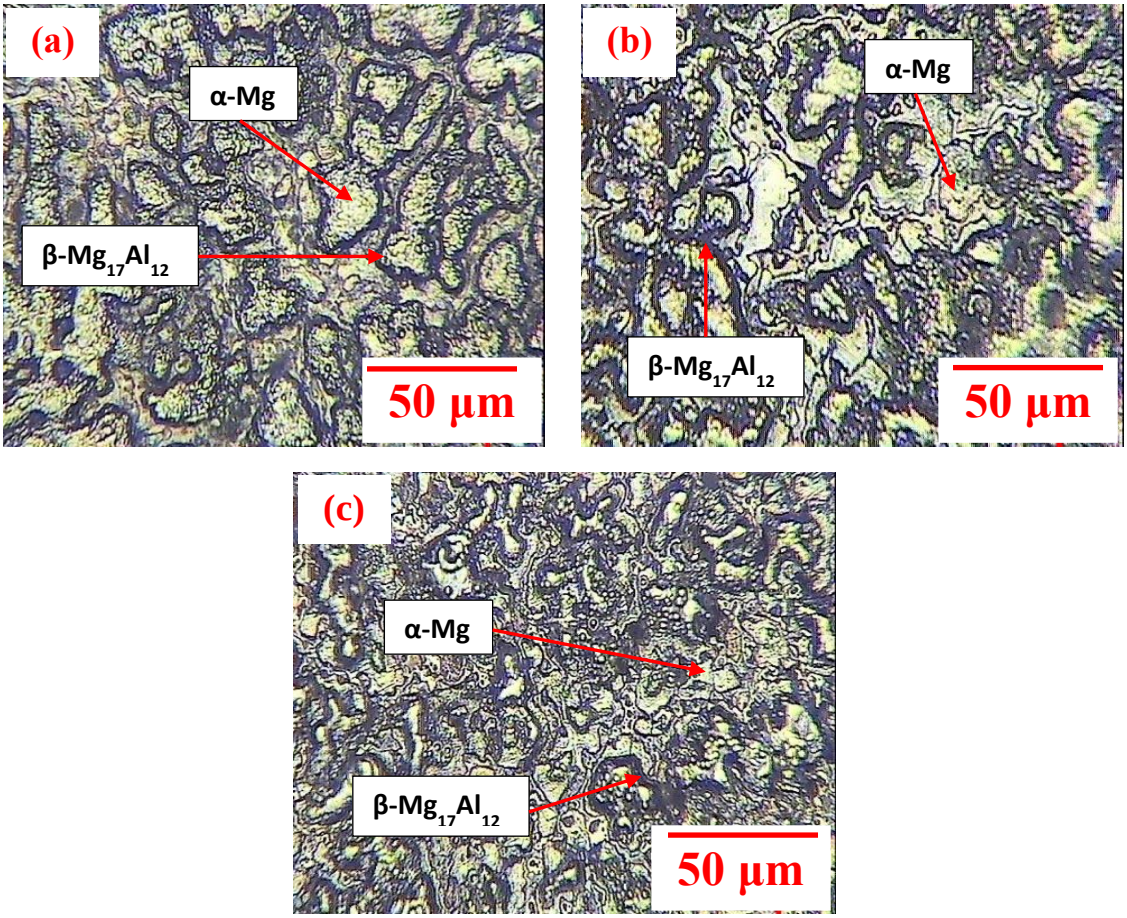

Figure 4.9 Optical microstructures of AZ91 alloy at 15 Hz – 1mm at 200x (a) Top section (b) Middle section (c) Bottom section.

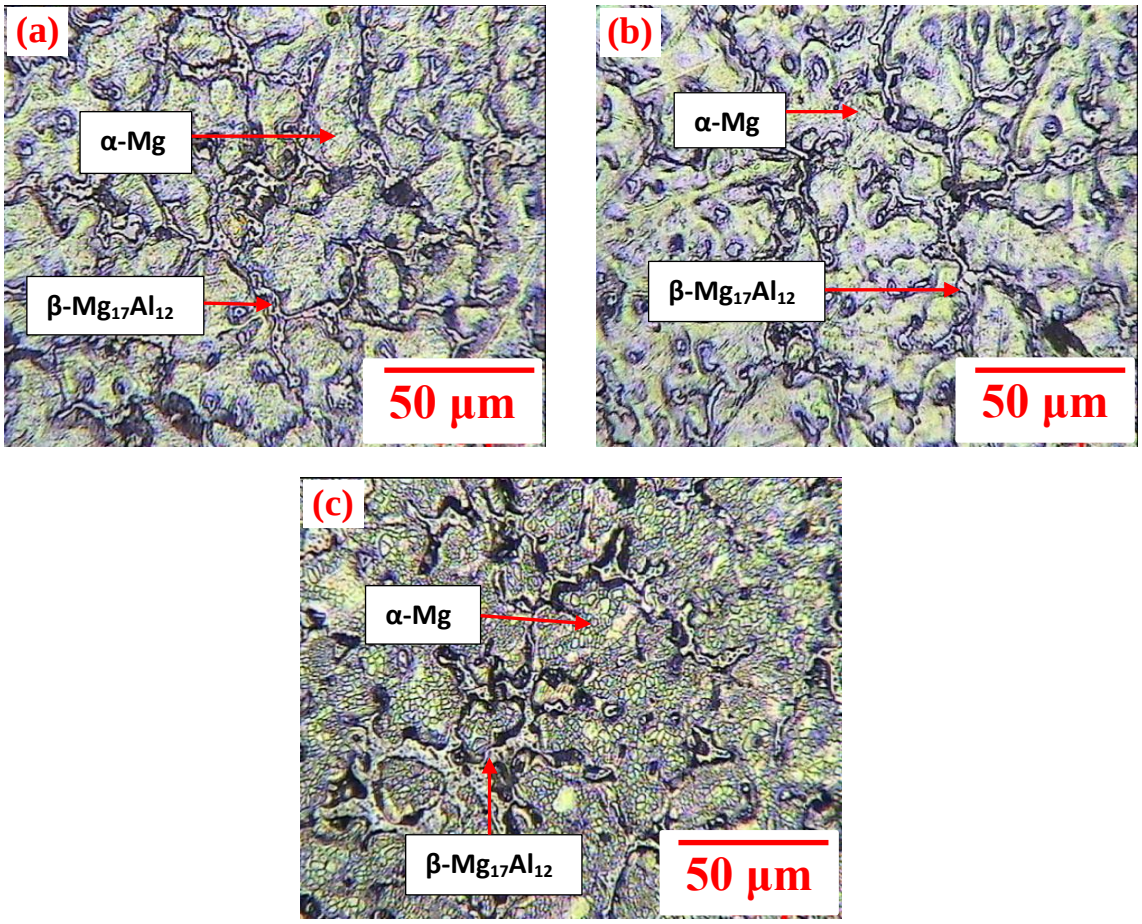

Figure 4.10 Optical microstructures of AZ91 alloy at 15 Hz – 2mm at 200x (a) Top section (b) Middle section (c) Bottom section.

On further increasing the amplitude to 3 mm- 15 Hz frequency (Fig.4.11) grains became coarser. This coarsening occurs may be due to the reduction in surface energy which is the driving force for coarsening. Coalescence and Ostwald ripening are the two mechanisms of coarsening. Amalgamation of neighboring dendritic arms leads to coarsening. This is known as coalescence. Due to increasing diffusion flux from the interfaces primary solid phases of small sizes dissolve in liquid, i.e. interfaces from high roundness to low roundness results in decrease in density of solid particles in final microstructures. This agglomerated solid particle play a dominant role in coarsening. This is known as Ostwald ripening mechanism [53].

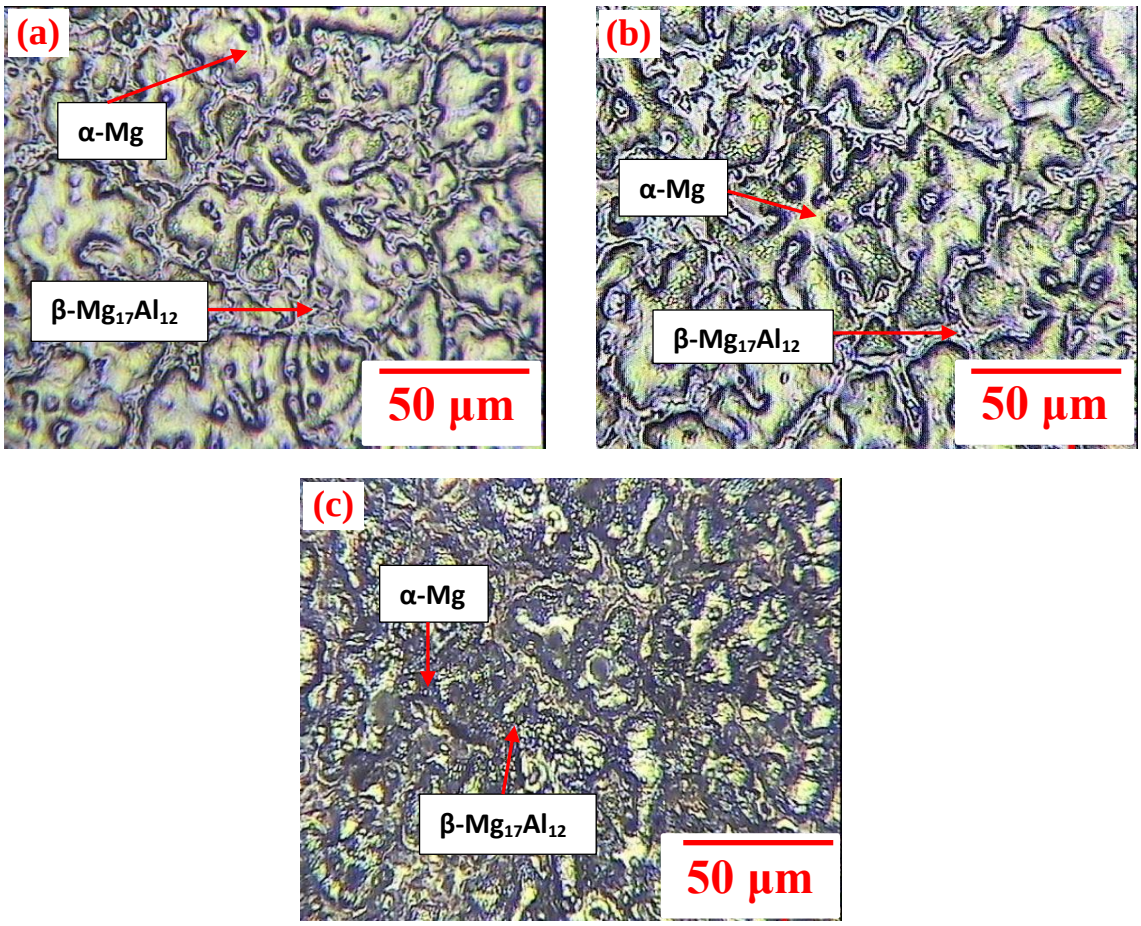

Figure 4.11 Optical microstructures of AZ91 alloy at 15 Hz – 3mm at 200x (a) Top section (b) Middle section (c) Bottom section.

Figure 4.12 shows the effect of amplitude of vibration on the grain size of the alloy.

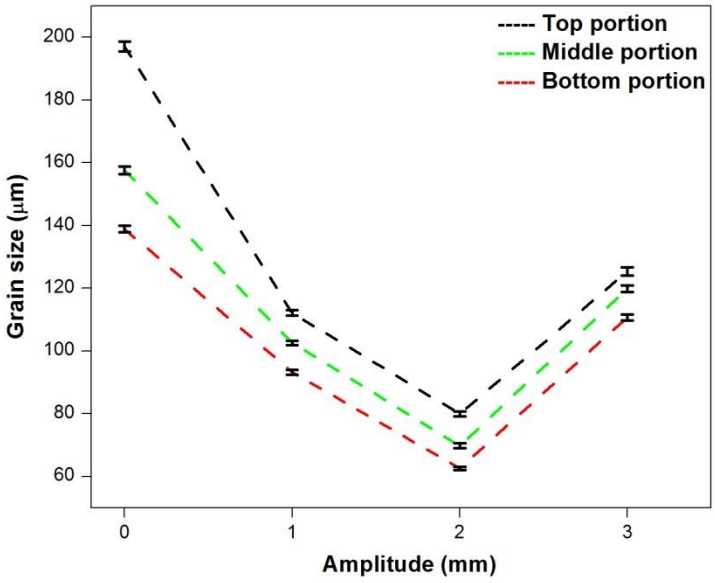

Figure 4.12 Effect of amplitude of vibration on grain size of AZ91 alloy.

Mechanism of the grain refinement through mechanical vibrations

Substantial refinement in the microstructure through imposition of mechanical vibration during solidification could be explicated by the following mechanisms:

(i) The liquid solidifies fast as soon as it comes in contact with the cold mold wall.

Mechanical vibration helps in the fragmentation of the initially solidified dendritic structure formed on the cold mold wall. Besides, forced convection in molten metal is induced by vibrational energy and on dendritic arms in the flow direction; the external forces are inserted by flows generated by vibration resulting in the breaking off the dendrites in the melt. The forced convection into the bulk melt brings the detached dendrite arms that act as new nuclei. As a result, with the further detachments of dendrite arms, the nucleation rate significantly increases, resulting in a considerable refinement of the microstructure [53].

(ii) Guo et al. [98] stated that subsequent growth conditions following heterogeneous nucleation are important factors for the solidification of metals. During solidification, these are substantially affected by heat extraction and fluid flow.

Nucleation and growth both are responsible for the final microstructure. Through vibration high solidification rate occurs by the alternate movement of a molten metal due to the generation of high heat transfer inside the molten metal to the mold interface. In molten metal, vibration causes higher cooling rate that result in a higher undercooling. Thus, encourage more number of existing nuclei in the molten metal to onset spontaneous heterogeneous nucleation, ensuing more refinement in the microstructure. Moreover, stronger forced convection ensues due to higher vibrational frequency. This signifies the fragmentation of the dendrites and generation of more nuclei in the melt. In the meantime, heat transfer rate of the molten metal also increases. Consequently, larger vibrational frequency promotes refinement of the microstructure.

(iii) The formation of bubbles or cavities in the liquid is known as cavitation. These cavities or bubbles could either be filled air or vapor or they could be almost empty. With the passage of suitable frequency and intensity of sonic or ultrasonic waves, these cavities are generated in the liquid. The oscillation of the medium causes formation of regions of compression and rarefaction. In rarefaction region, air or vapor bubbles are formed due to tension (negative pressure). Generally, in liquid metals, the pre- existing gas pockets are responsible for the formation of very small bubbles. But the unexpected expansion of undissolved gas bubbles result in the evaporation of produced liquid into the partial void. The production of very high pressure on the collapse of the cavities makes it effective in cleaning, dispersion and grain refinement. Extremely powerful shock waves arise on the ultimate disappearance of the bubbles, which are responsible for most of the phenomenon brought about by cavitation. Therefore, during solidification of metals and alloys, growing crystals dislocate by the forces allied with cavitation. This fragmentation of crystals efficiently generates more nuclei around which new crystals could form. So, in this way, crystals never grow beyond a certain size [99].

(iv) Zhao et al. [42] explained that generally solidification firstly occurs near the mold wall i.e in the low temperature zone. Then it expands towards the center. But the situation gets changed on imposing the mechanical vibration during solidification

process. Heat flow got disturbed during the crystal growth which affects heat and mass transport. It varies the structural and energy fluctuations in the melt making nucleation of the crystal easier. In the meantime, fragmentation of dendrites occur due to disturbance of mechanical vibration reducing the constitutional supercooling zone and controlling the growth of dendrites. These fragmented dendrites then grow into equiaxed grains. Therefore, it can be concluded that mechanical vibration imposed at the initiation of the solidification process, makes the nucleation arise in the whole molten metal or in a larger region. So during solidification only, these dendrites could be fragmented before growing into the larger dendrites.

(v) Tamura et al. [46] discovered that microstructural refinement also gets affected by the free space area for vibrating the melt. Under liquidus temperature, heterogeneous nucleation is promoted by mechanical vibration. According to Maltais et al. [44] through vibrations dendrites are broken down into pieces and heterogeneous nucleation is enhanced. Low frequency vibrations do not allow the melt to oscillate in a phase, so no mixing occurs in the melt. However, shearing occurs through the generation of surface waves at the free surface of the melt. Therefore, it can be said that these surface waves are responsible for the refinement of grains. But this mechanism is effective if nuclei are not remelted in the flowing metal. During filling, growing dendrites on the mold wall experience shear stress, some of them could be broken or detached by vibration, carried into the flowing metal and contribute to enhance grain refinement.

Under condition C: Addition of grain refiner without and with vibration

In the third set of experiments when 2 wt.% ZnO grain refiner was added without vibration to AZ91 Mg alloy (Fig.4.13), the grain sizes of α- Mg and β- $Mg_{17}Al_{12}$ decreased it was thought that Zn solute in the alloy has been liberated from ZnO. According to equation 2.8, ZnO is reduced to Zn on adding it to molten Mg. It is considered that Zn imparts grain growth restriction whereas remaining ZnO offer desirable sites for heterogeneous nucleation. It is reported that [100] heterogeneous nucleation occurs due to the good lattice matching between nucleating solid and grain

refiner. As both Mg and ZnO have similar crystal structure and lattice parameters (Table 2.2). Therefore, ZnO particles would act as heterogeneous nucleating sites for Mg due to aforementioned crystallographic resemblance. There is possibility that little amount of ZnO might have dissociated, resulting in the introduction of Zn into the melt. This extra Zn from ZnO may have assisted in the refinement of grains [6]. Hence, there could be two mechanisms for the grain refinement. One is ZnO acts as heterogeneous nucleating sites for Mg. Another is reaction of ZnO with Mg increase Zn solute in the melt resulting in growth restriction.

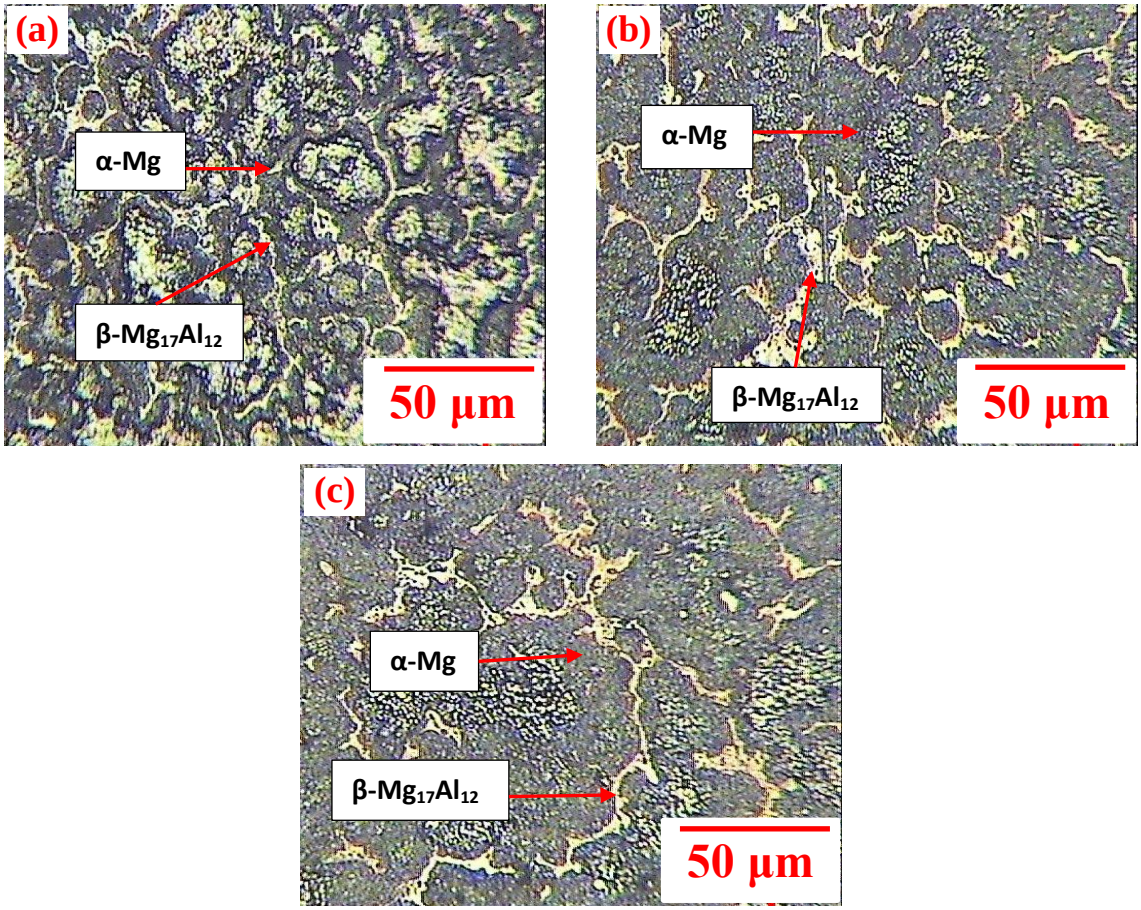

Figure 4.13 Optical microstructures of AZ91 alloy with 2% ZnO at 200x (a) Top section (b) Middle section (c) Bottom section.

The grains in the microstructure of the alloy given combined effect of mechanical vibration (15Hz- 2mm) and grain refiner (2 wt.%ZnO) became finer and uniformly distributed (Fig.4.14). This may be due to many heterogeneous nucleating sites are created prior to the formation of α- Mg with the addition of ZnO. Many of them turn into foundation of heterogeneous nucleation so the probability of nucleation of primary phase is increased. The increasing nuclei results in smaller particles. After the vibration was given to the melt, nuclei formed on the wall got fragmented. Moreover, there was a uniform distribution in the bulk which does not agglomerate. Subsequently, combined action of vibration and grain refiner resulted in finer and rounder particles [52].

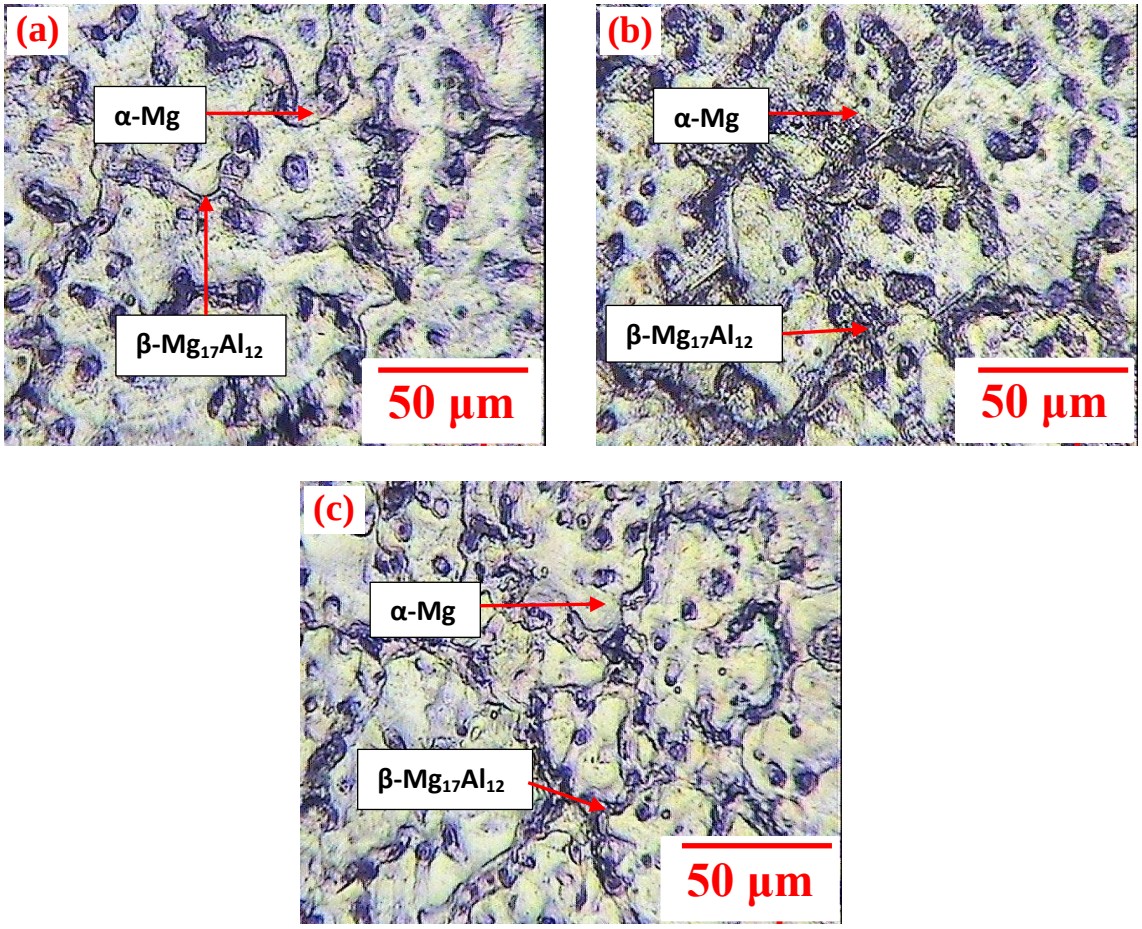

Figure 4.14 Optical microstructures of AZ91 alloy for 15Hz- 2mm + 2% ZnO at 200x (a) Top section (b) Middle section (c) Bottom section.

Figure 4.15 showing comparison in the grain size of the alloys given various treatments.

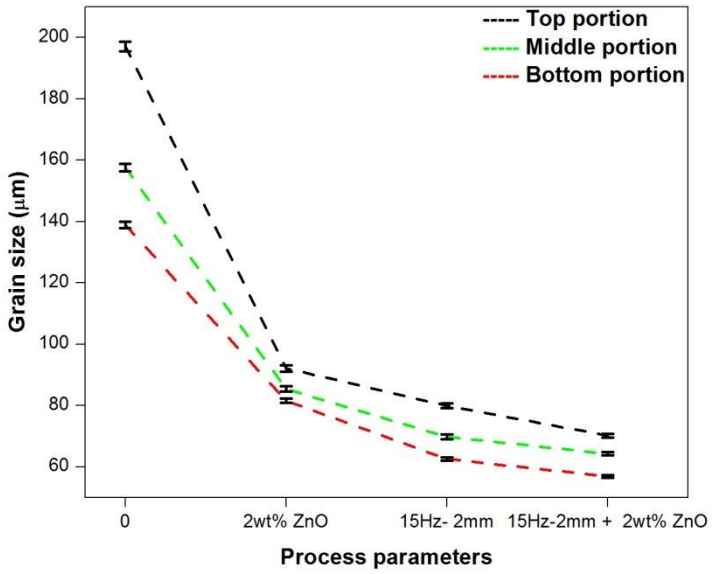

Figure 4.15 Effect of various process parameters on grain size of AZ91 alloy.

4.2.2 Scanning electron microscopy

The microstructure of AZ91 alloy is a mixture structure of α-Mg and precipitate of Al−Mg. The real cooling rate is difficult to be slow enough to maintain the equilibrium solidification; the actual solidification will deviate from the phase diagram. The eutectic temperature and the critical hypoeutectic content of aluminum both become lower under actual condition than those at equilibrium state [15]. The real solidification can be described using the dashed line in the non-equilibrium phase diagram, as shown in Fig. 2.1 (b). Figure 4.16 (a) shows the scanning electron micrographs of the bottom section of the as cast AZ91 Mg alloy. Figure 4.16 (b-d) shows the scanning electron micrographs of bottom section of the AZ91 alloy for condition A (imposition of mechanical vibrations at constant amplitude of 2mm and varied frequency 5- 25 Hz). It can be seen in Fig. 4.16 (a) that α-Mg grains are surrounded by coarse and reticular β- $Mg_{17}Al_{12}$ phase.

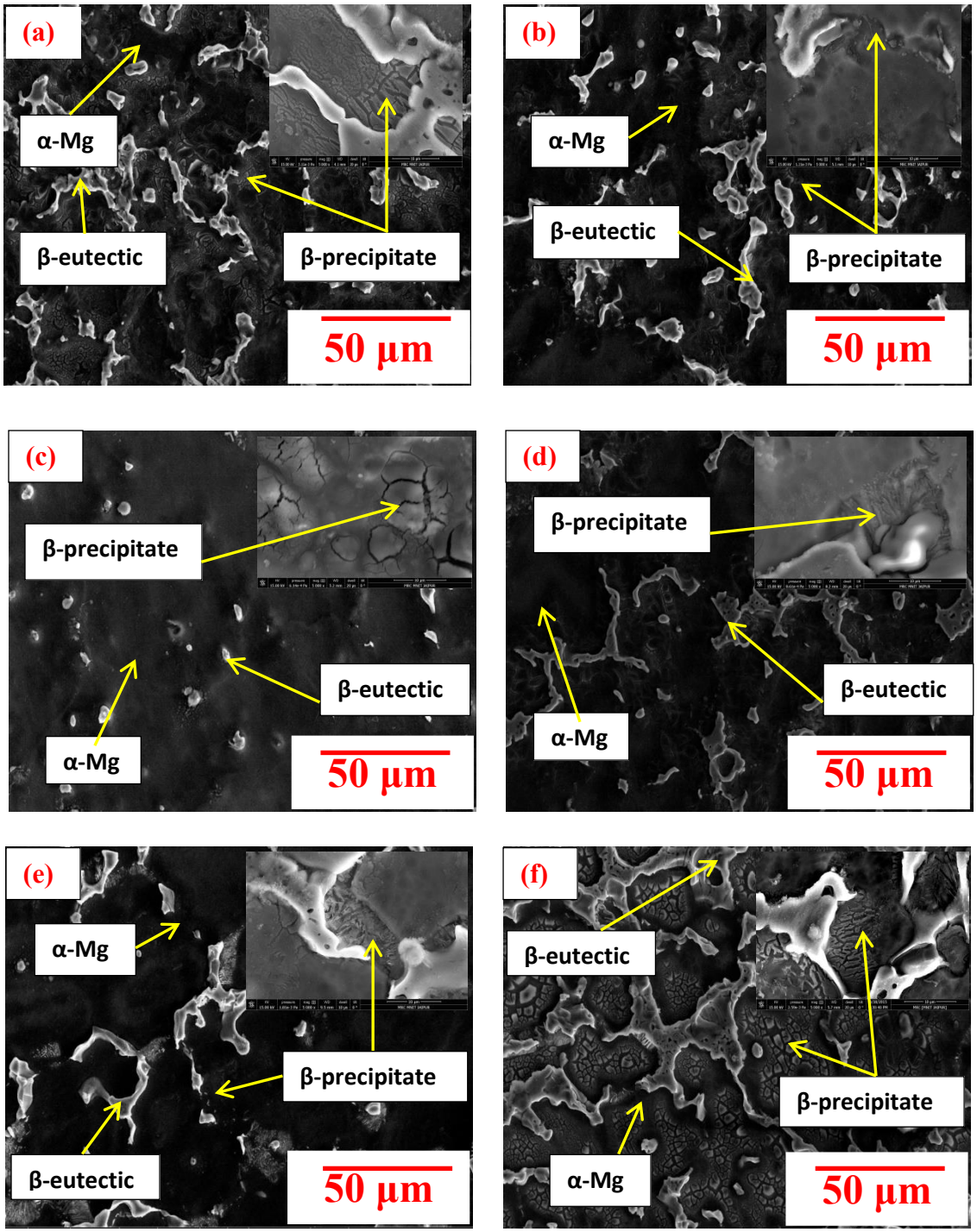

Figure 4.16 Scanning electron micrographs of the AZ91 alloy at 2 mm amplitude (a) as cast (b) 5 Hz (c) 10 Hz (d) 15 Hz (e) 20 Hz (f) 25 Hz.

The scanning electron micrograph exhibits three phases: α-Mg and β- ($Mg_{17}Al_{12}$) eutectic and β- precipitate. As stated above, the cooling rate is too high to maintain the homogeneity of aluminum during solidification resulting in high aluminum content in the remaining liquid at the end of solidification. In the further cooling procedure, β- $Mg_{17}Al_{12}$

precipitates into α-Mg matrix, especially in the divorced eutectic α-Mg matrix for its high aluminum content. The formation of the phases can be deduced as follows:

L → L + primary α → remaining L + primary α-Mg → divorced eutectic (α+β) + primary α-Mg → divorced eutectic (α+β) + precipitate β + primary α-Mg.

Figure 4.17 (a- b) shows the scanning electron micrographs of bottom section of the AZ91 alloy for condition B (imposition of mechanical vibrations at constant frequency of 15Hz and varied amplitude 0-3mm).

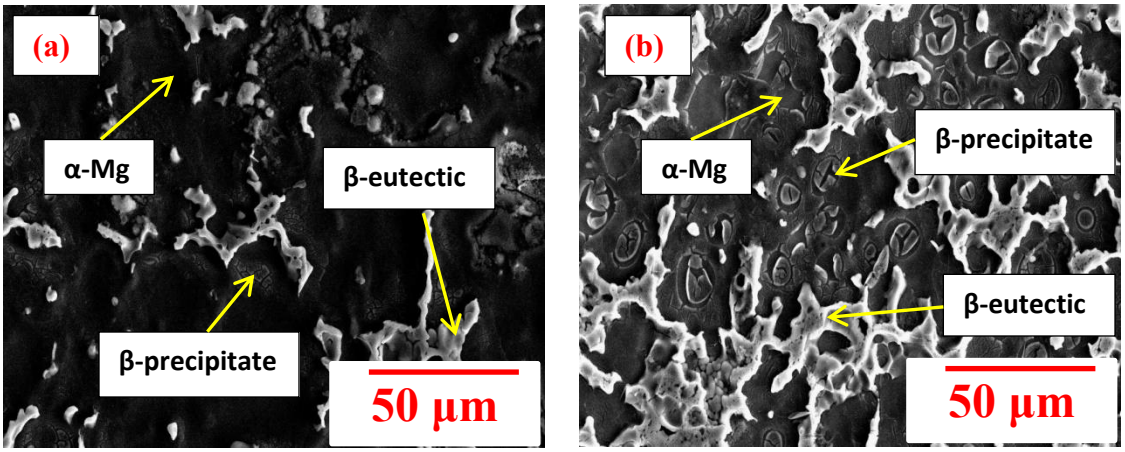

Figure 4.17 Scanning electron micrograph of the AZ91 alloy at 15 Hz (a) 1mm (b) 3mm.

$Mg_{17}Al_{12}$ phase is very brittle and its morphology, size, quantity and distribution have a great influence on the plasticity of Mg−Al alloys and leads to the limited ductility during deformation. In contrast, a structure of fine β- $Mg_{17}Al_{12}$ distributing in α-Mg matrix improves the formability of magnesium alloys significantly.

Figure 4.18 (a-b) shows the scanning electron micrographs of bottom section of the AZ91 alloy for condition C (addition of 2 wt% ZnO without and with vibration: 15 Hz- 2mm) respectively. In order to obtain perfect morphology of β- $Mg_{17}Al_{12}$ phase, mechanical vibrations were imposed and grain refiner (without and with vibration: 15 Hz- 2mm) was added to the AZ91 alloy.

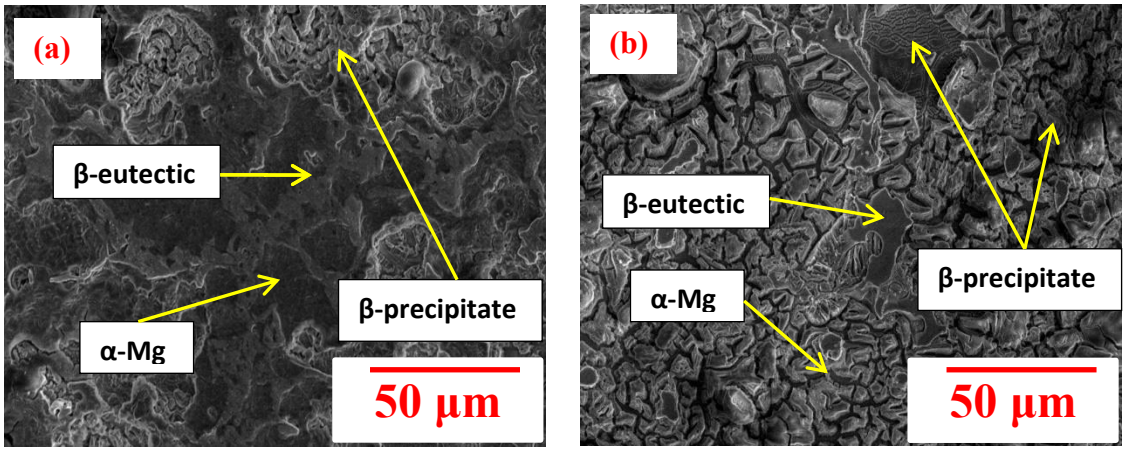

Figure 4.18 Scanning electron micrographs of AZ91 alloy (a) 2% ZnO (b) combination of 15Hz- 2mm + 2%ZO.

4.3 Porosity Measurement

Figure 4.19 shows the density of the AZ91 alloy for condition A with imposition of mechanical vibration at constant amplitude and varied frequency. The average density of the as-cast ingot obtained to be 1.795g/cm^3. When the alloy was given mechanical vibration at constant amplitude of 2mm and frequency of 5 Hz, the density of the alloy initially rises slowly. A further increase in frequency up to about 10 Hz- 2mm amplitude, the average density increases to a value of 1.8g/cm^3. The density of the alloy reaches to maximum of 1.812g/cm^3 at 15 Hz frequency and 2 mm amplitude of vibration. On further increasing the frequency at 20 Hz- 2mm amplitude and 25 Hz- 2mm amplitude, the density of the alloy decreases. This is because of the entrapment of air between the melt and the mold caused by the agitation in the melt through vibrations. [50].

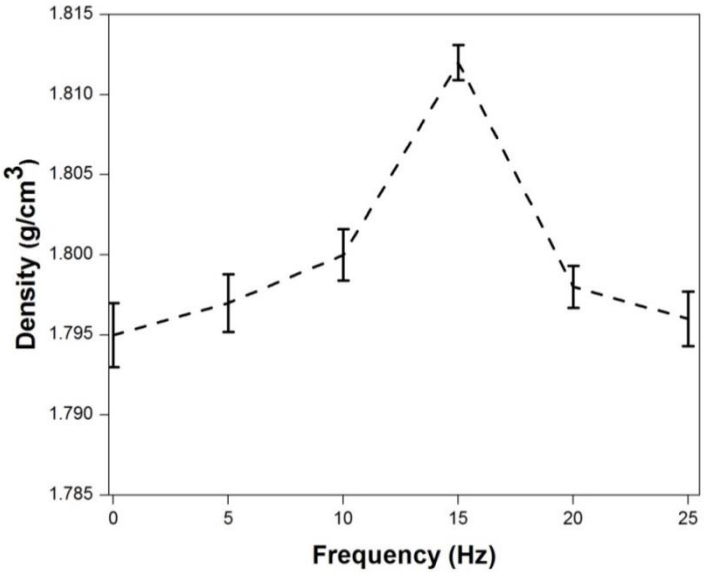

Figure 4.19 Effect of frequency at constant amplitude of 2mm on the density of the AZ91 Mg alloy.

Similarly, for condition B (Fig.4.20), at constant frequency of 15 Hz and increasing the amplitude at 1 mm and 2 mm the value of density increased, but on further increasing the amplitude to 3 mm and 15 Hz of frequency the density of the alloy decreased.

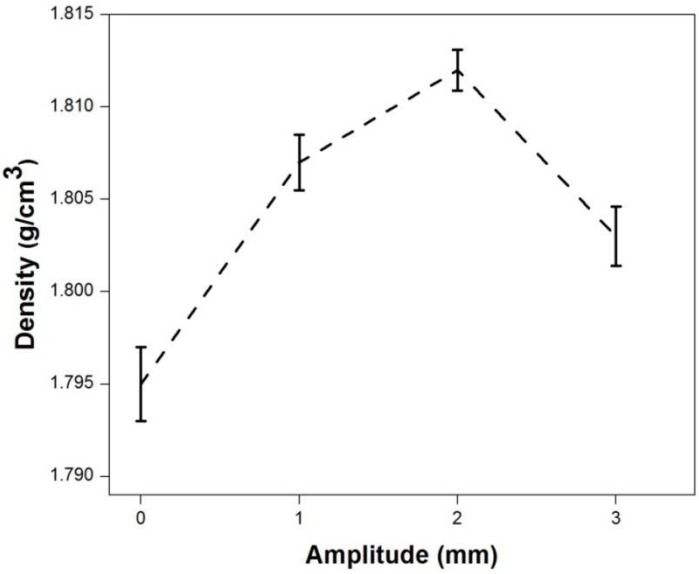

Figure 4.20 Effect of amplitude at constant frequency of 15Hz on the density of the AZ91 Mg alloy.

Figure 4.21 show the density for condition C i.e. alloy with the addition of 2 wt.% ZnO grain refiner without and with vibration (15 Hz- 2mm). On addition of grain refiner (2 wt.% ZnO) without vibration the value of density decreased as compared to the as cast alloy. This is probably because the melt has been oxidized with the addition of 2 wt.% ZnO without vibration. On, addition of the grain refiner (2 wt.% ZnO) along with the imposition of vibration the value of density increased and became almost similar to that of the vibration (15Hz – 2mm) imposed alloy. It is indicated that although unsoundness occurs due to gas porosity, imposition of the vibration and grain refiner affects largely the porosity. The result of this investigation shows the optimum results for alloy given combined effect of grain refiner and vibrations.

Combined action of addition of grain refiner (2 wt.% ZnO) along with the imposition of mechanical vibration (15 Hz- 2 mm) helps in the promotion of nucleation, reducing hydrogen, reducing porosities due to improved metal feeding and homogeneous microstructure [101]. The porosity existing in the structure of casting ingot is due to dissolved hydrogen in liquid and insufficient mass feeding of liquid both into spaces between dendrite arms [76]. In stationary condition, solidification starts at nucleation sites. The dendrites grow continuously and between the dendrite arms. The liquid in front of solid–liquid interface becomes enriched in hydrogen. Therefore, at the end of solidification, the increased hydrogen content in the spaces between dendrite arms allow hydrogen bubbles or pores to form. If the amount of dissolved hydrogen in the liquid is higher, gas is rejected and diffuses into bubbles during solidification. Thus, the size of the bubbles increased. The shrinkage causes a drop in local pressure of hydrogen in the liquid providing an additional driving force for cavity formation. However, bubbles that moved from interdendritic regions toward remaining liquids have not sufficient time to exit and elevate to the top of the mold during solidification. Therefore, they remain into the non-solidified liquids. Imposition of mechanical vibration led to decrease the size of primary α-Mg phase and fragmentation of β- $Mg_{17}Al_{12}$ phase. Due to decrease in the size of primary α-Mg and β- $Mg_{17}Al_{12}$ phases, amount of interdendritic channels increase while, volume of liquid between channels decreases. Then, size of gas cavities decreases and it facilitates their movement toward outside of interdendritic spaces. Addition of grain refiner (2 wt.% ZnO) along with the imposition of vibration (15 Hz- 2mm) during

solidification directly affects the dendritic structure. The liquid metal passes through the interdendritic channels to the pores easily as a result of combined action of addition of grain refiner (2 wt.% ZnO) along with the imposition of mechanical vibration (15 Hz- 2 mm). Vibration also acts to segregate the liquid from the solid by packing the solid down and displacing the liquid up. In this way, unidirectional solidification from the bottom is simulated and shrinkage porosity is suppressed. Porosity thus occurs chiefly in the upper part of the ingot since in this region the packing action by the solid crystals as a result of combined action is rather poor.

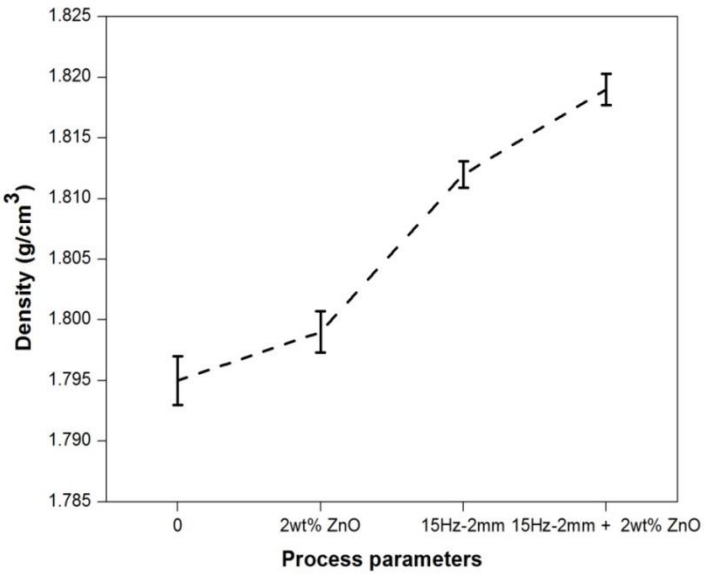

Figure 4.21 Effect of various process parameters on the density of the AZ91 Mg alloy.

4.4 Mechanical Properties

The mechanical properties of magnesium alloys depend on several factors viz. grain size and microstructure, porosity and distribution of intermetallic constituents. In the case of magnesium alloys fine grains is one of the important factors that lead to improvement in mechanical properties.

4.4.1 Tensile properties

Figure 4.22 reveals the tensile properties for condition A i.e. the mechanical vibration treated AZ91 alloy at constant amplitude of 2 mm and varied frequency (5- 25 Hz).

Figure 4.23 and Fig. 4.24 show the tensile properties for condition B i.e. the mechanical vibration treated AZ91 alloy at constant frequency (15 Hz) and varied amplitude (1- 3 mm) and for condition C i.e. addition of grain refiner (2 wt.% ZnO) without and with vibration (15 Hz- 2mm) respectively. Cast magnesium alloy shows 140 MPa UTS. Imposition of mechanical vibrations increases the UTS of the alloy. For condition A, when the alloy was given mechanical vibration at constant amplitude of 2 mm and varied frequency (5- 25 Hz) the value of UTS increases. The maximum value of UTS of 168 MPa is observed at frequency of 15 Hz and 2 mm amplitude of vibrations. On further increasing the frequency of vibration at 20- 25 Hz at 2 mm of amplitude, the strength decreases. In accordance with the previous investigations, it was found that as cast alloy exhibited lower tensile strength of 111 MPa and yield strength of 73 MPa [102]**.** According to Olufemi et al. [40] mechanical vibrations enhanced the ultimate tensile strength of the alloy by 15% until maximum value is attained between 12 and 16 Hz. The existence of the coarse eutectic β- $Mg_{17}Al_{12}$ network at the grain boundaries, lessens the strength of the as cast alloy and also leads to the formation of cracks under lower stress during tensile deformation. While, after imposition of the vibration considerable splitting up of the coarse eutectic β- $Mg_{17}Al_{12}$ phase and substantial grain refinement results in higher strength of the alloy. Thus, lowering the probability of crack and debonding of the β-$Mg_{17}Al_{12}$ phase under lower stress, enhance ductility and strength of the sample. The UTS increase first with the increase in frequency of vibration till maximum UTS is reached. On further increasing the frequency of mechanical vibration the value of UTS dropped. Similar trend was observed for yield strength and % elongation.

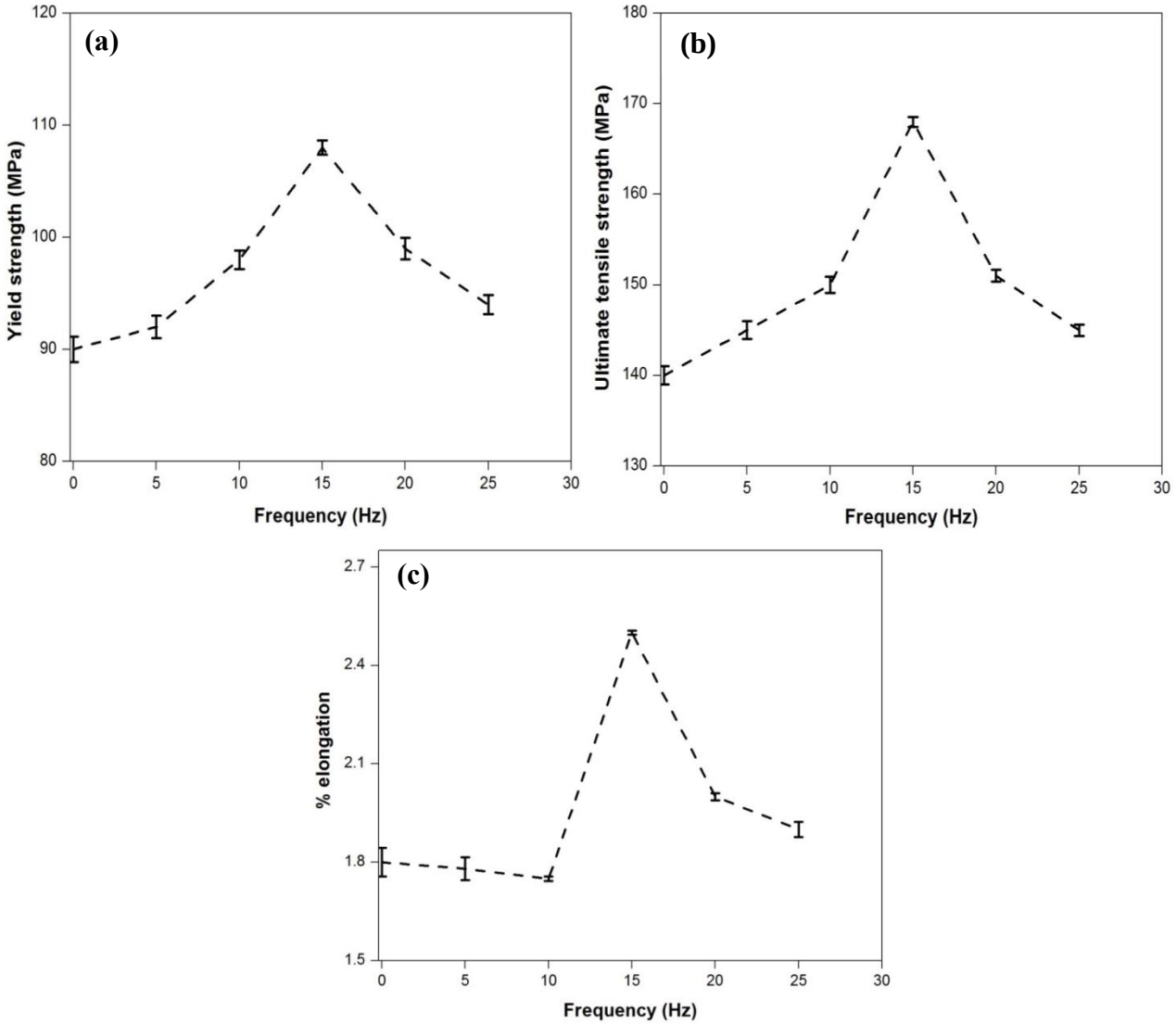

Figure 4.22 Effect of frequency at constant amplitude of 2mm on the tensile properties of the AZ91 Mg alloy.

For condition B, when the mechanical vibrations were imposed on the alloy at constant frequency (15 Hz) and varied amplitude (1mm- 3 mm) , it was found that the strength of the alloy increased on increasing the amplitude upto 2 mm- 15 Hz frequency. On further increasing the amplitude at 3 mm and 15 Hz frequency, the value of UTS decreased. Here also similar pattern was observed for yield strength and % elongation. According to Mollard et at. [103] mechanical vibrations are effective in increasing fluidity. Dendrites form during the solidification of the alloy. The dendritic structure of the alloy tends to have sharp-edged rims which commence region of stress- concentration.

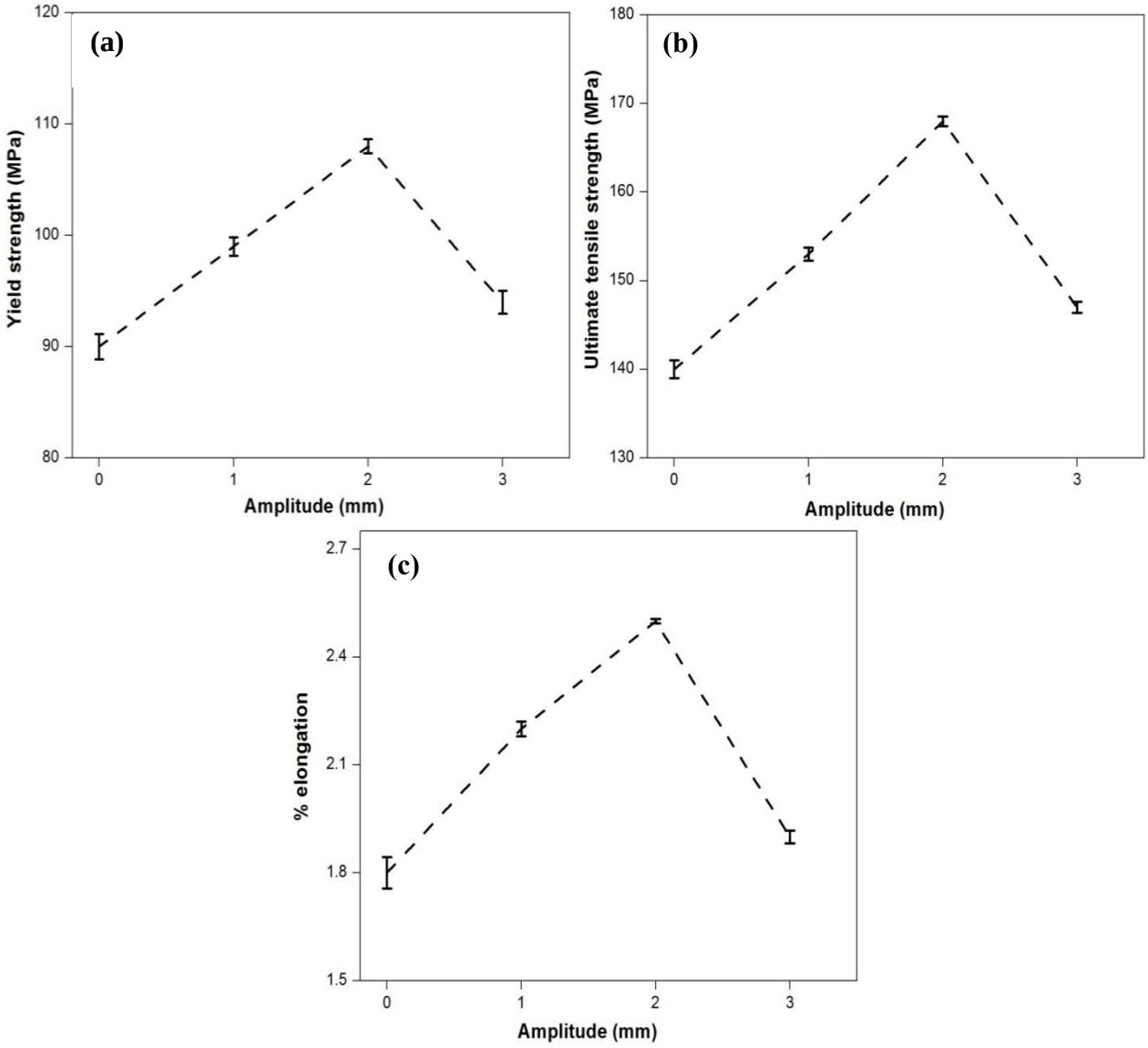

Figure 4.23 Effect of amplitude at constant frequency of 15Hz on tensile properties of the AZ91 Mg alloy.

For condition C, the ultimate tensile strength of the alloy was increased slightly when 2 wt.% ZnO was added without vibration as compared to the as-cast alloy. This may be due to the fine distribution of the β-phase which could perhaps enhance the strength of the alloy compared to the base alloy which has continuous brittle β-intermetallic phases. Owing to increased Zn solute with the addition of ZnO, solid solution strengthening of the alloys is thought to be accountable for the increased tensile strength. On giving the combined (2 wt.% ZnO + 15 Hz- 2mm) effect to the alloy, the tensile properties got enhanced. This may be due to the finer and uniform distribution of α- Mg and β-$Mg_{17}Al_{12}$ phases. As grain size is inversely proportional to the strength of the alloy. So, as the grain size decreases, strength of the alloy increases. HCP metals/ alloys have only 3 slip systems, while at least 5 active slip systems are required deformation to take place. HCP metals show strong impact of grain size on the strength as they have limited slip systems [104] in comparison to FCC and BCC metals. Thus, it can be said that fine grained Mg based materials have high strength.

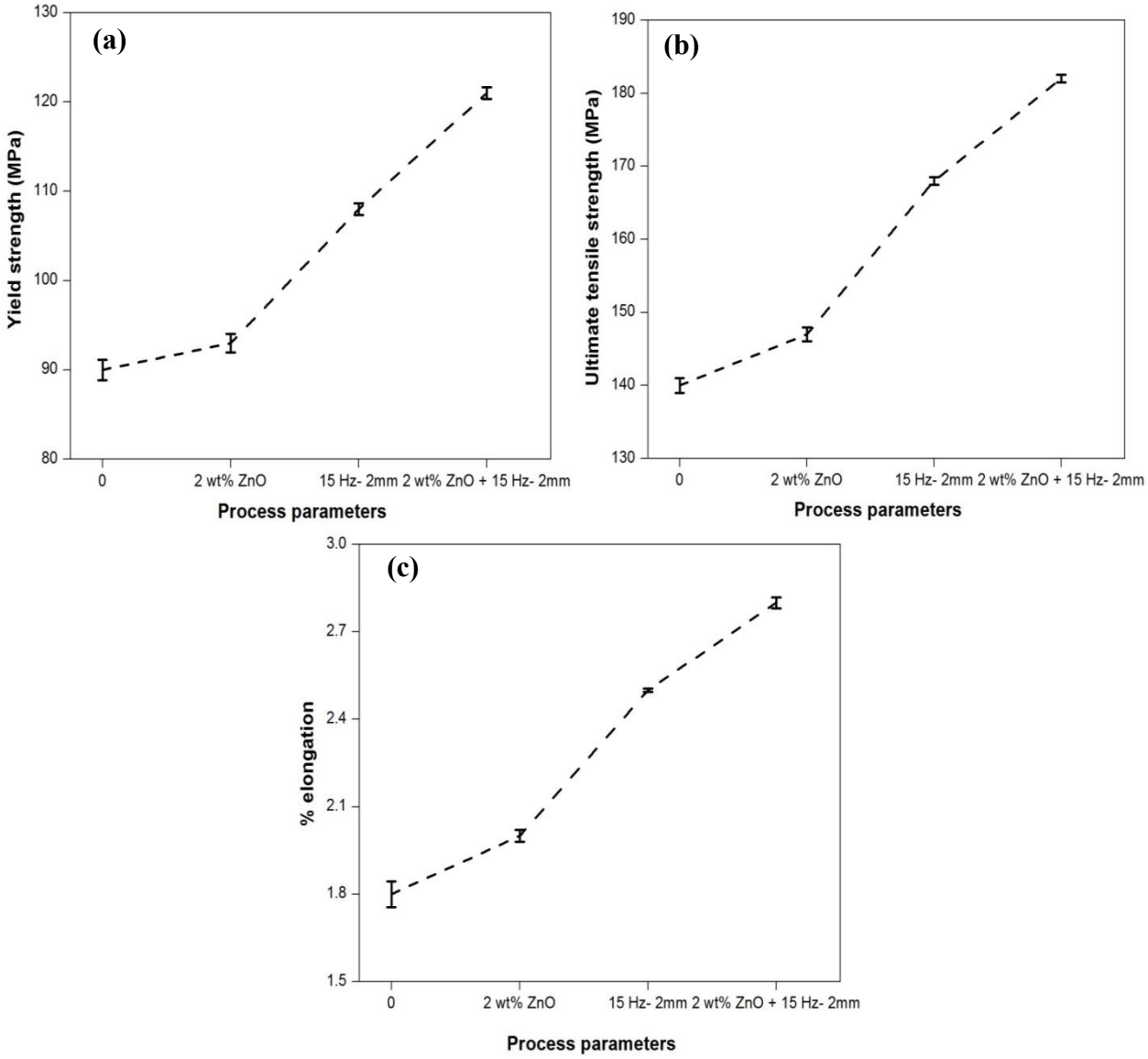

Figure 4.24 Effect of various process parameters on the tensile properties of the AZ91 Mg alloy.

4.4.2 Fractography

The number of active independent slip systems during deformation is responsible for the ability of Mg alloy to plastic deformation. For homogeneous plastic deformation to take place at least five independent slip systems are required. In HCP metals/ alloys, slip is much more limited and very difficult to exhibit the entity of five independent slip systems [105]. Therefore, HCP metals/ alloys are generally brittle. It has also been observed that lattice parameters perform a vital role in the determination of the operative slip system. In Mg alloys an ideal atomic packing exists when c/a = 1.632. Magnesium has slip planes at {0001} and slip directions of <1120>. Therefore, a total of three slip systems exist in magnesium alloys. Additional slip or twin systems needs to be activated for arbitrary plastic deformation which requires a much higher resolved shear stress resulting in the brittle behavior of magnesium alloys [106]. In magnesium alloys, the typical fracture modes are Cleavage and quasi- cleavage. $Mg_{17}Al_{12}$ phase is the chief strengthening intermetallic. The incompatibility of the BCC structure of $Mg_{17}Al_{12}$ with HCP structure of Mg- matrix escorted the fragility of Mg/ $Mg_{17}Al_{12}$ interface [107]. The SEM fractographs of tensile sample of AZ91 magnesium alloy without vibration and without addition of grain refiner (Fig.4.25 a) shows a brittle fracture behavior and cleavage crack. It can be elucidated by the fact that the sample without vibration has coarse and dendritic structure. The elongated particles fracture more often and easily than the spherical particles because they are the chief cause of stress concentration. There is a virtual continuous wall of β-eutectic surrounding the dendritic cell. During plastic deformation process, the dendrite cell act as grains and strong interaction between the particles and slip bands occur at the grain boundaries. Consequently, the final fracture path is liable to go through the β-eutectic particles and shows a brittle fracture nature indicating poor ductility. Figure 25 (b) shows deep and well distributed dimples with a high density at 15 Hz vibration frequency and 2mm of amplitude. The discontinuous cell boundaries in the microstructure are due to the refinement of the α-Mg and β-$Mg_{17}Al_{12}$ phases causing strong interaction between slip bands and plastic flow in the grain boundaries. The fractured β- particles generated in the grain boundaries permitting the final fracture path to traverse the β-$Mg_{17}Al_{12}$ phase besides the grain boundaries of primary α-Mg phase. That is why dimple rupture with cracked β- particles is responsible for the occurrence of fracture resulting in

a superior ductility [108]. When 2 wt.% ZnO was added to the AZ91 alloy, finer microstructure along with some secondary cracks and few dimples was observed. The combined action of grain refiner (2 wt.% ZnO) as well as vibrations (15 Hz- 2mm) showed the best results. The fracture surfaces were dominated by shallow dimple along with small cleavage planes that were more quasi-cleavage in nature, indicating higher ductility in alloys refined with the combined action of grain refiner (2 wt.% ZnO) and vibrations (15 Hz- 2mm). The alloy given combined action also has a finer, more fragmented and uniformly distributed β- phase. This might be responsible for the enhanced strength of the grain boundaries [6].

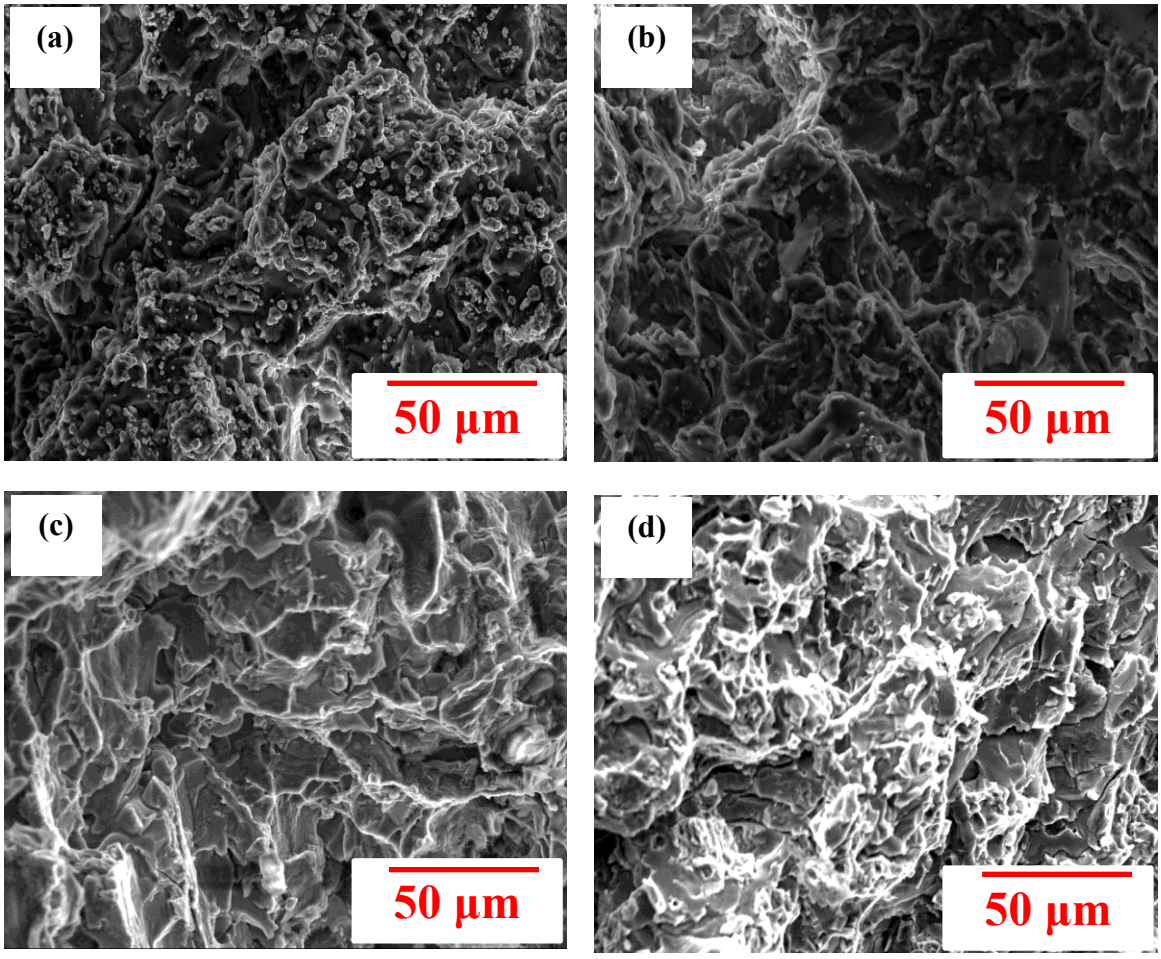

Figure 4.25 SEM fractographs of tensile test failed specimens (a) as cast (b) 15Hz - 2 mm (c) AZ91+ 2 wt.% ZnO (d) AZ91+ 2 wt.% ZnO + 15Hz - 2 mm.

4.4.3 Hardness

Figure 4.26 shows the influence of vibrations at constant amplitude and varied frequency (condition A) on hardness of the AZ91 alloy. The brinell hardness at the top section of the as cast alloy is 53 BHN while at the middle and bottom section hardness value is 55 BHN and 58 BHN respectively. Similar trend is observed in mechanically vibrated samples under different conditions. The brinell-hardness increases from 53 BHN to 66 BHN at 15 Hz frequency and 2 mm amplitude for the top section whereas for the middle and bottom portion the hardness increased from 55 BHN to 73 BHN and 58 BHN to 78 BHN respectively. On further increasing the frequency up to 25 Hz and 2 mm of amplitude the hardness of the top, middle and bottom portion decreases to 54 BHN, 56 BHN and 61 BHN respectively.

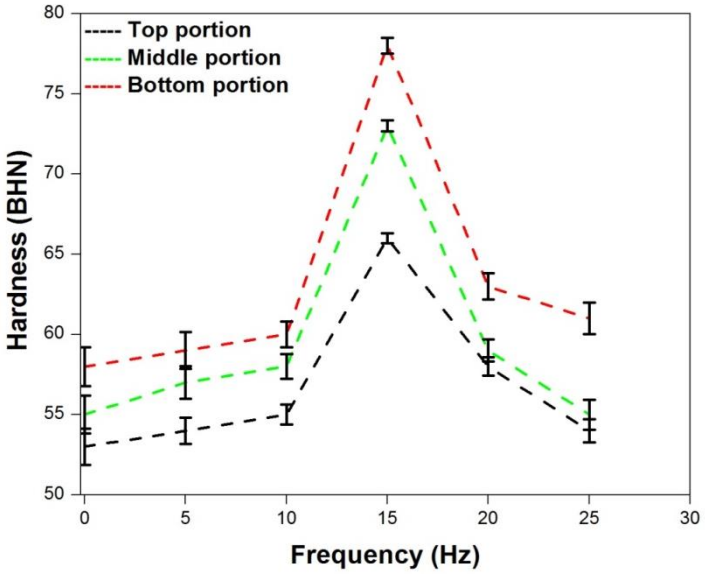

Figure 4.26 Effects of frequency of vibration on the hardness of the AZ91 sample (a) Top portion (b) middle portion (c) bottom portion.

Similarly for condition B, when the alloy was given mechanical vibration at constant frequency of 15 Hz and varied amplitude from 1- 3mm, the hardness for the bottom portion was the maximum as compared to middle and top portions (Fig.4.27). For 1mm amplitude - 15 Hz frequency the hardness at the top, middle and bottom sections was 64BHN, 69BHN and 72BHN respectively. On increasing the amplitude to 2mm- 15 Hz frequency, it has already been seen that the hardness for the top, middle and bottom

sections was 66BHN, 73BHN and 78BHN. While on further increasing the amplitude to 3 mm- 15 Hz frequency the hardness decreases to 64BHN, 70BHN and 72BHN for the top, middle and bottom sections respectively.

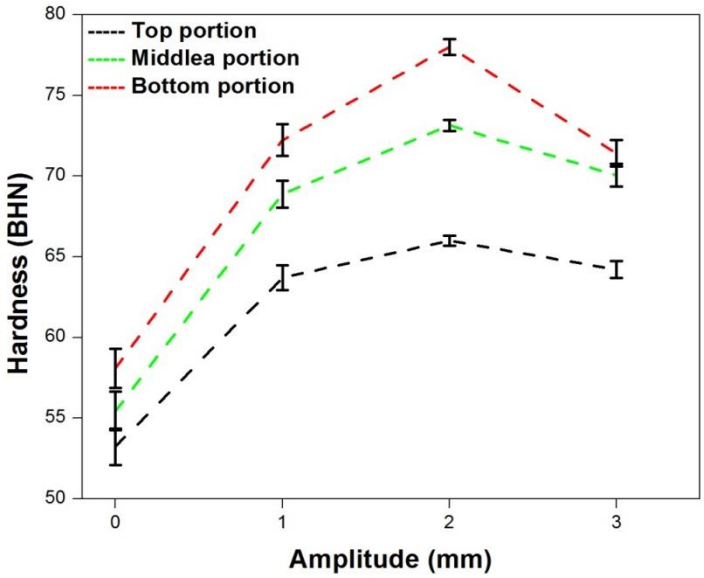

Figure 4.27 Effects of amplitude of vibration on the hardness of the AZ91 sample (a) Top portion (b) middle portion (c) bottom portion.

It is conspicuously revealed that the hardness of samples increases with the frequency and amplitude of vibration, reaches the maximum and then begins to fall to the minimum. The high hardness obtained at the bottom of each sample is attributed to the high cooling rate at the bottom of sample which promotes formation of fine grains. The fine grained material is harder and stronger than the coarse grained material as fine grained material has large grain boundary area to impede dislocation motion [18]. In addition to this the structures of the AZ91 alloys consist of a β- $Mg_{17}Al_{12}$ intermetallic phase at the grain boundaries. As the β- $Mg_{17}Al_{12}$ intermetallic phase solidifies last and fills interdendritic cavities, porosity, and the development of cracks get affected [40]. The uniform distribution and character of these brittle intermetallic compounds are also responsible for the increase in hardness. Therefore, combined effect of cooling rate and uniform distribution of β- $Mg_{17}Al_{12}$ are responsible for the increase in hardness. In condition C, when 2 wt.% ZnO grain refiner was added to the alloy without imposing the vibration the hardness of the alloy increased as compared to the as cast alloy. For top, middle and bottom sections, the hardness observed was 60BHN, 64BHN and 69BHN respectively.

The increase in hardness of the alloy with ZnO addition may also be related to solid solution strengthening of the matrix. On adding the grain refiner (2 wt.% ZnO) along with the imposition of vibration (15 Hz- 2 mm), the hardness of the alloy increased to a great extent (Fig.4.28). For this combined effect the hardness values for the top, middle and bottom sections were 72BHN, 79BHN and 92BHN respectively. This is again due to the finer and uniform microstructure of the alloy as well as increased density.

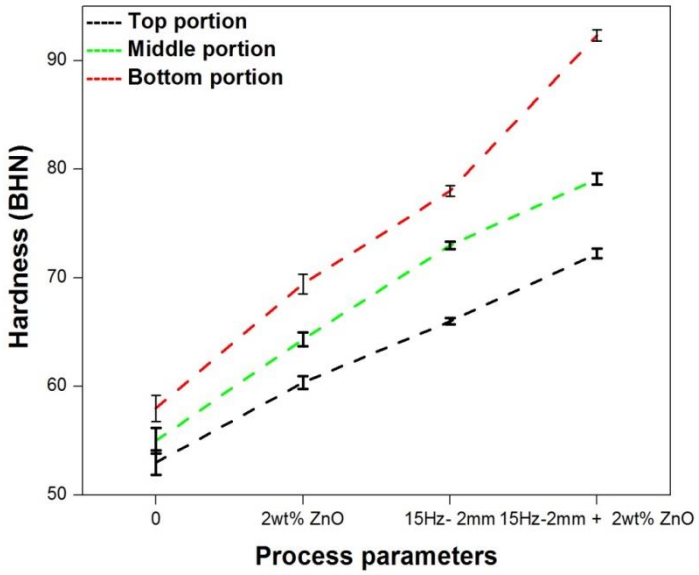

Figure 4.28 Effects of various parameters on the hardness of the AZ91 sample (a) Top portion (b) middle portion (c) bottom portion.

4.4.4 Friction coefficient and wear rate

The wear behavior of the AZ91 alloy at lower load of 5N and higher load of 10N was studied. Figure 4.29 (a) and Fig. 4.29 (b) show the coefficient of friction and wear rate respectively of the AZ91 alloy for condition A: with the imposition of mechanical vibration at varying frequencies (5- 25 Hz) and constant amplitude (2 mm). Figure 4.30 (a) and Fig. 4.30 (b) show the coefficient of friction and wear rate respectively of the AZ91 alloy for condition B: mechanical vibration treated alloy at varying amplitude (1 mm- 3 mm) and constant frequency (15 Hz). Figure 4.31 (a) and Fig. 4.31 (b) show the coefficient of friction and wear rate respectively of the AZ91 alloy for condition C: with the addition of 2 wt.% ZnO grain refiner without and with vibration (15 Hz- 2 mm) respectively.

When sample comes in contact with rotating disc, frictional heat generates due to which softening of the pin surface may take place. For condition A, at lower load of 5N, the value of coefficient of friction was maximum for as cast alloy (0.59) during sliding at $1ms^{-1}$ and it dropped to 0.41 when the alloy was given vibration at a frequency of 5Hz and 2 mm amplitude. The friction gradually decreased with the increase in frequency, and reaches minimum to 0.26 at a frequency of 15Hz and 2 mm amplitude. This is due to the refinement and uniform distribution of the β- phase. This value of coefficient of friction once again increases on increasing the frequency of vibration up to 25Hz and 2 mm amplitude. This increase in the value of COF is because of the coarse structure (Fig.4.6 and Fig.4.7) and increase in porosity of the alloy at higher frequencies. Similar pattern was observed for 10N load (Fig.4.29 a). However, at 10N load the coefficient of friction values were higher with corresponding values of load at 5N.The specific wear rates of the AZ91 alloy are plotted against the applied loads at 5N and 10N (Fig.4.29 b). At 5N load, there was a change in the slope of the wear rate curve at low frequency of 5Hz and 2 mm amplitude. The specific wear rate for the as cast alloy and the alloy with the imposition of vibration at 5 Hz frequency and 2 mm amplitude was 1.07 $x10^{-6}mm^3/Nm$ and 0.79 $x10^{-6}mm^3/Nm$ respectively. On further increasing the frequency, there was a decrement in wear rate and it reaches to minimum to a value of 0.51 $x10^{-6}mm^3/Nm$ when the vibration frequency was 15Hz and 2 mm amplitude. This is attributed to the fine and uniform distribution of the β- phase in the matrix and reduced porosity. The wear rates increased as frequency of vibration increases further to 20Hz- 2 mm amplitude and 25Hz- 2 mm amplitude, similar trend was also observed at 10N of load. However, at 10N load the specific wear rate was higher with corresponding values of load at 5N. The results commended that wear rate of AZ91 magnesium alloy considerably get affected by frictional heat that is been generated by the relative motion between AZ91 magnesium alloy and EN31 steel surface. At both the loads specific wear rate is decreasing upto 15 Hz and then increasing on further increasing the frequency to 20 Hz- 2 mm amplitude and 25 Hz- 2 mm amplitude.

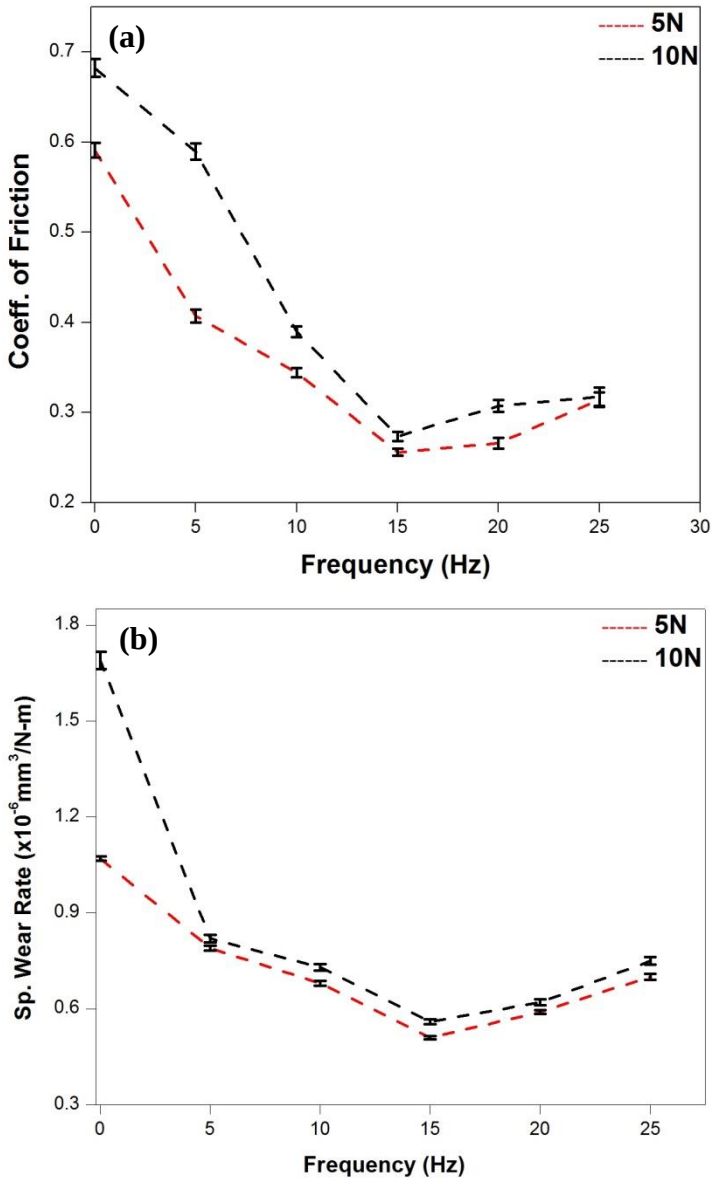

Figure 4.29 Effect of frequency of vibration at constant amplitude of 2mm on AZ91 at 5N and 10N loads (a) coefficient of friction (b) Sp. wear rates.

Figure 4.30 (a) and Fig.4.30 (b) show the coefficient of friction and wear rate respectively of the AZ91 alloy for condition B also when the alloy was treated with mechanical vibration at varied amplitude (1 mm- 3 mm) and constant frequency (15 Hz). On increasing the amplitude at 1mm and 15 Hz frequency there was drastic reduction (0.29) in the coefficient of friction as well as in the specific wear rate (0.88 $x10^{-6}mm^3/Nm$) of the alloy. On increasing the amplitude to 2mm and 15 Hz frequency, both the coefficient of friction and specific wear rate were minimum i.e 0.26 and 0.51 $x10^{-6}mm^3/Nm$. On further increasing the amplitude to 3mm and 15 Hz frequency the coefficient of friction and specific wear rate increased once again to a value of 0.28 and 0.68 $x10^{-6}mm^3/Nm$. It may be due to the coarse and non- uniform structure of the alloy. Similar trend was also observed at 10N of load.

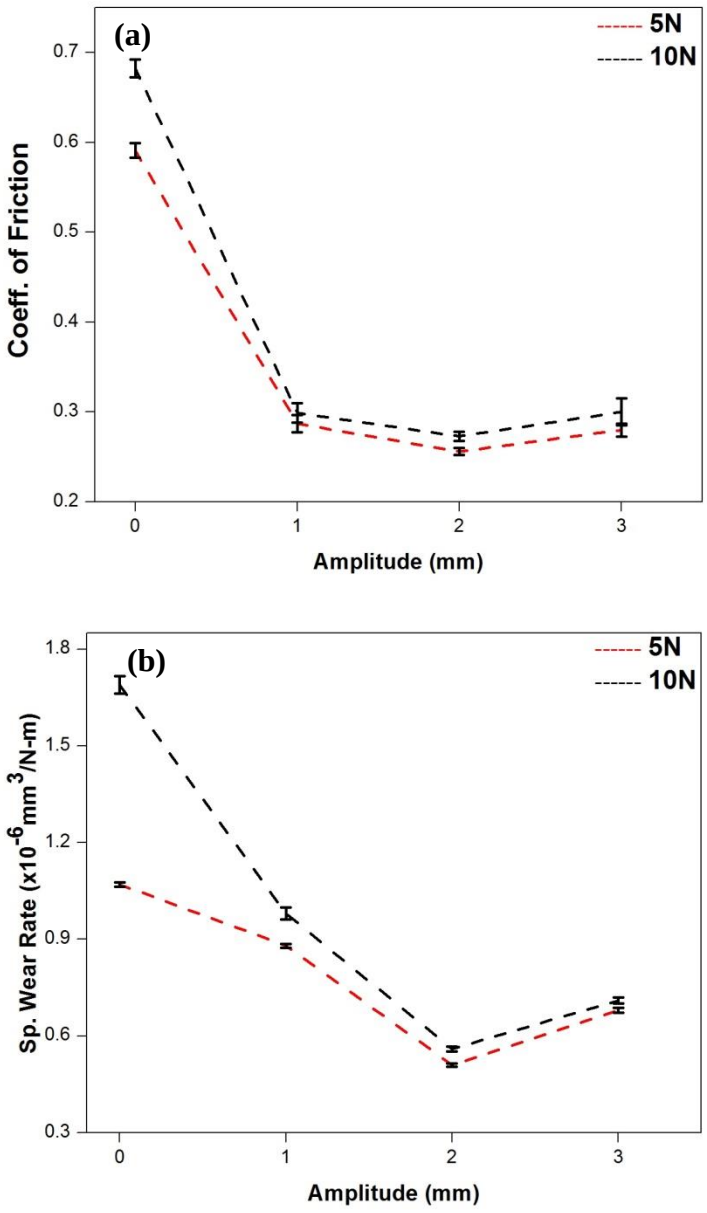

Figure 4.30 Effect of amplitude at constant frequency of 15 Hz on AZ91 at 5N and 10N loads (a) coefficient of friction (b) Sp. wear rates.

For condition C, it was found that on adding the grain refiner (2 wt.% ZnO) without vibration, both the coefficient of friction and specific wear rate were decreased to a value of 0.32 and 0.58 $x10^{-6}mm^3/Nm$, whereas, when the alloy was given combined effect of addition of grain refiner (2 wt.% ZnO) along with the imposition vibration (15 Hz- 2 mm), the coefficient of friction and specific wear rate showed the minimum values of 0.13 and 0.43 $x10^{-6}mm^3/Nm$. These minimum values of coefficient of friction and specific wear rate may be because of the fine and uniform distribution of the β- $Mg_{17}Al_{12}$ phase [109]. Here also similar trend was observed at 10N of load. Further, on comparing the COF and specific wear rates at both the loads, it was seen that the wear resistance of the alloy is much at 5N of load. Figure 4.31 (a) and Fig. 4.31 (b) show the coefficient of friction and wear rate of the AZ91 alloy for condition C with the addition of 2 wt.% ZnO grain refiner without and with vibration (15 Hz- 2mm) respectively. According to Iianaganar et al. [88] the actual area of contact to nominal area would increase on increasing the load leading increased frictional force between two sliding surfaces. The increased frictional force and real surface area in contact cause higher wear. Therefore, it could be said that on increasing the applied load, the wear resistance of the alloy with vibration at constant amplitude and varied frequency decreases. The best results were obtained for the given combined action of addition of grain refiner (2 wt.% ZnO) and imposition of vibrations (15Hz- 2mm) at both the loads.

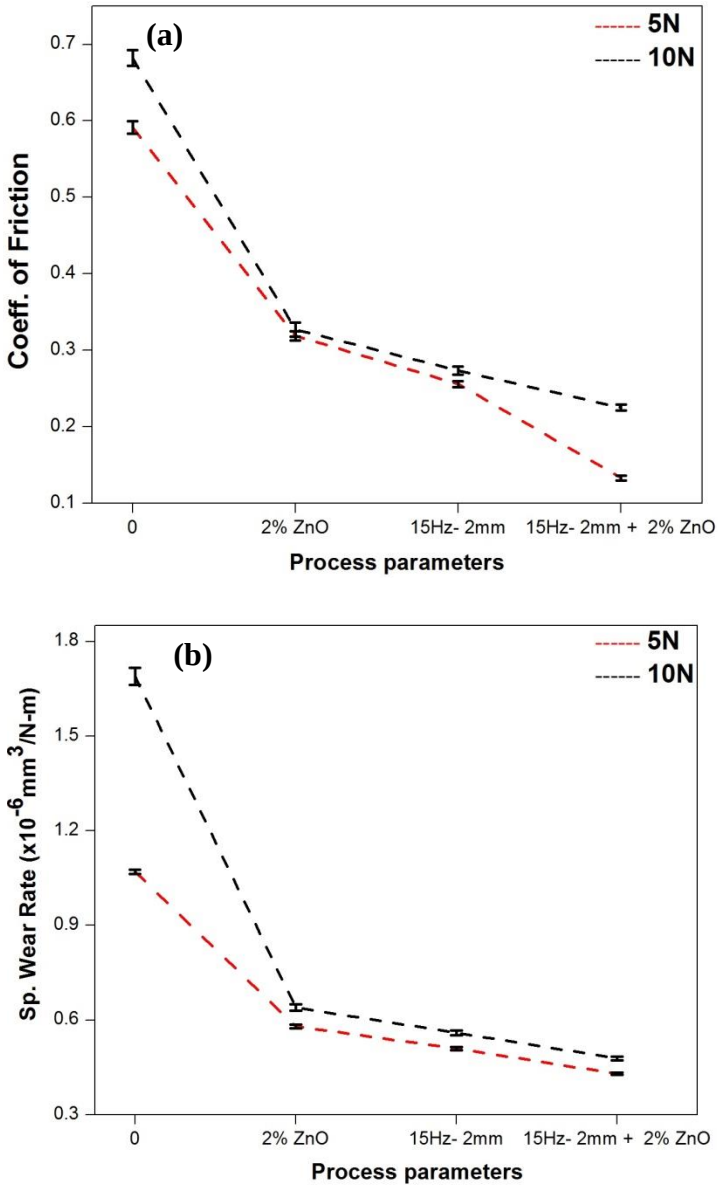

Figure 4.31 Effect of various process parameters on AZ91 at 5N and 10N loads (a) coefficient of friction (b) Sp. wear rates.

4.4.5 Analysis of worn surfaces

The worn pin surfaces under scanning electron microscope examination recognized four wear mechanisms operating under various processing conditions. They are abrasion, delamination, oxidation and plastic deformation. In the following sections, the observed wear mechanisms in relation to the processing conditions are identified for better understanding of the tribological behavior of AZ91 magnesium alloy.

Figure 4.32 (a- d) and Fig. 4.33 (a- d) show the FESEM micrographs of worn surfaces of the as cast and for condition A i.e. mechanically vibrated AZ91 alloy at constant amplitude of 2mm and varied frequency (5 Hz, 15 Hz, 25 Hz) at 5 N and 10 N loads respectively.

Analysis of worn surface of the as cast alloy

The wear track generated on as-cast AZ91 magnesium alloy is uneven/ irregular with deep and wide abrasive grooves as shown in Fig. 4.32 (a). When the as-cast AZ91 alloy pin slides on EN31 steel disc, it is plastically deformed and wear debris are formed [110]. Since, as-cast AZ91 pin is softer than tool steel disc, the loose worn debris embedded at the contact region of as-cast AZ91 pin. The entrapped debris particles produce further damage on both surfaces as a third-body abrasive and the debris itself undergoes delamination during the sliding. It is due to high friction caused by coarse grain size as well as inhomogeneous hardness of matrix and secondary phases. Similarly, at 10 N load worn surfaces of as-cast AZ91 magnesium alloy showed the same features and trends as observed at 5 N load (Fig. 4.33 (a)). However, the features of abrasive grooves, embedded debris and fracture fragments are more prominent than observed at 5 N loads. Wear remained oxidative in nature at both 5N and 10N loads.

Analysis of worn surfaces for condition A

Abrasive grooves, fracture fragments (delamination), oxides and embedded debris are also observed in vibration induced alloy at frequency of 5Hz and 2 mm amplitude (Fig. 4.32 (b)). However, these features are slightly lesser than that observed in as-cast AZ91 magnesium alloy. From the Fig. 4.32 (c), it can be seen that as the frequency of the

vibration is increased to 15 Hz and 2 mm amplitude, wear track generated are smooth with mild abrasive grooves. The reason for the low friction is due to optimum surface hardness and fine grain structure which reduced adhesion. The fine distributed second phase particles in vibrated (15Hz- 2mm) AZ91 magnesium alloy could also be beneficial for high wear resistance, as it has the tendency to provide some hardness in the matrix. As the frequency of vibration is increased further to 25Hz and 2 mm amplitude (Fig. 4.32 (d)), severe plastic deformation can be seen in large number. It is due to the increase the volume fraction of secondary phases after imposition of vibration at 25Hz and 2 mm amplitude, which provides inhomogeneous surface hardness. Similarly, at 10 N load worn surfaces of vibrated (at frequencies 5Hz, 15Hz, 25Hz and constant amplitude of 2 mm) AZ91 magnesium alloy showed the same features and trends as observed at 5 N load (Fig. 4.33 (b-d)). The features of abrasive grooves, embedded debris and fracture fragments are more prominent than observed at 5 N loads. These features are indicating the occurrence

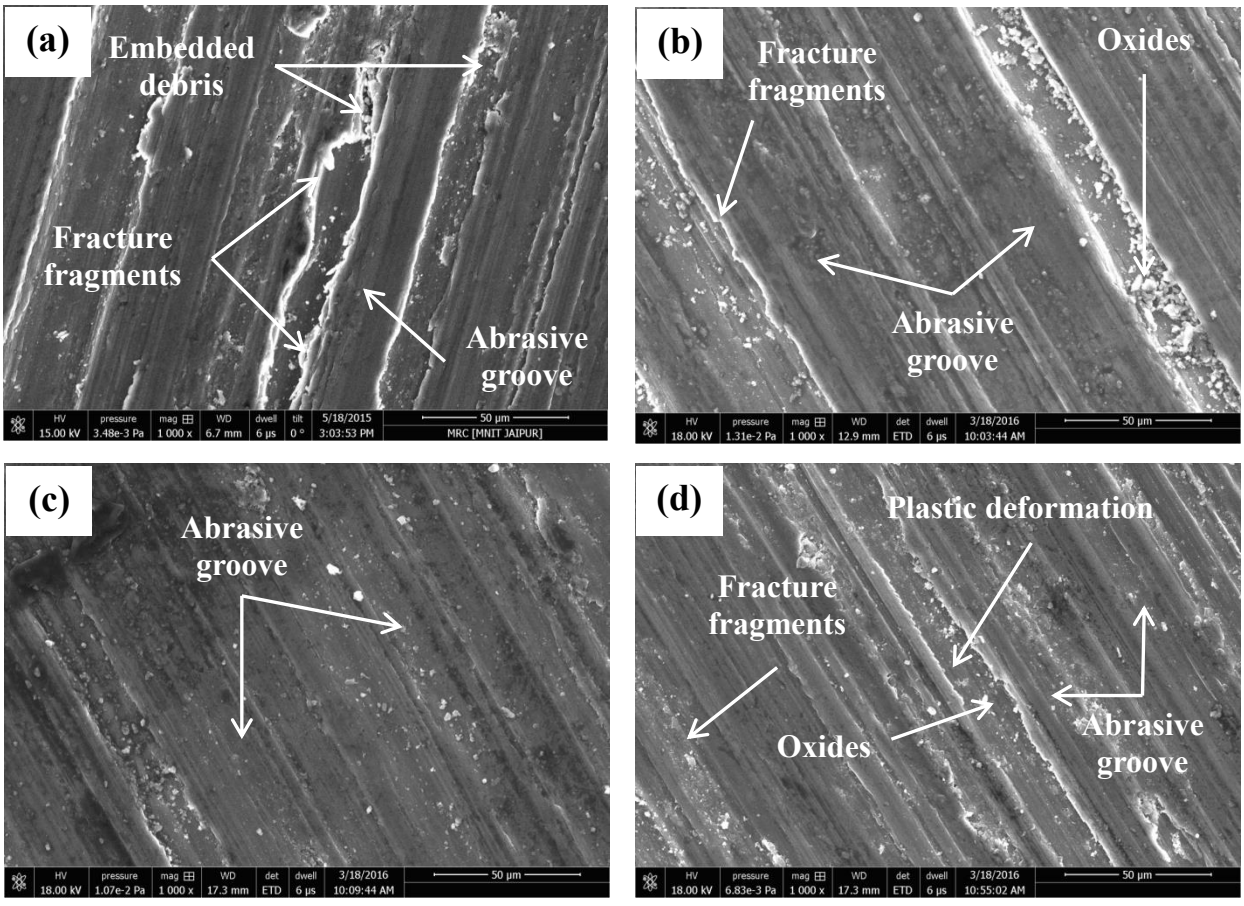

Figure 4.32 FESEM micrographs of worn surfaces of AZ91 magnesium alloy at 5 N load: (a) as-cast, (b) 5 Hz (c) 15 Hz (d) 25 Hz respectively.

of severe wear. The transition to severe wear accompanied by a significant increase in the roughness of worn surface of the samples [88]. It is observed that AZ91 magnesium alloy vibrated at 15Hz at both the loads (5N and 10N) could resist adverse conditions of wear better in comparison to the other vibrated alloys under similar conditions. In case of AZ91 Mg alloy vibrated at 15Hz, the presence of fine eutectic phase strengthens the magnesium matrix. In such cases, improvement in wear resistance was due to fine grains.

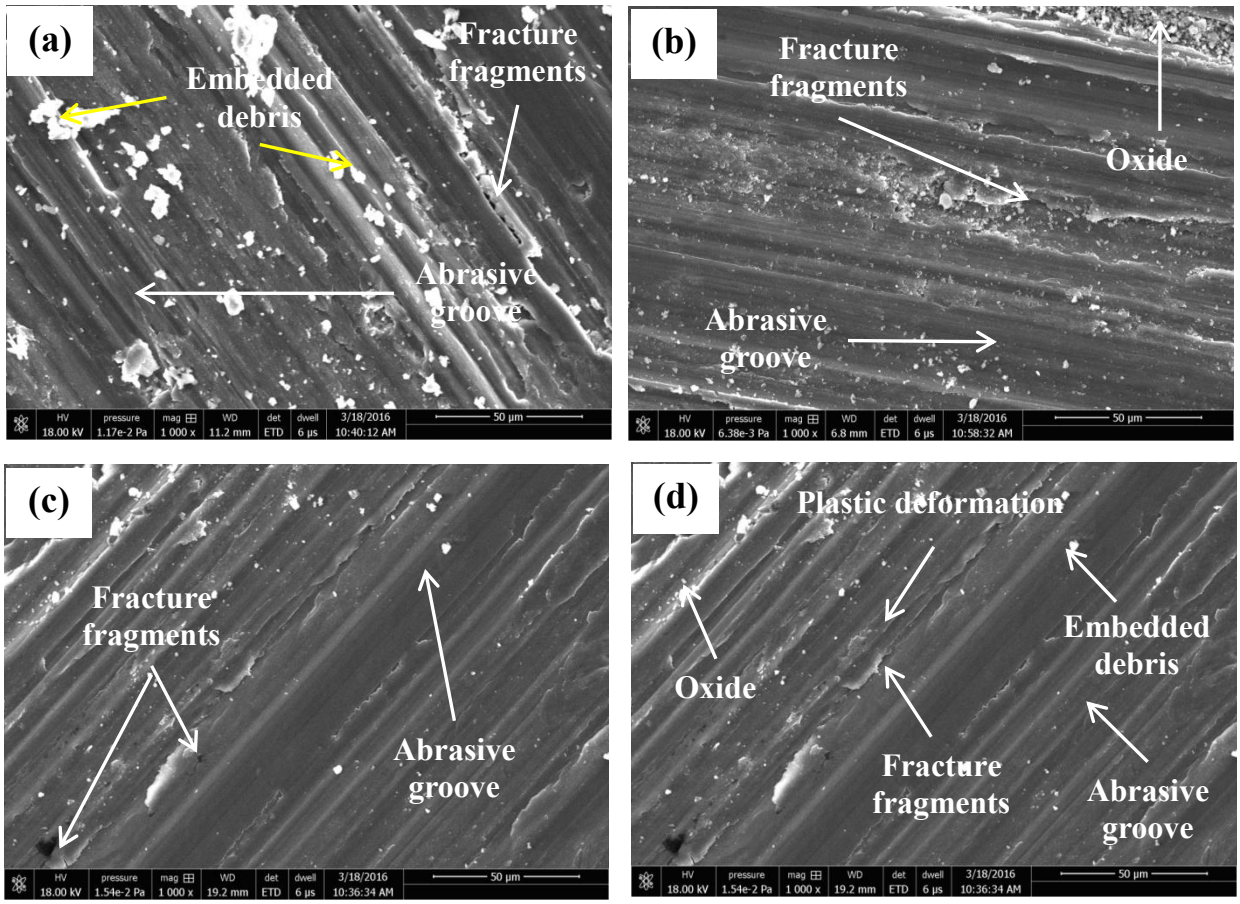

Figure 4.33 FESEM micrographs of worn surfaces of AZ91 magnesium alloy at 10 N loads: (a) as-cast (b) 5 Hz (c) 15 Hz (d) 25 Hz respectively.

Analysis of worn surfaces for condition B

Figure 4.34 (a and b) and Fig.4.35 (a and b) show the FESEM micrographs of worn surfaces for condition B i.e. mechanically vibrated AZ91 alloy at constant frequency of 15 Hz and varied amplitude (1 mm and 3 mm) at 5 N and 10 N loads respectively.

Similar features of abrasive grooves, fracture fragments (delamination), oxides and embedded debris are also observed in vibration induced alloy at 1 mm amplitude and 15 Hz frequency (Fig. 34 (a)). Here also these features are slightly lesser than that observed in as-cast AZ91 magnesium alloy. As the amplitude of vibration is further increased to 3 mm and 15 Hz frequency in Fig. 4.34 (b), abrasive grooves, fracture fragments, oxides and embedded debris can be seen lesser in number as compared to 1 mm but higher than that of 2 mm and 15 Hz frequency. As the amplitude of vibrations increase the yield strength decreases and alloy gets softened. As a result the material becomes prone to fracture fragments and the debris spread out of the contact surface in the direction of sliding as well as by moving sideways [110]. Similarly, at 10 N load worn surfaces of vibrated (at 1 mm and 3 mm of amplitude) AZ91 magnesium alloy showed the same features and trends as observed at 5 N load (Fig. 4.35 (a and b)). The features of abrasive grooves, embedded debris, oxides and fracture fragments are more prominent for 10 N load than observed at 5 N load. Among the all worn surfaces of the vibration imposed AZ91 alloy, alloy vibrated at 15Hz- 2mm showed the best results in terms of worn feature like abrasive grooves (Fig. 4.32 (c) and Fig.4.33 (c)). It could be due to the combination of the sufficient hardness coupled with fine grain structure of vibrated (15Hz- 2mm) AZ91 magnesium alloy. From SEM observations of worn pin, it is seen that no single wear mechanism is responsible for damage of the pin surface. There are several mechanisms occurring during wear. Therefore, this is a complex phenomenon. The optimum mechanical properties are observed at 15Hz frequency and 2mm amplitude as the grain size was the fine at 15Hz frequency and 2mm amplitude.

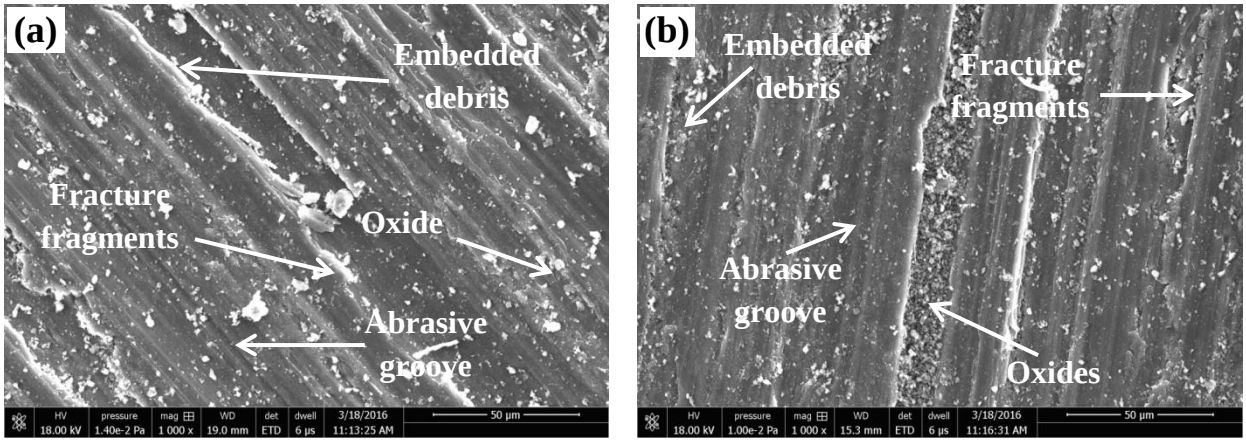

Figure 4.34 FESEM micrographs of worn surfaces of AZ91 magnesium alloy at 5 N load at 15 Hz: (a) 1mm (b) 3mm.

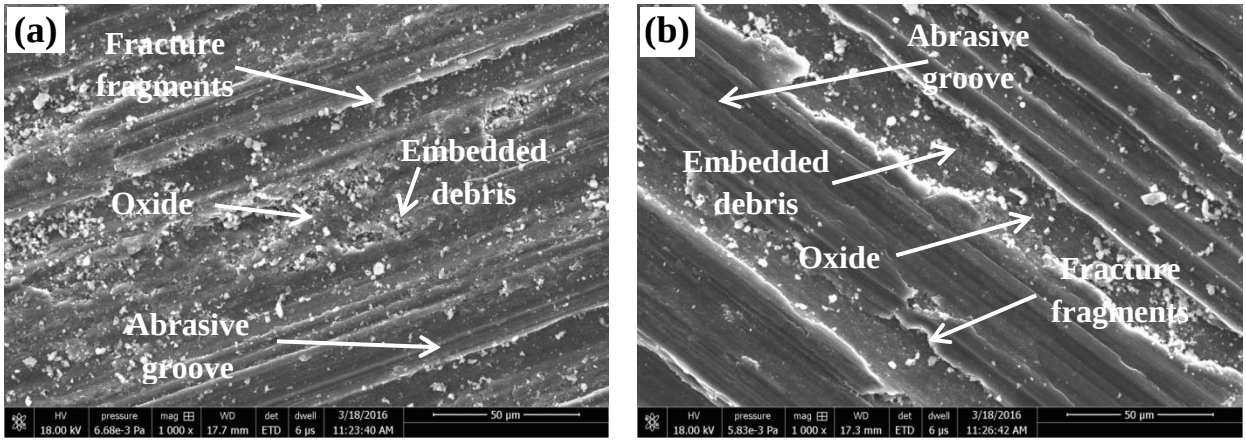

Figure 4.35 FESEM micrographs of worn surfaces of AZ91 magnesium alloy at 10 N load at 15 Hz: (a) 1mm (b) 3mm.

Analysis of worn surfaces for condition C

Figure 4.36 (a- b) and Fig.4.37 (a- b) show the FESEM micrographs of worn surfaces for condition C i.e. with the addition of 2 wt.% ZnO grain refiner to the AZ91 alloy without and with vibration (15 Hz- 2 mm) at 5 N and 10 N loads respectively.

When the alloy was given combined effect of addition of 2 wt.% ZnO grain refiner without imposition of vibration, features of abrasive grooves, fracture fragments (delamination) and severe plastic deformation are observed at 5 N load (Fig.4.36 (a)). The conversion to severe wear was complemented by a substantial increment in the roughness of the worn surface [78]. Similarly, at 10 N loads worn surface showed the same features and trends as observed at 5 N loads (Fig. 4.37 (a)). The features of abrasive grooves,

embedded debris and fracture fragments are more prominent for 10 N loads than observed at 5 N loads; again it is because of applied higher load, which helps to initiate high friction during wear process. When the 2 wt.% ZnO grain refiner was added to AZ91 alloy along with the imposition of vibration (15 Hz- 2mm), there were only abrasive grooves present on the worn surface at 5 N load, whereas on increasing the load to 10 N worn surface showed features of abrasive grooves, embedded debris and fracture fragments in very less amount.

It is observed that AZ91 magnesium alloy given combined effect of grain refiner (2 wt.% ZnO) and vibration (15 Hz- 2mm) at both the loads (5N and 10N) could resist adverse conditions of wear better in comparison to the other processed alloys under similar conditions.

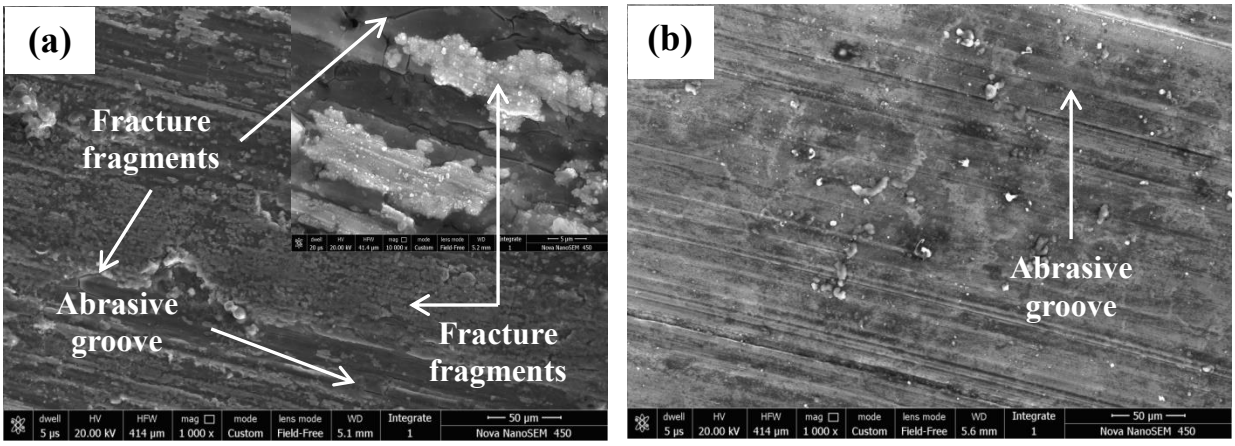

Figure 4.36 FESEM micrographs of worn surfaces of AZ91 magnesium alloy at 5 N load: (a) AZ91 + 2wt.% ZnO (b) AZ91 + 2wt% ZnO + 15Hz- 2mm.

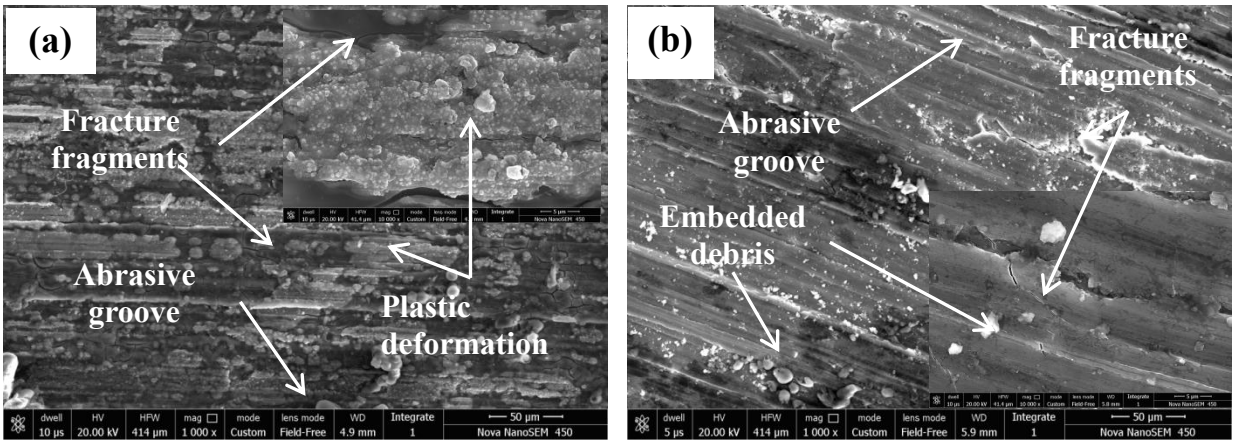

Figure 4.37 FESEM micrographs of worn surfaces of AZ91 magnesium alloy at 10N load: (a) AZ91 + 2wt.% ZnO (b) AZ91 + 2wt% ZnO + 15Hz- 2mm.

The presence of fine eutectic phase strengthens the magnesium matrix. In such cases, improvement in wear resistance was due to fine grains. Therefore, it is clear that the decrease in grain size results increase in wear resistance of grain refined AZ91 alloy. So, grain size is a vital parameter for better wear resistance [109].

4.4.6 Examination of wear debris

FESEM micrographs of wear debris of as-cast alloy and alloy with the imposition of vibration (15Hz- 2mm) and alloy with the addition of grain refiner (2 wt.% ZnO) without and with vibration (15 Hz- 2 mm) collected after sliding wear test at 5 N and 10 N are shown in Fig. 4.38 and Fig. 4.39 respectively. The as-cast AZ91 magnesium alloy at both 5 and 10 N load showed coarse debris as shown in Fig. 4.38 (a) and Fig. 4.39 (a). AZ91 magnesium alloy with the imposition of vibration at 15Hz frequency- 2mm amplitude

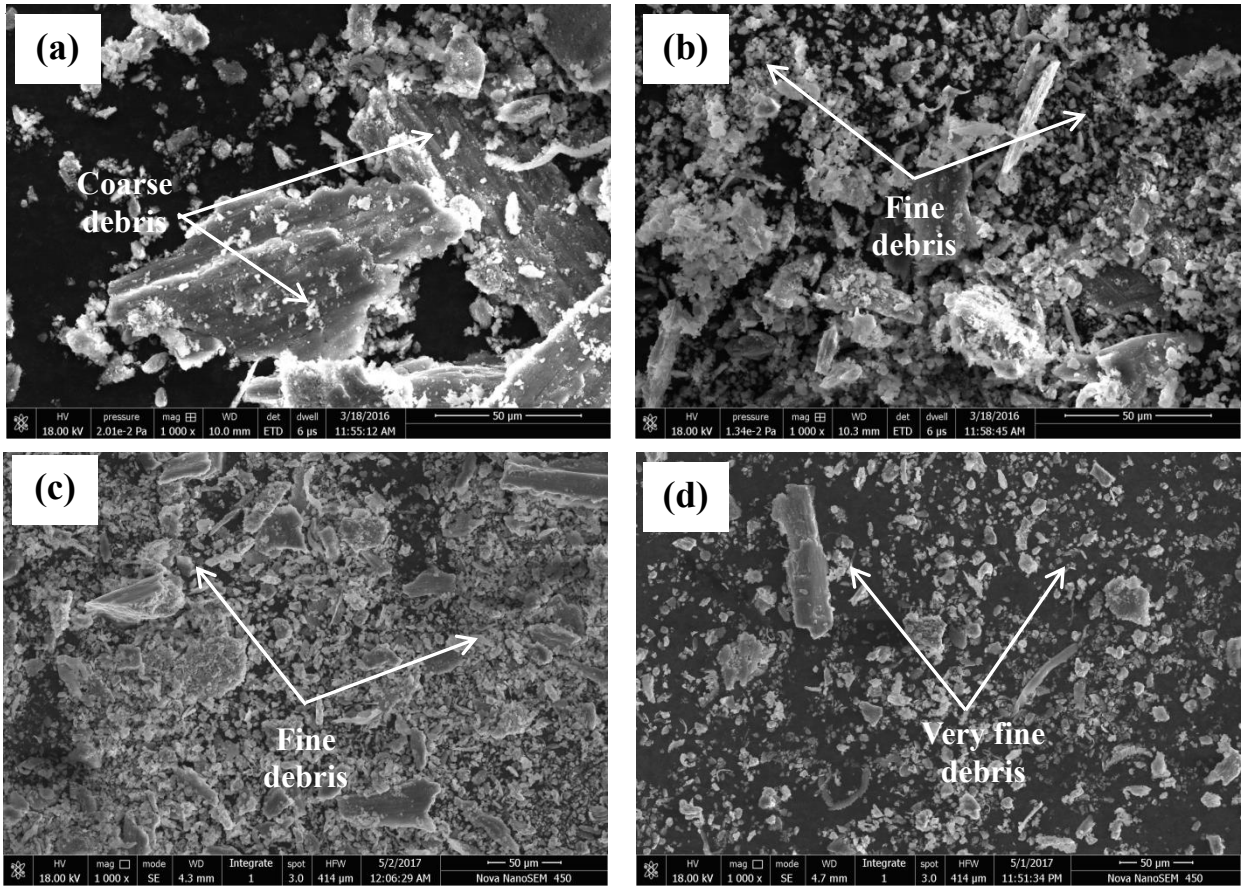

Figure 4.38 FESEM micrographs of worn debris of AZ91 magnesium alloy collected after wear test at 5 N loads (a) as-cast (b) AZ91+ 2 wt.% ZnO (c) 15 Hz- 2mm (d) AZ91+ 2 wt.% ZnO + 15 Hz- 2mm.

showed the fine debris as shown in Fig. 4.38 (b) and Fig. 4.39 (b). Similarly, Debris of the alloy with the addition of 2 wt.% ZnO showed fine particles as shown in Fig.4.38 (c) and Fig. 4.39 (c). But the debris of the alloy given combined action of addition of 2 wt.% ZnO along with the imposition of vibration (15 Hz- 2mm) showed very fine debris. Generally, fine debris is beneficial in term of wear resistance because fine particles in the debris reattached to form a transfer film on the surface of disc coming under sliding contact.

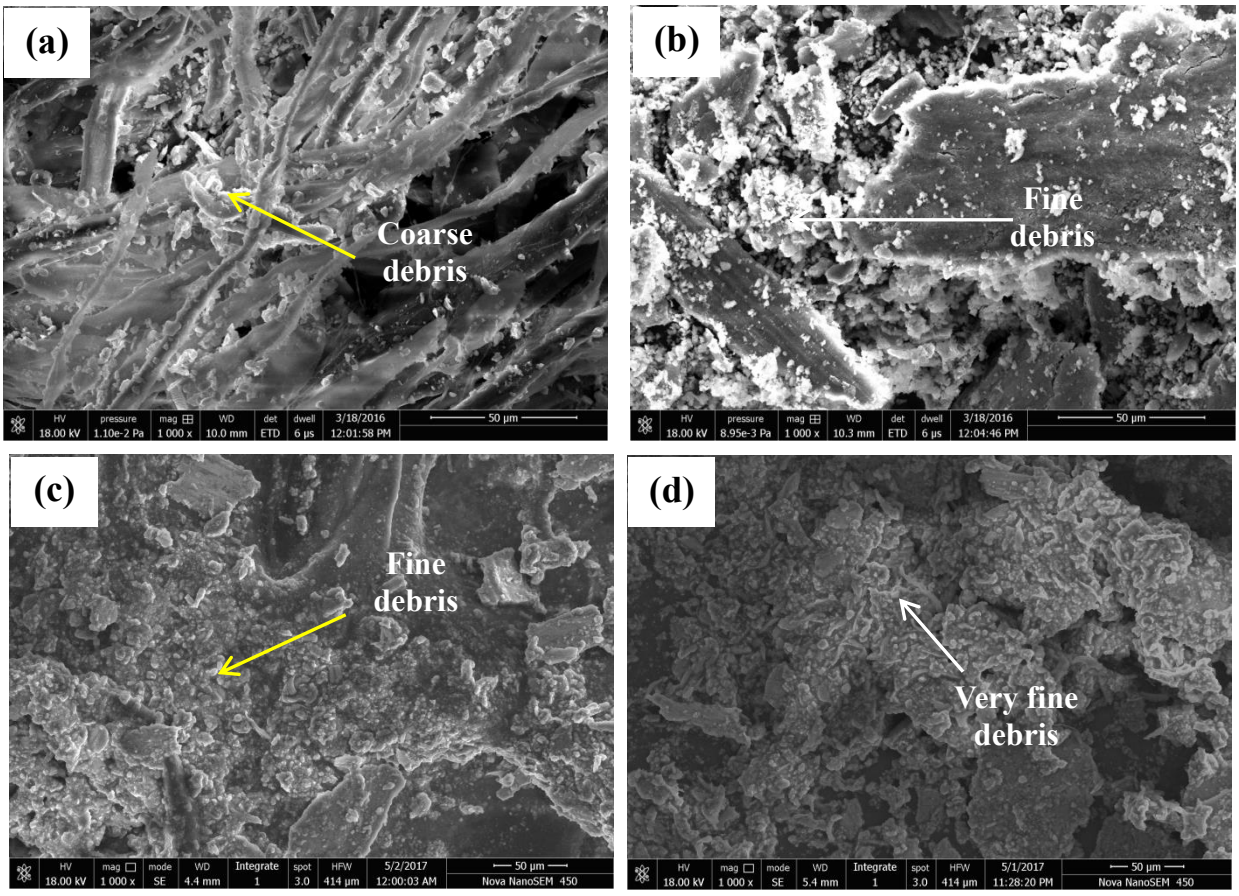

Figure 4.39 FESEM micrographs of worn debris of AZ91 magnesium alloy collected after wear test at 10 N loads (a) as-cast (b) AZ91+ 2 wt.% ZnO (c) 15 Hz- 2mm (d) AZ91+ 2 wt.% ZnO + 15 Hz- 2mm.

CHAPTER 5

CONCLUSIONS AND FUTURE WORK

This study was conducted with a view to examine the effectiveness of imposition of vibrations at various frequencies and amplitude and the addition of grain refiner (2 wt.% ZnO) without and with vibration in AZ91 magnesium alloy to determine its effects on grain refinement. The conclusions drawn from this study are as follows:

(i) Imposition of mechanical vibration at different frequency and amplitude to the solidifying AZ91 alloy leads to refinement of α- phase and fragmentation of the β- eutectic phase into small islands. The optimum results were obtained at 15 Hz frequency - 2mm amplitude of vibration.

(ii) The microstructure of the alloy when given combined action of vibration and grain refiner, α- phase became finer and spherical and the β- eutectic particles distributed uniformly and converted into small lamellae.

(iii) Imposition of mechanical vibration at different frequency and amplitude to the solidifying AZ91 alloy resulted in the increase in porosity. The optimum results of reduced porosity were obtained at 15 Hz frequency - 2mm amplitude of vibration ($1.812 g/cm^3$).

(iv) The combined action of vibration and grain refiner to the AZ91 alloy showed the minimum porosity. As the vibration along with the grain refiner promotes the filling ability and feeding capacity of the molten metal.

(v) Imposition of mechanical vibration at different frequency (5- 25 Hz) and amplitude (1- 3 mm) to the solidifying AZ91 alloy resulted in the increase in mechanical properties (ductility, % elongation, UTS and hardness) up to 15 Hz frequency and 2 mm of amplitude.

(vi) The combined action of vibration (15 Hz- 2mm) and grain refiner (2 wt.% ZnO) to the AZ91 alloy showed the best mechanical properties (ductility, % elongation, UTS and hardness) due to minimum porosity and much refined and fragmented α and β- phases respectively.

(vii) Fractographs of the fractured as- cast tensile samples showed brittle fracture behavior and cleavage crack. After imposing the vibrations up to 15 Hz frequency

- 2mm amplitude, alloy showed dimples which speaks of good plastic deformation prior to fracture.

(viii) The combined action of vibrations (15 Hz- 2mm) as well as grain refiner (2 wt.% ZnO) showed the best fractographs of the fractured tensile samples. The fracture surfaces were dominated by shallow dimple along with small cleavage planes that were more quasi-cleavage in nature, indicating higher ductility in alloys refined with the combined action of grain refiner and vibrations.

(ix) It is also observed that at both the loads (5N and 10N) AZ91 magnesium alloy vibrated at 15Hz- 2mm could resist adverse conditions of wear better than other respective conditions. The presence of fine eutectic phase strengthens the magnesium matrix which improved the wear resistance of the AZ91 alloy.

(x) The AZ91 magnesium alloy when given combined action (addition of 2 wt.% ZnO grain refiner along with the imposition of vibration at 15 Hz frequency and 2 mm amplitude) at both the loads (5N and 10N) showed best resistance to wear in comparison to the other processed alloys under similar conditions.

(xi) It is observed from worn surfaces of the samples, that different wear mechanisms occurred at 5 N and 10 N loads. However, the severity of wear was more at higher load of 10 N. At both the loads, the wear remained oxidative in nature.

From the above conclusions, it is observed that, among all the three conditions (i.e. condition A: At constant amplitude and varied frequency, condition B: At constant frequency and varied amplitude and condition C: Addition of grain refiner without and with vibration) the combined action of mechanical vibration along with addition of grain refiner has shown minimum porosity as combined action promoted the filling ability and feeding capacity of the molten AZ91 Mg alloy and thus lead to better mechanical properties such as ductility, % elongation, UTS, hardness and wear resistance.

Future Work

The suggestions for future work are;

(i) Tomography study on AZ91 Mg alloy may be done to get the internal structure of the alloy.

(ii) Transmission electron microscopy may be studied to examine the orientation relationship of the phases present in the alloy.

(iii) To study the effect of mechanical vibrations and combined action of mechanical vibrations and grain refiner on hot tearing during solidification.

(iv) To study the effect of mechanical vibrations at higher frequencies, acceleration, intensity and vibrational forces on AZ91 alloy.

REFERENCES

[1] Y. Kojima, Project of platform science and technology for advance magnesium alloys, Mater. Trans. 42 (2001) 1154–1159.

[2] M. Li, T. Tamura, N. Omura, K. Miwa, Effects of magnetic field and electric current on the solidification of AZ91D magnesium alloys using an electromagnetic vibration technique, J. Alloys Compd. 487 (2009) 187–193.

[3] Y. Mizutani, T. Tamura, K. Miwa, Effect of electromagnetic vibration frequency and temperature gradient on grain refinement of pure aluminum, Mater. Trans. 48 (2007) 538–543.

[4] U. Pandel, Studies on effect of vibrations during solidification on some cast Al- Si-Cu alloys, M.Tech. Thesis (1987).

[5] R.M. Pillai, K.S. Biju Kumar, B.C. Pai, A simple inexpensive technique for enhancing density and mechanical properties of Al-Si alloys, J. Mater. Process. Technol. 146 (2004) 338–348.

[6] S. Saha, C. Ravindran, Effects of Zinc oxide addition on the microstructure and mechanical properties of AZ91E Mg alloy, International Journal of Metal Casting 9 (2015) 39–48.

[7] H.M. Fu, D. Qiu, M.X. Zhang, H. Wang, P.M. Kelly, J.A. Taylor, The development of a new grain refiner for magnesium alloys using the edge-to-edge model, J. Alloys Compd. 456 (2008) 390–394.

[8] K. Lee, A study on grain refinement of AZ91E magnesium alloy with Al-5TiB2, Al- Al4C3 and ZnO additions, Master of Applied Science Thesis (2011).

[9] E.Meza Garcia, Ingenieurwissenschaften, Influence of alloying elements on the microstructure and mechanical properties of extruded Mg-Zn based alloys, Ph.D Thesis (2010).

[10] M.N. Khan, Solidification study of commercial magnesium alloys, Master of Applied Science Thesis, Concordia University Montreal, Quebec, Canada, (2009).

[11] Properties of Magnesium Alloys, http://mg.tripod.com/asm_prop.htm.

[12] A. Azad, Grain refinement of magnesium alloy AZ91E, Master of Applied Science Thesis (2012).

[13] F. Mordike, Magnesium technology- metallurgy, design data, applications, Springer, (2006).

[14] A.A. Luo, W. Sun, W. Zhong, J.C. Zhao, Computational thermodynamics and kinetics for magnesium alloy development, Adv. Mater. Process. 173 (2015) 26–30.

[15] J.Y. Li, J.X. Xie, J.B. Jin, Z.X. Wang, Microstructural evolution of AZ91 magnesium alloy during extrusion and heat treatment, Trans. Nonferrous Met. Soc. China 22 (2012) 1028–1034.

[16] S. Nafisi, Effects of grain refining and modification on the microstructural evolution of semi solid 356 alloy, Ph.D Thesis (2006).

[17] V. Raghvan, Materials science and engineering: A first course, PHI Learning (2004).

[18] W. Callister, Materials science and enginering, Wiley India (2009).

[19] F.C.Campbell, Phase Diagrams—understanding the basics, ASM International (2012) 429–446.

[20] J. Grandfield, D.G. Eskin, I. Bainbridge, Direct-Chill Casting of Light Alloys: Science and Technology, (2013) 424.

[21] K.U. Kainer, Magnesium: Proc. 7th Int. Conf. Magnes. Alloy. Their Appl., Germany (2007) 6–7.

[22] T.K. Loughnane, The Effect of Grain Refinement on the Castability of Magnesium-Aluminium Alloys, Ph.D Thesis, The University of Waikato, (2007).

[23] M. Easton, D. StJohn, Grain refinement of aluminum alloys: Part II. Confirmation of, and a mechanism for, the solute paradigm, Metall. Mater. Trans. A. 30 (1999) 1625–1633.

[24] A.K. Dahle, Y.C. Lee, M.D. Nave, P.L. Schaffer, D.H. StJohn, Development of the as-cast microstructure in magnesium - aluminium alloys, J. Light Met. 1 (2001)

61–72.

[25] D.H. StJohn, A.K. Dahle, T. Abbott, M.D. Nave, M. Qian, Solidification of cast magnesium alloys, Essent. Readings Magnes. Technol. (2014) 193–198.

[26] A.A. Shabana, Theory of vibrations - An introduction, Springer (1996).

[27] Eskin, Ultrasonic Treatment of Light Alloy Melts, CRC Press Taylor & Francis Group (2015).

[28] J. Campbell, Effects of vibration during solidification, Int. Mater. Rev. 26 (1981) 71–108.

[29] O. V Abramov, High-Intensity Ultrasonics: theory and industrial applications, CRC Press Taylor & Francis Group (1999).

[30] A. Ramirez, M. Qian, B. Davis, T. Wilks, D.H. StJohn, Potency of high-intensity ultrasonic treatment for grain refinement of magnesium alloys, Scr. Mater. 59 (2008) 19–22.

[31] M. Qian, A. Ramirez, A. Das, D.H. StJohn, The effect of solute on ultrasonic grain refinement of magnesium alloys, J. Cryst. Growth. 312 (2010) 2267–2272.

[32] Y.S. Yang, J.C. Wang, T. Wang, C.M. Liu, Z.M. Zhang, Effects of ultrasonic treatment on microstructures of AZ91 alloy, Trans. Nonferrous Met. Soc. China 24 (2014) 76–81.

[33] Z.H. Wang, X.D. Wang, Y.X. Zhao, W.B. Du, SiC nanoparticles reinforced magnesium matrix composites fabricated by ultrasonic method, Trans. Nonferrous Met. Soc. China 20 (2010) 1029–1032.

[34] M. Khosro Aghayani, B. Niroumand, Effects of ultrasonic treatment on microstructure and tensile strength of AZ91 magnesium alloy, J. Alloys Compd. 509 (2011) 114–122.

[35] D. Gao, Z. Li, Q. Han, Q. Zhai, Effect of ultrasonic power on microstructure and mechanical properties of AZ91 alloy, Mater. Sci. Eng. A. 502 (2009) 2–5.

[36] K.B. Nie, X.J. Wang, K. Wu, M.Y. Zheng, X.S. Hu, Effect of ultrasonic vibration and solution heat treatment on microstructures and tensile properties of AZ91

alloy, Mater. Sci. Eng. A. 528 (2011) 7484–7487.

[37] C.F.B. Kadir Kocatepe, Effect of low frequency vibration on macro and micro structures of LM6 alloys, Mater. Des. 28 (2007) 1767–1775.

[38] N. Abu-Dheir, M. Khraisheh, K. Saito, A. Male, Silicon morphology modification in the eutectic Al-Si alloy using mechanical mold vibration, Mater. Sci. Eng. A. 393 (2005) 109–117.

[39] N. Abu-Dheir, M. Khraisheh, K. Saito, A. Male, Effect of mold vibration on the solidification process during gravity die casting of AA 356, Solidification of Aluminum Alloys, TMS, 2004: pp. 361–368.

[40] A. Fatai Olufemi, I. Simeon Ademola, Effects of melt vibration during solidification on the mechanical property of Mg-Al-Zn alloy, Int. J. Metall. Eng. 1 (2012) 40–43.

[41] A. Abugh, I.K. Kuncy, Microstructure and mechanical properties of vibrated castings and weldments : A review, J. Eng. Stud. Res. 19 (2013) 7–12.

[42] Y.G. Zhao, Y.H. Liang, Q.D. Qin, W. Zhou, Q.C. Jiang, Effect of mechanical vibration on the microstructure, impact toughness and thermal fatigue behavior of cast hot working die steel, ISIJ Int. 44 (2004) 1167–1172.

[43] D.B. Goel, Effect of vibration during solidification on structure and mechanical properties of aluminum alloys, Ph.D Thesis, University of Roorkee, 1978.

[44] A. Maltais, M. Fiset, D. Dubé, Grain refinement of magnesium alloy AZ91D cast in permanent mold using mechanical vibrations, Mater. Sci. Forum. 426–432 (2003) 527–532.

[45] H.M. Guo, A.S. Zhang, X.J. Yang, M.M. Yan, Y. Ding, Microstructure formation and mechanical properties of AZ31 magnesium alloy solidified with a novel mechanical vibration technique, Metall. Mater. Trans. A. 45 (2014) 438–446.

[46] T.Tamura, T. Matsuki, K. Miwa, Effect of mechanical vibrations on microstructure refinement of Al-7 mass % Si alloys, Light Metals (2011) 827–830.

[47] K. Miwa, T. Tamura, M.J. Li, N. Omura, Y. Murakami, Effect of vibration during solidification to obtain high potential metallic materials, Mater. Sci. Forum. 690

(2011) 162–165.

[48] T.M. and K.M. Takuya Tamura, Refinement factors of mechanical vibrations on microstructure of Al-7 mass % Si alloys, Mater. Trans. 52 (2011) 830–833.

[49] M.H. and M.Y. Naoki Omura, Yuichiro Murakami, Mingjun Li, Takuya Tamura, Kenji Miwa, Hideki Furukawa, Eff ects of mechanical vibration on macrostructure and mechanical properties of AC4C aluminum alloy castings, Mater. Trans. 50 (2009) 2578–2583.

[50] N. Omura, Y. Murakami, M. Li, T. Tamura, K. Miwa, H. Furukawa, M. Harada, Effects of mechanical vibration on cooling rate and DAS of AC4C aluminum alloy gravity die castings, Mater. Trans. 50 (2009) 2604–2608.

[51] N. Omura, Y. Murakami, M. Li, T. Tamura, K. Miwa, H. Furukawa, M. Harada, M. Yokoi, Effects of Mechanical Vibration on Macrostructure and Mechanical Properties of AC4C Aluminum Alloy Castings, Mater. Trans. 50 (2009) 2578–2583.

[52] JW Zhao, SS Wu, LZ Xie, AN Ping, YW Mao, Effects of Vibration and grain refiner on microstructure of semisolid slurry of hypeoeutectic Al-Si alloy, Trans. Nonferrous Met. Soc. China. 18 (2008) 842–846.

[53] F. Taghavi, H. Saghafian, Y.H.K. Kharrazi, Study on the ability of mechanical vibration for the production of thixotropic microstructure in A356 aluminum alloy, Mater. Des. 30 (2009) 115–121.

[54] Y. Osawa, X. Liu, S. Takamori, H. Somekawa, T. Mukai, Effect of ultrasonic vibration pretreatment on microstructural evolution and mechanical properties of extruded AZ91 alloy, Mater. Trans. 49 (2008) 972–975.

[55] Y. Mizutani, T. Tamura, K. Miwa, Eff ect of electromagnetic vibration frequency and temperature gradient on grain refinement of pure aluminum, Mater. Trans. 48 (2007) 538–543.

[56] S. Guo, Q. Le, Y. Han, Z. Zhao, J. Cui, The effects of electromagnetic vibration on macrosegregation in AZ80 magnesium alloy billets, Mater. Trans. 47 (2006) 392–398.

[57] Y. Mizutani, Y. Ohura, K. Miwa, K. Yasue, T. Tamura, Y. Sakaguchi, Effect of the electromagnetic vibration intensity on microstructural refinement of Al-7%Si alloy, Mater. Trans. 45 (2004) 1944–1948.

[58] X.F. TIAN, Z.T. FAN, N.Y. HUANG, Effect of mechanical vibration on microstructure and mechanical properties of lost foam casting magnesium alloy, Chinese J. Nonferrous Met. 16 (2006) 1838–1844.

[59] T. Tamura, T. Matsuki, K. Miwa, Refinement Factors of Mechanical Vibrations on Microstructure of Al-7 mass% Si Alloys, Mater. Trans. 52 (2011) 830–833.

[60] F. Taghavi, H. Saghafian, Y.H.K. Kharrazi, Study on the effect of prolonged mechanical vibration on the grain refinement and density of A356 aluminum alloy, Mater. Des. 30 (2009) 1604–1611.

[61] Z. Zhao, Z. Fan, X. Dong, B. Tang, D. Pan, J. Li, Influence of mechanical vibration on the solidification of a lost foam cast 356 alloy, China Foundry. 7 (2010) 24–29.

[62] T. Motegi, Grain-refining mechanisms of superheat-treatment of and carbon addition to Mg-Al-Zn alloys, Mater. Sci. Eng. A. 413–414 (2005) 408–411.

[63] S. Karlsen, D.O.Oymo, D.Westengen, H.Pinfold, P.M.D. Stromhaug, Development of grain refiner for Al-containing Mg-alloys, Light Met. Process. Appl. (1993) 397–408.

[64] F. Xue, W. Du, Y. Sun, Microstructure refinement of magnesium based alloy, Mater.Sci.Forum 488–489 (2005) 143–146.

[65] L. Lu, A.K. Dahle, D.H. StJohn, Grain refinement efficiency and mechanism of aluminium carbide in Mg-Al alloys, Scr. Mater. 53 (2005) 517–522.

[66] Q. Jin, J.P. Eom, S.G. Lim, W.W. Park, B.S. You, Grain refining mechanism of a carbon addition method in a Mg-Al magnesium alloy, Scr. Mater. 52 (2005) 421–

[67] Y. Pan, X. Liu, H. Yang, Role of C and Fe in grain refinement of an AZ63B magnesium alloy by Al-C master alloy, J.Mater.Sci.Technol. 21 (2005) 822–826.

[68] D.H. StJohn, M. Qian, M.A. Easton, P. Cao, Z. Hildebrand, Grain refinement of magnesium alloys, Metall. Mater. Trans. A. 36 (2005) 1669–1679.

[69] P. Cao, M. Qian, D.H. StJohn, Effect of manganese on grain refinement of Mg-Al based alloys, Scr. Mater. 54 (2006) 1853–1858.

[70] R.C. Elsayed, K. Lee, Effect of Ca and Mn additions on the castability and mechanical properties of AZ91D Mg alloy permanent mold castings, AFS Trans. 117 (2009) 659–672.

[71] J. Du, J. Yang, M. Kuwabara, W. Li, J. Peng, Effects of manganese and/or carbon on the grain refinement of Mg-3Al alloy, Mater. Trans. 49 (2008) 139–143.

[72] Y. Wang, X. Zeng, W. Ding, Effect of Al-4Ti-5B master alloy on the grain refinement of AZ31 magnesium alloy, Scr. Mater. 54 (2006) 269–273.

[73] Y. Wang, H.Y. Wang, Y.F. Yang, Q.C. Jiang, Solidification behavior of cast TiB2 particulate reinforced Mg composites, Mater. Sci. Eng. A. 478 (2008) 9–15.

[74] J. Buha, Grain refinement and improved age hardening of Mg-Zn alloy by a trace amount of V, Acta Mater. 56 (2008) 3533–3542.

[75] S.S. Mishra, S.S. Sahu, V. Ray, Effect of mold vibration on mechanical and metallurgical properties of Al-Cu alloy, IJTRE 3 (2015) 131–134.

[76] K. Kocatepe, Effect of low frequency vibration on porosity of LM25 and LM6 alloys, Mater. Des. 28 (2007) 1767–1775.

[77] G. Chirita, I. Stefanescu, D. Soares, F.S. Silva, Influence of vibration on the solidification behaviour and tensile properties of an Al-18 wt%Si alloy, Mater. Des. 30 (2009) 1575–1580.

[78] A.W. El-Morsy, Dry sliding wear behavior of hot deformed magnesium AZ61 alloy as influenced by the sliding conditions, Mater. Sci. Eng. A. 473 (2008) 330–335.

[79] H. Hiratsuka, A. Enomoto, T. Sasada, Friction and wear of A12O3, ZrO2 and SiO2 rubbed against pure metals, Wear. 153 (1991) 361–373.

[80] A.Alahelisten, F.Bergman, M.Olsson, S.Hogmark, On the wear of aluminium and magnesium metal matrix composites, Wear. 165 (1993) 221–226.

[81] C.S.P.Rao, G. B. V. Kumar, N. Selvaraj, Mechanical and tribological behavior of

particulate reinforced aluminum metal matrix composites – A review, J. Miner. Mater. Charact. Eng. 10 (2011) 59–91.

[82] H. Chen, A.T. Alpas, Sliding wear map for the magnesium alloy Mg-9Al-0.9Zn (AZ91) 246 (2000) 106–116.

[83] J. An, R.G. Li, Y. Lu, C.M. Chen, Y. Xu, X. Chen, L.M. Wang, Dry sliding wear behavior of magnesium alloys, Wear 265 (2008) 97–104.

[84] P.J. Blau, M. Walukas, Sliding friction and wear of magnesium alloy AZ91D produced by two different methods, Tribol. Int. 33 (2000) 573–579.

[85] N.N. Aung, W. Zhou, L.E.N. Lim, Wear behaviour of AZ91D alloy at low sliding speeds, Wear. 265 (2008) 780–786.

[86] R. Jun, M. Ying, TJ Chen, X. Tao, YD Li, Friction and wear characteristic of AZ91D magnesium alloy under dry fricttion reciprocating sliding motion, Proceeding 4th China Int. Symp. Tribol., (2004) 285–291.

[87] A.J. Lopez, P. Rodrigo, B. Torres, J. Rams, Dry sliding wear behaviour of ZE41A magnesium alloy, Wear. 271 (2011) 2836–2844.

[88] E. Ilanaganar, S. Anbuselvan, Wear mechanisms of AZ31B magnesium alloy during dry sliding condition, Materials Today: Proceeding (2016) 1-9.

[89] Suh, The delamination theory of wear, Elsevier Sequoia, 1978.

[90] S. Das, S. V. Prasad, T.R. Ramachandran, Microstructure and wear of cast (Al-Si alloy)- graphite composites, Wear 133 (1989) 173–187.

[91] C.Y.H. Lim, S.C. Lim, M. Gupta, Wear behaviour of SiCp-reinforced magnesium matrix composites, Wear 255 (2003) 629–637.

[92] S. Das, A.T. Morales, A.T. Alpas, Microstructural evolution during high temperature sliding wear of Mg-3% Al-1% Zn (AZ31) alloy, Wear. 268 (2010) 94–103.

[93] A. K. Mondal, B.S.S. Chandra Rao, S. Kumar, Wear behaviour of AE42+20% saffil Mg-MMC, Tribol. Int. 40 (2007) 290–296.

[94] A. Zafari, H.M. Ghasemi, R. Mahmudi, An investigation on the tribological

behavior of AZ91 and AZ91 + 3 wt% RE magnesium alloys at elevated temperatures, Mater. Des. 54 (2014) 544–552.

[95] C. Taltavull, B. Torres, A.J. Lopez, J. Rams, Dry sliding wear behavior of AM60B magnesium alloy, Wear. 301 (2013) 615–625.

[96] A. Kumar, R. Kumar, S. Ansari, S.S. Mishra, Effect of mould vibration on microstructure and mechanical properties of casting during solidification, IJERT 3 (2014) 90–92.

[97] Y.J. Chen, W.N. Hsu, J.R. Shih, The effect of ultrasonic treatment on microstructural and mechanical properties of cast magnesium alloys, Mater. Trans. 50 (2009) 401–408.

[98] H.M. Guo, A.S. Zhang, X. Yang, M.M.Yan, Grain refinement of Al−5%Cu aluminum alloy under mechanical vibration using meltable vibrating probe, Trans. Nonferrous Met. Soc. China. 24 (2014) 2489–2496.

[99] C. Vivès, Grain refinement in aluminum alloys by means of electromagnetic vibrations including cavitation phenomena, JOM-E. 50 (1998) 1–8.

[100] M.X. Zhang, P.M. Kelly, M. Qian, J.A. Taylor, Crystallography of grain refinement in Mg-Al based alloys, Acta Mater. 53 (2005) 3261–3270.

[101] T.R. Vijayaram, M. Sayuti, S. Sulaiman, Effect of mechanical vibration on the properties , microstructure and fractography of titanium carbide particulate-reinforced LM6 alloy composite castings, Indian foundry Journal 58 (2012) 23–33.

[102] A.H. Feng, Z.Y. Ma, Enhanced mechanical properties of Mg-Al-Zn cast alloy via friction stir processing, Scr. Mater. 56 (2007) 397–400.

[103] F.R. Mollard, M.C. Flemings, E.F. Niyama, Aluminum fluidity in casting, JOM 39 (1987) 34.

[104] K. Kubota, M. Mabuchi, K. Higashi, Review processing and mechanical properties of fine-grained magnesium alloys, J. Mater. Sci. 34 (1999) 2255–2262.

[105] W. Soboyejo, Mechanical properties of engineered materials, CRC Press, (2002).

[106] J. Pelleg, Mechanical properties of materials, Springer (2013).

[107] Y.Z. Lu , Q.D. Wang, W.J. Ding, X.Q. Zeng, Y.P. Zhu, Fracture behavior of AZ91 magnesium alloy, Mater. Lett. 44 (2000) 265–268.

[108] W. Jiang, X. Chen, B. Wang, Z. Fan, H. Wu, Effects of vibration frequency on microstructure, mechanical properties, and fracture behavior of A356 aluminum alloy obtained by expendable pattern shell casting, Int. J. Adv. Manuf. Technol. 83 (2016) 167–175.

[109] P.C. Meena, A. Sharma, S. Singh, Effect of grain refinement on microstructure and wear behavior of cast Al-7Si alloys, La Metall. Ital. 1 (2015) 25–34.

[110] G.V. Bhaskar, B. Sharmila, P.N. Chetty, Wear Resistance behavior study of AZ31B Mg alloy, IJERT 3 (2014) 2778–2782.

Appendix I

Table 1: Effect of frequency of mechanical vibration at constant amplitude on the density of the alloy

Frequency	Density	Standard deviation
0	1.795	0.002
5	1.797	0.0018
10	1.8	0.0016
15	1.812	0.0011
20	1.798	0.0013
25	1.796	0.0017

Table 2: Effect of amplitude of mechanical vibration at constant frequency on the density of the alloy

Amplitude	Density	Standard deviation
0	1.795	0.002
1	1.807	0.0015
2	1.812	0.0011
3	1.803	0.0016

Table 3: Effect of grain refiner without and with vibration parameters on the density of the alloy

Process parameters	Density	Standard deviation
0	1.795	0.002
AZ91 + 2 wt.% ZnO	1.799	0.0017
15Hz-2mm	1.812	0.0011
Combined	1.819	0.0013

Table 4: Effect of frequency of mechanical vibration at constant amplitude on the tensile properties of the AZ91 Mg alloy

Frequency of vibration (Hz)	Yield Strength (MPa)	UTS (MPa)	% Elongation
0	90±1.14	140±1.024	1.8±0.044
5	92±1	145±0.977	1.78±0.035
10	98±0.83	150±0.913	1.75±0.007
15	108±0.638	168±0.532	2.5±0.006
20	99±0.974	151±0.666	2.0±0.011
25	94±0.865	145±0.631	1.9±0.023

Table 5: Effect of amplitude of mechanical vibration at constant frequency on the tensile properties of the AZ91 Mg alloy

Amplitude of vibration (Hz)	Yield Strength (MPa)	UTS (MPa)	% Elongation
0	90±1.14	140±1.024	1.8±0.044
1	99±0.825	153±0.726	2.2±0.021
2	108±0.638	168±0.532	2.5±0.006
3	94±1.03	148±0.625	1.9±0.018

Table 6: Effect of grain refiner without and with vibration on the tensile properties of the AZ91 Mg alloy

Process parameters	Yield Strength (MPa)	UTS (MPa)	% Elongation
0	90±1.14	140±1.024	1.8±0.044
AZ91 + 2 wt.% ZnO	93±1.04	147±0.953	2±0.021
15Hz-2mm	108±0.638	168±0.532	2.5±0.006
Combined	121±0.65	182±0.536	2.8±0.019

Table 7: Effect of frequency of mechanical vibration at constant amplitude on the hardness of the alloy

Frequency	Hardness		
	Top portion	Middle portion	Bottom portion
0	53 ± 1.13	55 ± 1.18	58 ± 1.20
5	54 ± 0.81	57 ± 1.01	59 ± 1.15
10	55 ± 0.62	58 ± 0.75	60 ± 0.81
15	66 ± 0.3	73 ± 0.33	78 ± 0.49
20	58 ± 0.56	59 ± 0.69	63 ± 0.82
25	54 ± 0.72	55 ± 0.93	61 ± 0.98

Table 8: Effect of amplitude of mechanical vibration at constant frequency on the hardness of the alloy

Amplitude	Hardness		
	Top portion	Middle portion	Bottom portion
0	53 ± 1.13	55 ± 1.18	58 ± 1.207
1	64 ± 0.77	69 ± 0.82	72 ± 0.98
2	66 ± 0.3	73 ± 0.33	78 ± 0.49
3	64 ± 0.52	70 ± 0.71	71 ± 0.81

Table 9: Effect of grain refiner without and with vibration on the hardness of the alloy

Process parameters	Hardness		
	Top portion	Middle portion	Bottom portion
0	53 ± 1.13	55 ± 1.18	58 ± 1.207
AZ91 + 2 wt.% ZnO	60 ± 0.6	64 ± 0.64	69 ± 0.92
15Hz-2mm	66 ± 0.3	73 ± 0.33	78 ± 0.49
Combined	72 ± 0.42	79 ± 0.49	92 ± 0.52

Table 10: Effect of frequency of mechanical vibration at constant amplitude on the COF of the AZ91 Mg alloy

Frequency	COF at 5N	COF at 10N
0	0.59 ± 0.0081	0.68 ± 0.01
5	0.41 ± 0.007	0.58 ± 0.009
10	0.34 ± 0.005	0.38 ± 0.006
15	0.26 ± 0.004	0.27 ± 0.0052
20	0.27 ± 0.006	0.30 ± 0.0066
25	0.31 ± 0.008	0.32 ± 0.01

Table 11: Effect of frequency of mechanical vibration at constant amplitude on the specific wear rate of the AZ91 Mg alloy

Frequency	Sp. Wear rate at 5N	Sp. Wear rate at 10N
0	1.07 ± 0.007	1.69 ± 0.027
5	0.79 ± 0.008	0.82 ± 0.012
10	0.68 ± 0.008	0.73 ± 0.01
15	0.51 ± 0.005	0.56 ± 0.008
20	0.59 ± 0.006	0.62 ± 0.009
25	0.7 ± 0.009	0.75 ± 0.012

Table 12: Effect of amplitude of mechanical vibration at constant frequency on the COF of the alloy

Amplitude	COF at 5N	COF at 10N
0	0.59 ± 0.0081	0.68 ± 0.01
1	0.29 ± 0.0096	0.3 ± 0.0011
2	0.26 ± 0.004	0.27 ± 0.0052
3	0.28 ±0.0072	0.32 ± 0.015

Table 13: Effect of amplitude of mechanical vibration at constant frequency on the specific wear rate of the alloy

Amplitude	Sp.wear rate at 5N	Sp.wear rate at 10N
0	1.07 ± 0.007	1.69 ± 0.027
1	0.88 ± 0.006	0.98 ± 0.018
2	0.51 ± 0.005	0.56 ± 0.008
3	0.68 ± 0.008	0.71 ± 0.009

Table 14: Effect of grain refiner without and with vibration on the COF of the alloy

Process parameters	COF at 5N	COF at 10N
0	0.59 ± 0.0081	0.68 ± 0.01
AZ91 + 2 wt.% ZnO	0.32 ± 0.006	0.33 ± 0.009
15Hz-2mm	0.26 ± 0.004	0.27 ± 0.0052
Combined	0.13 ± 0.0032	0.23 ± 0.0037

Table 15: Effect of grain refiner without and with vibration on the specific wear rate of the alloy

Process parameters	Sp. Wear rate at 5N	Sp. Wear rate at 10N
0	1.07 ± 0.007	1.69 ± 0.027
AZ91 + 2 wt.% ZnO	0.58 ± 0.006	0.64 ± 0.01
15Hz-2mm	0.51 ± 0.005	0.56 ± 0.008
Combined	0.43 ± 0.004	0.479 ± 0.006

Appendix II

List of publications

International Journal

1. Vatsala Chaturvedi, Ashok Sharma, Upender Pandel, **"Effect of mechanical vibrations on grain refinement of AZ91 Mg alloy",** Materials Research Express **4** (2017).
2. Vatsala Chaturvedi, Upender Pandel, Ashok Sharma, **"Effect of mechanical vibrations on the wear behavior of AZ91 Mg alloy",** Scopus (Accepted).
3. Vatsala Chaturvedi, Upender Pandel, "**Improvement of mechanical properties by mechanical vibration on AZ91 during solidification**", International Journal of Engineering Technology, Management and Applied Sciences, **Pearson Publications 3 (**2015) Special Issue, ISSN 2349-4476.

National Journals

1. Vatsala Chaturvedi, Upender Pandel, Ashok Sharma, "**Melting practice for magnesium alloys"** Indian Foundry Review (2014)**.**
2. Vatsala Chaturvedi, Upender Pandel, Ashok Sharma, "**Energy efficiency in casting of magnesium alloys"** Indian Foundry Journal (2014).

International and National Conferences

1. Vatsala Chaturvedi, Upender Pandel, **"Study of mechanical vibration on structure and properties of Mg-9Al alloy during solidification",** Proceedings of the 17th Int. AMME Conference, organized by Military Technical College Kobry El-Kobbah, Cairo, Egypt, 2016.
2. Vatsala Chaturvedi, Upender Pandel, "**Improvement of mechanical properties by mechanical vibration on AZ91 during solidification**", International

Conference on Emerging Trends of Engineering, Science, Management and its Applications, organized by JNU Delhi, 2015.

3. Vatsala Chaturvedi, Upender Pandel, Ashok Sharma, Abstract "**Grain refinement of magnesium alloys through vibrations**", The Indian Institute of Metals NMD ATM, 2014.

4. Vatsala Chaturvedi, Upender Pandel, Ashok Sharma, "**An overview of improvement of properties of AZ91 magnesium alloy by grain refinement through vibrations**", International conference on advance trends in engineering & technology (ICATET), 2013.

5. Vatsala Chaturvedi, Upender Pandel, Ashok Sharma, "**An overview of effect of vibration on AZ91 Mg alloy during solidification**", National conference on recent trends in materials engineering", 2013.